Methodology for Designing and Analyzing an Ideal Convergent-Divergent Nozzle

Omar Andrés Fuentes Manrique

A Dissertation Submitted in Partial Fulfillment of the Requirements for the Degree of Mechanical Engineering

Thesis Advisor

Manuel Martinez

Ph.D Mechanical Engineering

Universidad Industrial de Santander

School of Mechanical Engineering

Bucaramanga

2019

I dedicate this thesis to my beloved parents for their support during all of my life, that means so much to me, and I owe them everything I have accomplished.

Next, I want to remember my immediate family, my three sisters, my aunt and cousin, the people with whom I raised. The same way, I am glad about my dear girlfriend Lizeth, my companion, and the person who has supported me since the beginning of my major with her genuine belief in me and her unconditional love.

Last but not least important, I dedicate this to my friends Dayal, German, Diego, and Robinson, people that have been my study and fun fellows.

All of them helped me until I finished this piece of work.

Acknowledgments

I welcome this opportunity to thank my advisor, Prof. Manuel Martinez for giving me the opportunity to conduct this dissertation, next, for his theoretical assistance and encouragement to complete this project, which was solely pursued due to my interest in the topic, also, for the continuing sanity checks because of my ideas about the thesis. His exceptional ability and speed for grasping new concepts and responding to them have taken me several times by surprise.

Besides, I want to thank Prof. William Pinto for being a "second advisor" in many respects, including the long office lectures on optimization algorithms. I am profoundly grateful for all his help and dedication in teaching me always in the kindest way because, without it, I would not have had the opportunity to do this work.

Finally, I would also like to acknowledge with appreciation to my friend Dayal Castro for his patience and guidance with the handling and interpretation of the software ANSYS. His experience was an immense source to draw upon.

Preface

Strengthening the pillars of the current School of Mechanical Engineering at UIS is one of the reasons for undertaking this piece of work since this almost the only dissertation thesis related to compressible flow through nozzles and the only that treat the design of a convergent-divergent nozzle.

This thesis pretends to show the reader a way to design this type of nozzle from a closer perspective to the basic undergraduate concepts of Fluid Mechanics and Thermodynamics. Understanding that handling topics such us compressible fluid dynamics, CFD, and propulsion is complicated for mean students, the purpose is to show a step by step process to derive, apply, and understand the design and analysis of an ideal CD nozzle. Implementing these topics in the thesis dissertation of the school of Mechanical Engineering at UIS is one of the most robust objectives of the author.

The decision to work in this subject is due to the author's interest in aeronautics and astronautics. The fact that all kinds of jet engines, rockets, and wind tunnels have a nozzle to produce thrust or fit a flux is an approximation to develop knowledge in the topics and is the cause of how this book came about. The scope of this book is analytical, theoretical, and numerical; the experimental part is a limitation of this work. The references for this project is an important part to mention, as most of them are relevant articles, thesis, and books on the field. Last, it is essential to suggest the reader read in the order that is offered and no other.

Table of Contents

List of Tables

List of Figures

List of Appendices

(Appendices can be seen in either the CD or the library database at UIS)

Symbols

π_n	Nozzle total pressure ratio
p	Pressure
s	Entropy
R	Gas constant
γ	Specific heat ratio of the gas
C	Specific heat, Coefficient
$\dot{m}$	Mass flow rate
ρ	Density, radius
V	Velocity
u	Axial velocity
v	Radial velocity
c	Sound velocity
A	Area
T	Temperature
M	Mach number
F	Nozzle gross thrust
L	Length
x	x-axis coordinate
y	y-axis coordinate
ϵ	Origin of Sauer reference frame
α	Mach angle, Coeff. of the linear axial perturbation velocity
Γ	Circulation
w	Rotation in a fluid
φ	Potential velocity function

θ	Streamline angle
λ	Characteristic line slope
σ	Coefficient indicating either two-dimensional or axisymmetric problem
$Q,\ R,\ S,\ T$	Finite differential compatibility equation coefficients

Subscripts

t	Throat
T	Total
0	Ambient
$Crit$	Critic
D	Discharge
e	Effective
g	Gross
p	Pressure
V	Volume
i	Ideal
A	Angular
$down$	Downstream
up	Upstream
a	Dimensionless
IV	Initial-Value line
$Cham$	Chamber
$-*$	Corrector variables
$x,\ y$	Derivative in x or y

Superscripts

$*$	Critic

Abstract

Title: Methodology for Designing and Analyzing an Ideal Convergent-Divergent Nozzle.[1]

Author: Omar Andrés Fuentes Manrique[2]

Keywords: nozzle, supersonic, convergent-divergent, ANSYS-Fluent, characteristics, methodology, algorithm, programming, Matlab.

Description: The lack of a robust procedure in the design of convergent-divergent supersonic nozzles and the dispersion of reference material creates a vacuum in the undergraduate students. This thesis tries to fill the gaps in the literature, presenting all the concerned concepts to carry out a nozzle design. That includes the derivation of the method of characteristics from the concepts of fluid mechanics. Also, a methodology and an algorithm for programming in Matlab of the design and analysis of a steady axisymmetric isentropic convergent-divergent supersonic nozzle is presented. An example of the methodology application was carried out. Numerical simulation of CFD in the packaged software ANSYS-Fluent was computed to compare and validate the results from the application of the methodology. Both methods showed the same behavior of the flow, and the uniformity index computed in Fluent was 0.99. All the compared results between both methods had an error lower than 1%.

[1]Dissertation
[2]School of Mechanical Engineering. Advisor: Manuel Martinez, Ph.D. Mechanical Engineering.

Resumen

Título: Metodología para Diseñar y Analizar una Tobera Convergente-Divergente Ideal.[3]

Autor: Omar Andrés Fuentes Manrique[4]

Palabras clave: tobera, supersónica, convergente-divergente, ANSYS-Fluent, características, metodología, algoritmo, programar, Matlab.

Descripción: La falta de un procedimiento robusto en el diseño de toberas convergentes-divergentes supersónicas, y la dispersión bibliográfica crea un vacío en los estudiantes de pregrado. Esta tesis trata de llenar los vacíos en la literatura, presentando todos los conceptos involucrados para llevar a cabo un diseño de este tipo de toberas. Eso incluye la derivación del método de características desde los conceptos de mecánica de fluidos. Además, se presenta una metodología y un algoritmo para programar en Matlab el diseño y análisis de una tobera supersónica convergente-divergente isentrópica en estado estable. Se realizó un ejemplo de la aplicación de la metodología. Se realizó una simulación numérica de CFD en el software empaquetado ANSYS-Fluent para comparar y validar los resultados de la aplicación de la metodología. Ambos métodos mostraron el mismo comportamiento del flujo, y el índice de uniformidad calculado en Fluent fue de 0.99. Todos los resultados comparados entre ambos métodos tuvieron un error inferior al 1%.

[3]Trabajo de grado

[4]Facultad de Ingenierías Fisico-Mecánica. scueka de Ingeniería Mecánica. Director: Manuel Martinez, Ph.D. Ingeniería Mecánica

Introduction

Modern aircraft are powered by gas turbine engines, which are also called jet engines. There are several different types of gas turbine engines, but all these have a nozzle to produce thrust, to conduct the exhaust gases back to the free stream, and to set the mass flow rate through the engine (NASA Glenn Research Center, 2015, at *Nozzles*, para. 1). Converging-diverging ducts also come up in aircraft engine inlets, wind tunnels, and in all sorts of piping systems designed to control gas flow. The nozzle begins where the chamber diameter begins to decrease and converts the potential energy of the gas stream from the high temperature and pressure into kinetic energy by expanding the gas stream to the high velocity at the nozzle exit (DeBonis, 2010, chap. 1).

A nozzle is relatively a simple device, just a specially shaped tube through which hot gases flow. Though, the mathematics which describes the operation of the nozzle takes some careful thought. Nozzles come in a variety of shapes and sizes depending on its use (NASA Glenn Research Center, 2015, at *Nozzles*, para. 2). The geometry to be treated in this research is a convergent-divergent (CD) nozzle. This kind of nozzles is composed basically for three parts, a primary or convergent nozzle, the throat, and a secondary or divergent nozzle. In a converging nozzle, the highest velocity at which a fluid can be accelerated is the sonic velocity or Mach 1. A secondary nozzle is used to accelerate the fluid at supersonic speeds beyond the throat through the gas stream expansion.

The design of a nozzle is divided into three principal stages, the subsonic, transonic, and supersonic stages. All of them are designed separately and have different methods of design. For the subsonic part, the formula of Vitoshinsky is utilized as it generates a smooth contour with uniform flow in the x-axis direction. The transonic section is designed by the Sauer method, and although there are some other methods to analyze the flow at near-critical speeds, it is the most

straightforward. In the diverging stage, there are two primary numerical techniques for the solution of completely supersonic, steady, and inviscid flows. These techniques are the method of characteristics and finite-difference methods. The method of characteristics is older and more developed and is limited to inviscid flows. In contrast, finite-difference techniques (along with finite-volume techniques) are still evolving as computational fluid dynamics grows and matures, and have much more general application to inviscid and viscous flows. Although, in this project, the method of characteristics is used to solve the problem of supersonic flow expansion through a CD nozzle, the utilization of CFD to corroborate the method will involve the finite-difference technique.

The method of characteristics has been used since the 1930s supersonic flow solutions in channels, and despite its maturity, its practical implementation for axisymmetric nozzles remains a tedious process; this is a direct consequence of the lack of satisfactory reference material, i.e., the open literature does not contain a robust methodology of its derivation and implementation. Consequently, authors of several papers have felt the need to supply their derivations, and many of the standard presentations are not very easy to follow or apply. This thesis tries to fill these gaps in the literature and provides the technical details required for the proper use of this method.

Hence, this work centered on providing a robust methodology for designing and analyzing an axisymmetric and ideal convergent-divergent nozzle. A design algorithm is presented for programming the methodology in Matlab. The results and the work itself are expected to strengthen the foundations of the School of Mechanical Engineering at UIS because, so far, 17 years ago, there is no history of the topic.

This dissertation has been organized into eight chapters; the first chapter corresponds to the objectives. The second chapter will help the reader with the literature concerning the performance and contour of the convergent-divergent supersonic nozzle. Chapter three presents the derivation of the method of characteristics and present the necessary formulas for applying the method of Sauer.

Chapter four explains the methodology in a step by step and provides the flowcharts for programming the methodology in Matlab. Chapter five includes the numerical simulation approach made in ANSYS-Fluent and the way to validate its convergence and results. Chapter six is the validation of the overall results. The two remaining chapters correspond to the conclusions and recommendations. All the references utilized are in the list of references organized alphabetically. Finally, the appendices include a chapter of complementary literature, a chapter of numerical analysis, and the programming of the methodology used for designing the example is attached to the CD and can be viewed in the UIS Library database. The reader is expected to follow the just described order and not others.

1. Objectives

1.1 General Objective

Provide a reliable methodology for designing and analyzing an ideal axisymmetric convergent-divergent nozzle, as well as make an algorithm for programming in Matlab. This proposal fulfills the objectives of innovation, technological development, and scientific progress proposed by the Universidad Industrial de Santander, in the search for expansion into new fields of study.

1.2 Specific Objectives

- Derive the method of the characteristics from the basic concepts of Fluid Mechanics since its usual derivation is made from the differential equation of the velocity potential. In this way, it seeks to consolidate its use and understanding.
- Provide an algorithm for the design of a convergent-divergent nozzle applying the method of the characteristics, providing only the pressure and stagnation temperature, the ratio of specific heats, the radii of the combustion chamber, and the throat, the water radii up and down the throat and the Mach design number.
- Corroborate the design method through a simulation in CFD, using ANSYS-Fluent, taking into account that the results are acceptable and that the difference in the results between the methods does not exceed 5%.

2. Convergent-Divergent or De Laval Nozzle

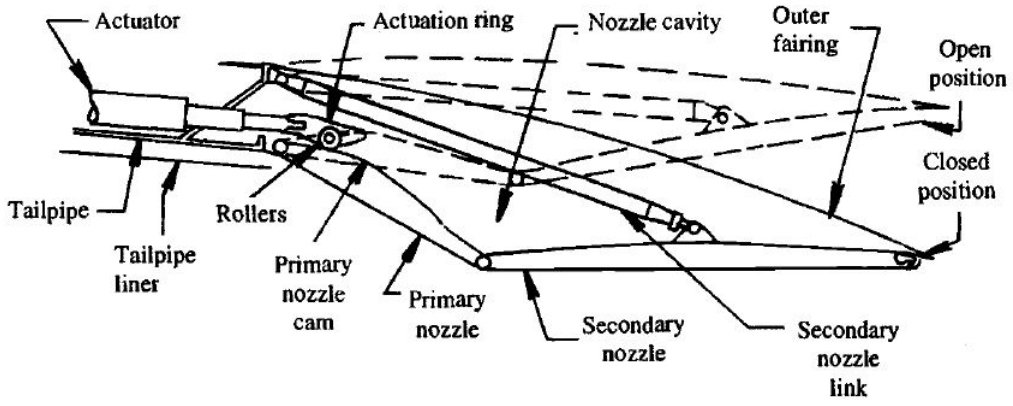

Figure 1.. Convergent-divergent nozzle schematic

Source: Oates (1989) at *Aircraft Propulsion Systems Technology and Design.*

The concept of an exhaust nozzle for jet engines has changed (most in military aircraft) from a single convergent duct to a multitasked component in modern designs that include a high-performance shape generally convergent-divergent with variable-geometry and some other functions (Farokhi, 2014, p. 8). Figure 1 shows a simplified aircraft CD-Nozzle with a fixed area for afterburner operation combined with the most common parts. The (CD) duct is used in order to expand a steady internal flow from subsonic to supersonic speed (DeBonis, 2010; John D. Anderson, 2003, p. 413). The subsonic flow is accelerated in the converging section up to the minimum area or throat. Here the gas velocity reaches a sonic speed (Mach number of one, M = 1). Then the nozzle accelerates the flow supersonically (M > 1) by providing a path of increasing flow area (El-Sayed, 2016, pp. 680 - 681). CD nozzles are used for high-speed applications, where the engine provides very high pressures, which must be expanded to the freestream pressure, i.e., is used if the nozzle pressure ratio $P_{T-inlet}/p_0$ is high (greater than about six) (Mattingly, 2006, p. 728).

NOTE: For reading about the functions of a CD nozzle and the history of the development and use of de Laval nozzle, read the appendix A.1 and A.2.

2.1 Nozzle Performance and Aerodynamics Remarks

Nozzle performance is generally measured in terms of the parameters, mass-flow, thrust, the pressure distribution, the area, and the efficiency (DeBonis, 2010; El-Sayed, 2016, p.681). These parameters are evaluated through empirical correction factors or dimensionless coefficients. These are the gross thrust coefficient, the discharge or flow coefficient, the velocity coefficient, the angularity coefficient, the pressure ratio, and the area ratio, which represent a variety of non-ideal phenomena (Mattingly, 2006; Oates, 1989). The thrust and discharge correction factors are yielded by the measurement of the combustion chamber pressure, the mass flow rates, the thrust force, and the throat and exit areas in the testing of propulsion systems. Correction factors are ratios of the actual to the formulated or ideal values and are used by engineers to predetermine performance ahead of testing and for preliminary designs (Sutton & Biblarz, 2010, p. 90). All these correction factors are interrelated one to another in terms of the nozzle performance measurement.

Pressure Distribution

Nozzle pressure distributions are used by mechanical designers to determine hardware structural loads and actuation system loads. These loads thus affect detailed mechanical design, weight, and cost and are, therefore, significant estimates to be provided by the aerodynamic designer. Internal pressure distributions can be estimated for the primary and secondary nozzle to cover all nozzle geometries and operating conditions. Although the external loads on the nozzle are generally much smaller than the internal loads, external pressure distributions need to be estimated at high-load conditions.

Throughout the pressure distribution, the behavior of the gas expansion within the nozzle can be seen. Imperfect expansion is the primary loss mechanism

in nozzle flows. In the case of a good design of de Laval nozzle, for a given nozzle area ratio (A_9/A_8), there is a single pressure ratio (NPR) or backpressure that provides maximum thrust, it is reached at the point $P_9 = P_0$. At any other pressure ratio, there will be a non-nominal state, and the flow will not be correctly expanded at the nozzle exit, resulting in a loss of thrust. Non-nominal states are reached through changes in the parameters of working gas at the inlet or the exit of nozzle (Škorpík, 2018, p. 10).

Pressure distributions can be obtained either from scale-model tests or from analytical methods, being the scale-model tests more accurate; however, it is not always possible to obtain test data (Oates, 1989, p. 330).

In the primary nozzle, since the flow consists primarily of subsonic flow, adequate accuracy of the pressure distribution can be obtained by utilizing the assumption of one-dimensional flow. However, this approach can produce errors in several ways.

Oates explains two of them. First, a small error that will occur at the forward hinge point near the nozzle entrance, where the one-dimensional calculation does not take into account the local turning of the flow. However, since this is close to the hinge, the impact of this error on actuator loads is usually negligible. Second and more significant, an error that can occur for nozzle designs with unusually long primary nozzles at afterburning conditions. As significant combustion can take place within the primary nozzle, there is a heat addition, and total pressure loss occurring within the primary nozzle. As a result, the real static pressure distribution will be significantly higher than the calculated one-dimensional pressure distribution. This error becomes very significant at the high fuel-air ratios. The correction for reheat burning effects must be applied to any analytical calculation and all scale-model data. For most applications, the primary nozzle is relatively short; thus, this effect is minimal, if not insignificant. However, it should always be checked.

In the secondary nozzle (Figure 2.2(b)), the prediction of the gas loads is not as straightforward as the primary nozzle for several reasons. Sudden overexpansion of the flow immediately downstream of the throat causes the pressure distribution

to deviate significantly from that predicted by a one-dimensional analysis. Also, the amount of cooling slot flow if present, but the real case is that even nozzles with no cooling slot will have some amount of leakage flow at the throat due to hardware stack-up tolerances. Thus, reliable analytical predictions can be made by only two methods: semi-empirical using test data and theoretical using computerized flowfield equations (Oates, 1989, pp. 332-334).

Independent of the method used, either primary or secondary nozzle pressure load estimates should be provided to the mechanical designer at a sufficient number of nozzle geometries settings to allow easy interpolation (see Figure 2). It is vital to provide the most precise load possible.

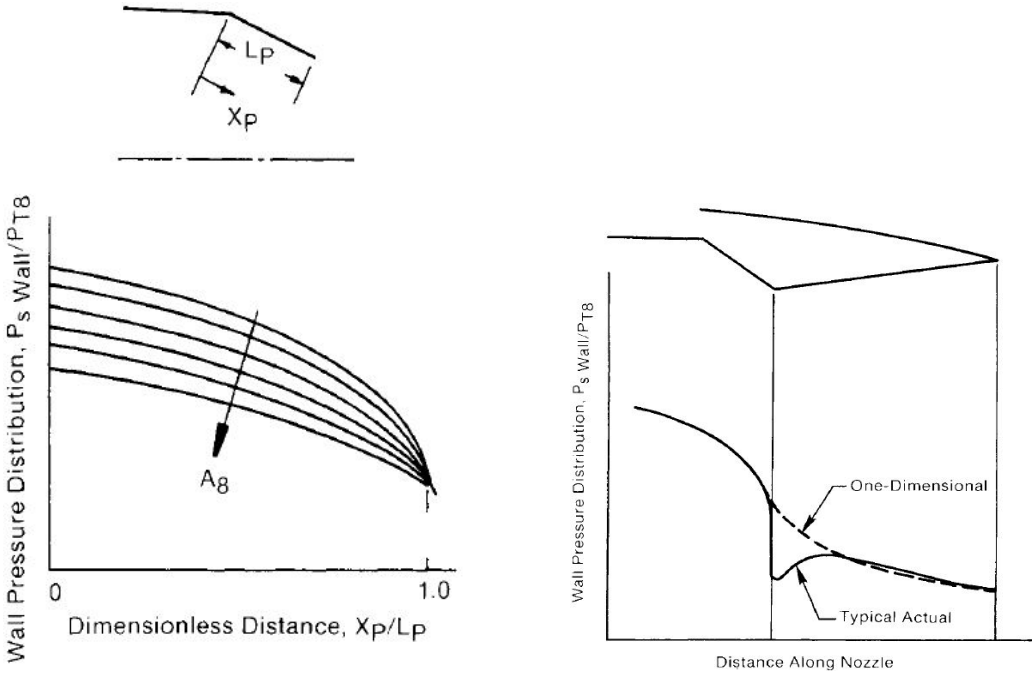

(a) Primary nozzle pressure distribution. (b) Sec. nozzle pressure distribution.

Figure 2.. Convergent-divergent nozzle pressure distribution.
Source: Oates (1989) at *Aircraft Propulsion Systems Technology and Design.*

Nozzle external pressure distributions will be dependent on many parameters, including specific nozzle geometry, propulsion system installation, local aircraft configuration including control surface position, Mach number, and nozzle

pressure ratio as well as Reynolds number and aircraft attitude (angle of attack, yaw). Because of the large number of variables, it is virtually impossible to devise semiempirical parametric curves that could be used to provide an initial estimate. By far, the most accurate pressure distributions are obtained from wind-tunnel tests of the exact nozzle/airplane configuration of interest at the appropriate operating conditions. Extrapolation or interpolation of these data is often necessary to provide load estimates at all the conditions of interest. In the absence of directly applicable wind-tunnel data, pressure distributions can be estimated by using previous wind-tunnel test data or by analytical methods. When using previous data, configurations, and conditions that most closely resemble the nozzle and installation of interest should be used for load estimates. Computerized analytical methods can also be used to predict external loads. This approach gives outstanding results for two-dimensional or axisymmetric configurations. In either case, engineering judgment will be required to interpret and apply the information to define load estimates accurately (Oates, 1989, p. 336).

Nozzle Total Pressure Ratio (π_n)

The total pressure ratio in a nozzle is the ratio of outlet total pressure P_{t9} to inlet total pressure P_{t7} (El-Sayed, 2016, p. 681).

$$\pi_n = \frac{p_{T-outlet}}{p_{T-inlet}} \tag{2.1}$$

This parameter is a direct measure of flow irreversibility due to friction and shock in the nozzle as the nondimensional entropy rise in an adiabatic process is the negative natural logarithm of total pressure ratio, namely, (Farokhi, 2014, p. 374).

$$\frac{\Delta s}{R} \approxeq -ln(\pi_n) \tag{2.2}$$

Nozzle Pressure Ratio (NPR)

The NPR across the nozzle controls the expansion process and the maximum thrust (Mattingly, Heiser, & Pratt, 1801, p. 473). The NPR signifies the nozzle flow expansion potential, i.e., from the stagnation or total state at the entry to the ambient static state. Even though it can be defined using the total pressure at the throat section without any significant difference (DeBonis, 2010, Chap. 2). Since p_0 is the ambient pressure, the nozzle pressure ratio is a strong function of altitude, demanding higher area expansion ratios of the nozzle with altitude. The choice of a convergent or a convergent-divergent nozzle can also be guided based on the magnitude of this parameter (Farokhi, 2014, p. 374).

$$NPR = \frac{P_{T-inlet}}{p_0} \tag{2.3}$$

The mass flow rate through a nozzle varies with nozzle pressure ratio until a speed of Mach 1 is reached at the nozzle throat. The NPR at this point is termed the critical NPR, i.e., the NPR_{Crit} leads to a sonic throat. Beyond this pressure ratio, the nozzle is said to be choked, and the nozzle flow rate does not respond to a variation in the downstream, exit pressure. Hence the nozzle flow rate will not be affected by changes in altitude. The mass flow is still affected by changes in plenum conditions (DeBonis, 2010, Chap. 2). The critical NPR for a perfect gas is:

$$NPR_{Crit} = \left(\frac{\gamma + 1}{2}\right)^{\frac{\gamma-1}{\gamma}} \tag{2.4}$$

NOTE: For reading about the relation of the NPR with the nominal and non-nominal states in the gas expansion, read the appendix A.3.

Massflow and Discharge Coefficient (C_D)

The nozzle must be able to pass the amount of mass flow that the engine cycle requires for all operating conditions. The minimum nozzle area, the throat area for a convergent-divergent nozzle, controls the mass flow rate for a given operating condition in an engine. From these conditions, the effective flow area at

the nozzle throat required to pass the total flow is determined (Oates, 1989, p. 307). Thus, the nozzle and engine mass flow are typically defined using the conditions at the nozzle throat (DeBonis, 2010).

The principle of the conservatism of mass in a steady flow with a single inlet and single outlet is expressed by equating the mass flow rate; this is known in mathematical form as the continuity equation (Sutton & Biblarz, 2010, p. 50). The ideal flow rate is based on the one-dimensional isentropic expansion of the gas to the freestream conditions. For a choked nozzle, the ideal mass flow can be expressed as a function of nozzle plenum and throat conditions (DeBonis, 2010), and it is equal to the mass flow at any section within the nozzle (Sutton & Biblarz, 2010).

$$\dot{m_{ideal}} = \rho_t V_t A_t = \frac{P_t A_t}{\sqrt{T_t}} \sqrt{\frac{\gamma}{R} \left(\frac{2}{\gamma + 1} \right)^{\frac{\gamma+1}{\gamma-1}}} \tag{2.5}$$

For an axisymmetric two-dimensional analysis, the properties ρ_t and V_t are taken from the axis, and the actual flow mass is computed numerically.

The discharge coefficient relates the actual total flow rate through the nozzle to the ideal flow rate. Also, this coefficient can be shown to be identically equal to the ratio of the effective one-dimensional flow area required to pass the total actual nozzle flow to the nozzle physical throat area (Mattingly, 2006, p. 737).

$$C_D = \frac{\dot{m_{actual}}}{\dot{m_{ideal}}} = \frac{A_{t-effective}}{A_{t-geometric}} \tag{2.6}$$

This coefficient is not a measure of efficiency, but rather a sizing parameter that allows the nozzle physical area to be matched to an engine cycle, i.e., in a design, the order is to determine the required effective area from the engine cycle calculations, and the flow coefficient is used to calculate the required nozzle physical throat area (Oates, 1989, p. 308). DeBonis (2010) considers that the CD factor represents the influence of internal losses as the presence of a boundary layer on a surface, which acts as a blockage of the geometric flow area and reduces the effective area of the nozzle, restricting the flow. There is also a total pressure loss associated

with the boundary layer formed on the wall (Farokhi, 2014). The buildup of the boundary layer is accounted until the throat is reached, at this location will be the minimum effective area.

Depending on the engine cycle/exhaust nozzle system selected, the actual flow in the flow coefficient can include not only the flow passing through the nozzle throat area A8, but it can also include primary nozzle leakage and, in some cases, bypass cooling air and knowing each of these flows, a total nozzle effective area can be determined (Oates, 1989).

$$\dot{m_{actual}} = \dot{m}_t + \dot{m_{leakage}} + \dot{m_{cooling}} \tag{2.7}$$

$$A_{e;total} = A_{t-e} + A_{e-leakage} + A_{e-cooling} \tag{2.8}$$

$$C_D = \frac{A_{t-e} + A_{e-leakage} + A_{e-cooling}}{A_t} \tag{2.9}$$

In these cases, the effective area at the nozzle throat comprises most of the total effective area. The leakage effective area is typically 0.5-1% of the total and the cooling effective area is typically 0-2% of the total (Oates, 1989).

Area Ratio

Nozzle area ratio ε (or nozzle expansion ratio) is defined as nozzle exit area divided by throat area. From isentropic relations:

$$\varepsilon = \frac{A_{Exit}}{A_{Throat}} = \frac{1}{M}\left(\frac{2+(\gamma-1)M^2}{\gamma+1}\right)^{\frac{\gamma+1}{2(\gamma-1)}} \tag{2.10}$$

Notice that $\varepsilon > 1$, but sometimes the inverse is also named 'area ratio' (this contraction area ratio is bounded between 0 and 1). However, although no confusion is possible when quoting a value (if it is (>1) refers to A_{Exit}/A_{Throat}, and if it is (<1) refers to A_{Throat}/A_{Exit}), one must be explicit when saying 'increasing area ratio' (Martinez, 2017).

As it is desirable to keep the thrust near to the maximum possible engine thrust ($p_e outlet = p_0$), then the nozzle area ratio has to be manipulated in order to achieve this aim. In modern aircraft, the exhaust nozzle throat of a CD nozzle works in a choked mode across a wide operating range within the flight envelope.

In case of a flow expansion different from $p_{outlet} = p_0$, it is remarkable to consider that a small amount of underexpansion is less harmful to aircraft and engine performance than overexpansion (Saeed Farokhi). Thus, the design area ratio A_{Exit}/A_{Throat} of convergent-divergent nozzles is selected such that the nozzle flow does not separate due to overexpansion for most throttle settings (Mattingly, 2006, p. 741).

The engine cycle and operating conditions set the nozzle throat area A_{Throat}, and the exit area A_{Exit} is established in either of two ways. First, Kinematically, by a linkage system in which case, there is a single value of A_{Exit} for each A_{Throat}, in this case, A_{Exit} is dependent on A_{Throat}, and the nozzle is said to have a fixed area ratio schedule (see *figure* 1). Second, A_{Exit} is set by its own linkage and actuation system independently of A_{Throat} and is said to have a variable area ratio schedule in which the area ratio can be set to provide maximum internal performance at any operating pressure ratio (Oates, 1989, p. 317). In this case, the maximum nozzle performance is characterized as a function of pressure ratio.

Variable-area nozzles are required for engine cycles where significant variations in nozzle exit area are necessary. When the airplane has an afterburning engine operation, the nozzle exit area assumes only two positions. One closed and the other open (with/without afterburner) (Farokhi, 2014, p. 389), and it is said to have two schedules: a low-speed mode and a high-speed mode (Mattingly, 2006, p. 732). In nearly all cases, this area variation has increments of 50-150% from non-afterburning to full afterburning operation (Oates, 1989, p. 301). What happens with an afterburner in operation is that the exhaust gas temperature increases significantly with a subsequent drop of density. A choked nozzle requires to open up its throat to accommodate a lower density gas and be able to pass almost the same mass flow rate as with no afterburner operation. Nowadays, the

limitation of only two positions for the nozzle exit area seems unnecessary, especially in light of the advanced propulsion control system of modern aircraft. Here, the purpose of nozzle area scheduling control is to achieve the highest possible performance with altitude, speed, aircraft attitude, and acceleration.

To provide the nozzle performance for an engine cycle, a sufficient number of C_{fg} curves should be defined to cover the nozzle operating range of interest and the minimum number of geometries at which C_{fg} curves should be defined.

For rockets and space vehicles, the nozzle area ratio could be as large as 50. The exhaust speed that can be achieved is governed by the nozzle area ratio, which in turn is determined by the design ambient pressure. Low ambient pressure leads to a high nozzle exit area, higher gas exit velocity, and hence, more thrust (El-Sayed, 2016, p. 682).

Velocity Coefficient (C_v)

It is the ratio of the actual exhaust velocity to the ideal exhaust velocity with no loss of total pressure $P_{outlt} = P_t$. It represents the effect of frictional loss in the boundary layer of the nozzle (Farokhi, 2014, p. 379).

$$C_v = \frac{V_{out}}{V_{out-i}} = \sqrt{\frac{1 - \left(\frac{p_{outlet}/p_0}{NPR.\pi_n}\right)^{\frac{\gamma-1}{\gamma}}}{1 - \left(\frac{p_{outlet}/p_0}{NPR.C_D^2}\right)^{\frac{\gamma-1}{\gamma}}}} \tag{2.11}$$

Because it is related to friction, this coefficient is mostly a function of the secondary nozzle surface area, Mach number near the wall, and Reynolds number (Oates, 1989, p. 315).

Angularity Coefficient (C_A)

In many systems, the flow exiting the nozzle is diverging and, therefore, not perfectly aligned with the thrust direction. The component of the velocity not

aligned with the thrust direction will not contribute to the thrust and is, therefore, a loss of thrust (DeBonis, 2010, p. 5). This loss of thrust is termed as the divergence loss. The flow angularity loss coefficient is proportional to the thrust loss due to the nonaxial exit of the exhaust gas (Mattingly, 2006, p. 739).

For a differential element of flow, this coefficient is the cosine of the local exit flow angle α_j (see *figure* 3). Since the exit angle α, varies from zero at the nozzle centerline to a maximum value at the outer radius, the overall nozzle angularity loss coefficient is the integral of $cos(\alpha)$, across the nozzle exit (Oates, 1989, p. 313).

$$C_{Aj} = \frac{V_{out-Axial}}{V_{out-i}} = cos(\alpha_j) \tag{2.12}$$

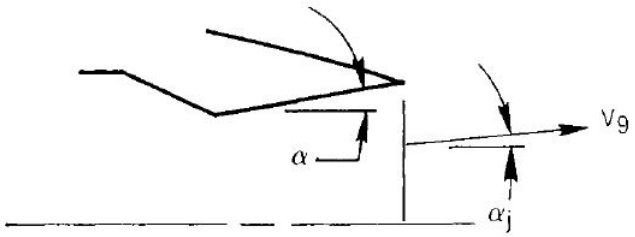

Figure 3.. Nozzle angularity coefficient

Source: Oates (1989) at *Aircraft Propulsion Systems Technology and Design.*

For the assumption of constant mass flow per unit area, the flow angularity is

$$C_A = \frac{1}{A_{Exit}} \int_{r=0}^{r=R_e} cos(\alpha_j) 2\pi r_j dr \tag{2.13}$$

For the case of a variable mass flow distribution, the equation would be adjusted to include the mass flow variation.

$$C_A = \frac{1}{\dot{m}} \int cos(\alpha_j) d\dot{m} \tag{2.14}$$

For one-dimensional adiabatic flow, CA = 1. In real nozzle geometries, there is also a slight loss in nozzle aerodynamic efficiency because the exit static pressure is not equal to ambient pressure across the entire nozzle exit area. For practical engineering purposes, this loss is included in the angularity coefficient.

It should be recognized that, while angularity and velocity coefficients can be determined separately by analytical studies, it is challenging and virtually impractical to determine the individual coefficients by experimental methods.

Nozzle Gross Thrust and Thrust Coefficient (C_{fg})

The nozzle contribution to engine thrust is called gross thrust and can be computed using the following equation.

$$F_{g-actual} = \dot{m}_{out} V_{out} + (p_{out} - p_0) A_{out} \tag{2.15}$$

The first term is the thrust generated due to the gas momentum and is termed the stream thrust (or vacuum thrust). The second term is the pressure-area term. It is zero when the flow is ideally expanded (DeBonis, 2010). The gross thrust of a nozzle is maximum when it operates fully expanded ($p_e = p_0$).

The momentum thrust is affected by total pressure losses and flow angularity at the exit (Farokhi, 2014, p. 386). These losses are seen as C_D, C_V, and C_A distributed throughout the nozzle, as shown in Figure below.

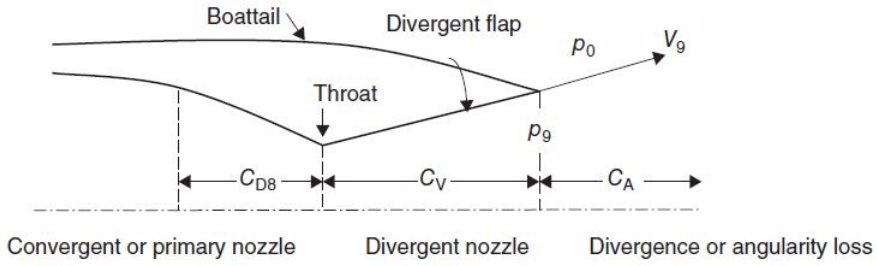

Figure 4.. Loss parameters in a CD nozzle

Source: Farokhi (2014) at *Aircraft Propulsion (2nd ed.).*

If all these loss parameters are taken into account, the equation of the actual thrust became in:

$$F_{g-actual} = C_D C_V \dot{m}_{t-i} V_{out-i} \left[C_A + \frac{1 - \frac{p_0}{p_{out}}}{\frac{2\gamma}{\gamma-1}\left[\left(\frac{p_{T-out}}{p_{out}}\right)^{\frac{\gamma-1}{\gamma}} - 1\right]} \right] \tag{2.16}$$

An ideal expansion in a nozzle leads to the maximum thrust. However, if the loss parameters are not considered, the ideal gross thrust available to the nozzle is achieved. This ideal thrust is based on the total airflow supplied to the nozzle, the total pressure, and temperature at the nozzle throat, and the fuel-air ratio at the nozzle throat (Oates, 1989, p. 305).

$$F_{g-ideal} = \dot{m}_{t-i} V_{out-i} \tag{2.17}$$

The ideal velocity is the velocity achieved if the flow were isentropically expanded to the freestream pressure and can be written as a function of nozzle pressure ratio and plenum temperature (DeBonis, 2010).

$$V_{ideal} = \sqrt{T_{T-t} \frac{2\gamma R}{\gamma - 1} \left(1 - NPR^{\frac{1-\gamma}{\gamma}}\right)} \tag{2.18}$$

Ideal thrust normalized by throat area and plenum pressure can be expressed as a function of nozzle pressure ratio (DeBonis, 2010, p. 3).

$$\frac{F_{g-ideal}}{p_{T-inlet} A_t} = \sqrt{\left(\frac{2\gamma^2}{\gamma - 1}\right) \left(\frac{2}{\gamma - 1}\right)^{\frac{\gamma+1}{\gamma-1}} \left(1 - NPR^{\frac{1-\gamma}{\gamma}}\right)} \tag{2.19}$$

Nozzle thrust can be expressed in non-dimensional form as thrust efficiency. The thrust coefficient is the ratio of actual nozzle gross thrust to the ideal available gross thrust (Oates, 1989, p. 305).

$$C_{fg} = \frac{F_{g-actual}}{F_{g-ideal}} \tag{2.20}$$

This coefficient represents the measure of nozzle efficiency and accounts for all nozzle losses. It includes the fundamental friction, angularity, and expansion losses and can include leakage and cooling air throttling losses if desired (Oates, 1989, p. 311).

The thrust coefficient is determined from the geometry and the engine/nozzle operating condition. The thrust coefficient is then used to calculate the actual gross thrust produced by the engine at the operating condition of interest.

While the flow coefficient definition is virtually universal, the thrust coefficient can be defined in several ways. The variations appear in the definition of an ideal thrust. For example, ideal thrust can be based on ideal airflow, or it can be based on nozzle exit velocity and pressure. Any definition will provide the correct nozzle gross thrust as long as it is consistently used from initial design and analysis (Oates, 1989, p. 307).

The gross thrust coefficient for one-dimensional flow of a calorically perfect gas in terms of the NPR, the pressure at the plenum and at the exit:

$$C_{fg} = C_D C_V \sqrt{\frac{1 - \left(\frac{\frac{p_{out}}{p_0}}{NPR.C_D^2}\right)^{\frac{\gamma-1}{\gamma}}}{\left(1 - NPR^{-\frac{\gamma-1}{\gamma}}\right)}} \left[C_A + \frac{\frac{\gamma-1}{2\gamma}\left(1 - \frac{p_0}{p_{out}}\right)}{\left(\pi_n NPR \frac{p_0}{p_{out}}\right)^{\frac{\gamma-1}{\gamma}} - 1}\right] \tag{2.21}$$

Figure 5 illustrates how thrust varies with nozzle pressure ratio. At the peak thrust coefficient condition, the ideal exit static pressure is equal to ambient pressure ($p_e = p_0$) and, by definition $V_{e-i} = V_e$. Therefore, the thrust equals the ideal thrust, and the peak thrust coefficient becomes the product of the angularity and velocity coefficients ($C_{fgPeak} = C_A C_V$). At any other NPRs, i.e. that both underexpansion ($p_e > p_0$) and overexpansion ($p_e < p_0$) make the nozzle thrust falls below the ideal value (DeBonis, 2010; Oates, 1989).

The angularity and velocity coefficients define the nozzle peak efficiency or maximum thrust coefficient. Once the nozzle peak thrust coefficient has been defined, a basic nozzle thrust coefficient curve can be calculated using one-dimensional fluid dynamics.

Leakage Losses

Nozzles that contain variable geometry require the moveable parts to be sealed to prevent flow leakage. Nevertheless, some leakage is inherent with this type

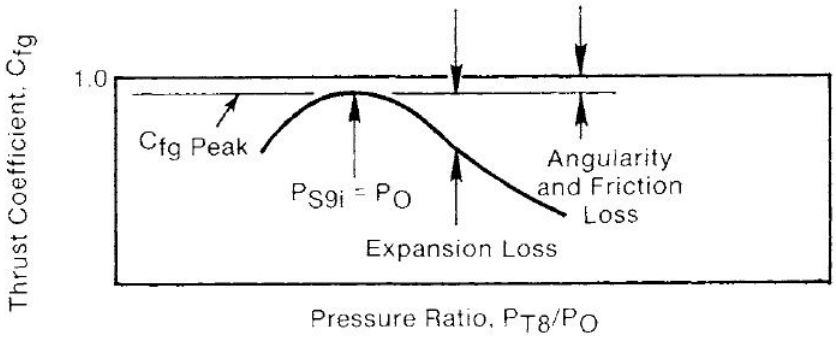

Figure 5.. Ideal thrust as a function of nozzle pressure ratio

Source: Oates (1989) at *Aircraft Propulsion Systems Technology and Design.*

of nozzles, and with high-pressure nozzle flow will occur, resulting in performance losses. Therefore, these gas leakage losses must be accounted for in performance estimates. This leakage occurs through the hinges, flaps, and seals for both the convergent and divergent actuated flow paths. Leakage losses affect both the discharge coefficient and the thrust coefficient. However, the percentage loss in mass flow is greater than the loss in thrust. Since it is impossible to simulate leakage areas in a scale-model test accurately, these thrust losses must be analytically calculated. The calculations require the use of nozzle wall pressure distributions to obtain the gas pressure loading and knowledge of the effective leakage areas in the nozzle.

2.2 Contour of De Laval Nozzle

A de Laval nozzle is a duct that is convergent-divergent in shape to expand a steady internal flow from subsonic to supersonic speed (John D. Anderson, 2003). Nozzles and chambers are usually of a circular cross-section. The aerodynamic design of a CD supersonic nozzle must be divided into three parts the subsonic, the throat (minimum cross-section) or transonic, and the supersonic sections. The wall surface throughout the nozzle should be smooth and shiny to minimize friction, radiation absorption, and convective heat transfer due to surface roughness. Gaps, holes, sharp edges, or protrusions must be avoided. This contour also must be parallel with streamlines to avoid a rise of turbulence through a sudden change of

path of flow velocity at the wall. It suggests the outlet velocity should be in the axial direction of the nozzle (Škorpík, 2018; Sutton & Biblarz, 2010, p. 8, p. 76).

Laval nozzles producing parallel and uniform flow are employed at some supersonic and hypersonic vehicles and wind tunnels, and there are some main types (El-Sayed, 2016, p.689): Ideal, Linear (cone), Bell, Annular. This thesis will treat with the ideal type without considering the boundary-layer formation.

Subsonic Converging Contour

It concerns the converging nozzle section between the chamber and the transonic nozzle section. This part is not critical in achieving high performance. The subsonic flow in this section can easily be turned at a very low-pressure drop. Any radius, cone angle, wall contour curve, or nozzle inlet shape is usually satisfactory, although an ideal contour should be smooth (Sutton & Biblarz, 2010, p.76). For that reason, the formula proposed by S. Vitoshinsky in the early twentieth century will be used to generate a contour of this part of the nozzle. Such a profile is useful for nozzles connecting two pipes of different diameters and is used in the design of subsonic and supersonic nozzles where it requires having a smoothly narrowing shape that approximates the distribution of speeds in exit section to uniform (Deych, 1961, p.297).

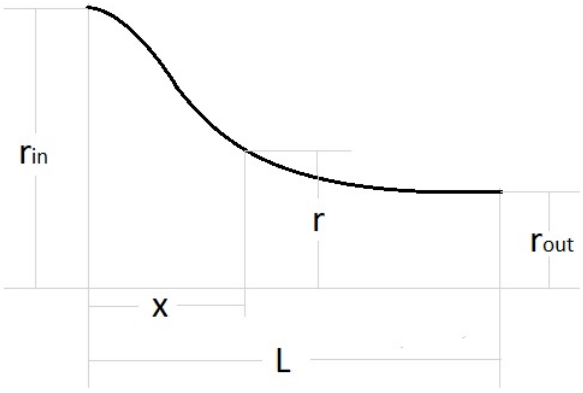

Figure 6.. Parameters for the Vitoshinsky formula.

$$r = \frac{r_{out}}{\sqrt{1 - \left[1 - \left(\frac{r_{out}}{r_{in}}\right)^2\right] \frac{\left(1 - \frac{x^2}{L^2}\right)^2}{\left(1 + \frac{x^2}{3L^2}\right)^3}}} \tag{2.22}$$

Vitoshinsky's studies deal with the aerodynamics of aircraft, while contractions must create flow with the least boundary layer at the exit. Nozzles (contractions) based on the Vitoshinsky equation have been studied at the VNIIM (Mendeleev All-Russia Research Institute of Metrology), starting in 1970 (Gutkin & Chistyakov, 2013).

In general, because of the multidimensionality of the converging subsonic flow, the sonic line is gently curved. However, for most applications, one-dimensional flow can be assumed in this part of the nozzle.

Transonic Contour

The analysis of the flowfield in the throat portion of the nozzle is, in most cases, the key to the design problem, because the location of the sonic line and the flow conditions on it are required in order to initiate the supersonic design (Ishii, 2014).

A significant source of error in determining the properties of the flow field in the diverging portion of the nozzle may be attributed to the approximations employed for determining the properties of the flow field in the neighborhood of the throat of the nozzle.

The determination of the flow pattern in the throat region of a two-dimensional CD nozzle under chocked flow conditions may be accomplished by applying small perturbation techniques to the equations governing choked flow. Small perturbation techniques are meritorious because they make it possible to obtain practical and useful results for a somewhat tricky flow problem (Zucrow & Hoffman Joe, 1977, p.95).

Figure 7 shows that the contour is axially symmetric concerning the x-axis, and the fluid flows in its positive direction. Also, it shows the sonic line (the locus

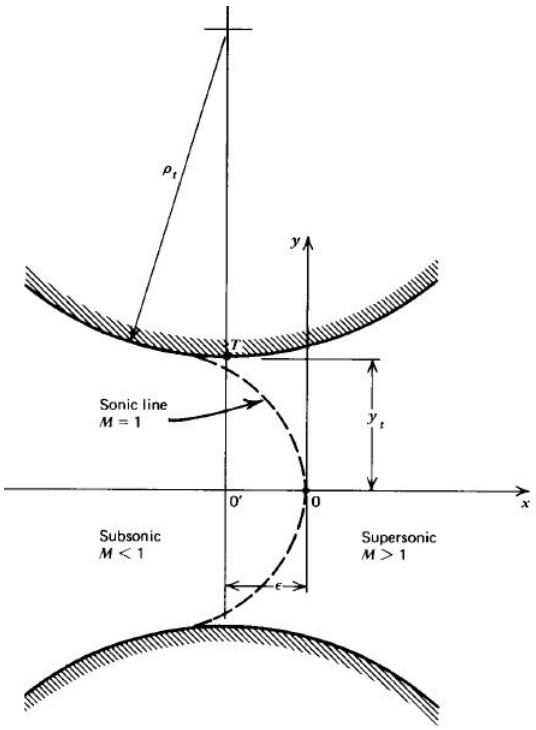

Figure 7.. General features of the throat region

Source: Zucrow and Hoffman Joe (1977) at *Gas Dynamics. Volume 2.*

of all of the points where the flow Mach number $M = 1$) as a parabola and it starts from the wall (in reality with the edge of the boundary layer) at a point slightly upstream from the throat and proceeds downstream until crosses the centerline at a point 0. This point represents the origin of the Sauer method plane. ϵ represents a distant of how far it is from the cartesian plane.

For designing the transonic part of the nozzle, this thesis will use the Sauer method. Nowadays, there are different methods and more accurate such as Hall, Kleigel, and Cline's methods. However, for the dimensionless ratio of $\rho_{up}/y_t \geq 2$ (Zucrow & Hoffman Joe, 1977, p.112), Sauer analysis yields consistent results that tends to approach for a one-dimensional and uniform flow and have similar results to others analysis and the available experimental data. Also, the analysis of Sauer is the most straightforward.

With Sauer method the sonic line is obtained, but to initiate a solution for the two-dimensional axisymmetric supersonic flow field by the method of

characteristics it is necessary to have an initial-value line that is in the range of influence of downstream the throat, and the sonic line is unsuitable because it begins upstream from the throat region (Zucrow & Hoffman Joe, 1977, p.102). Therefore, the line where $v = 0$ (velocity in the y direction) might be employed as it is shown in figure 8.

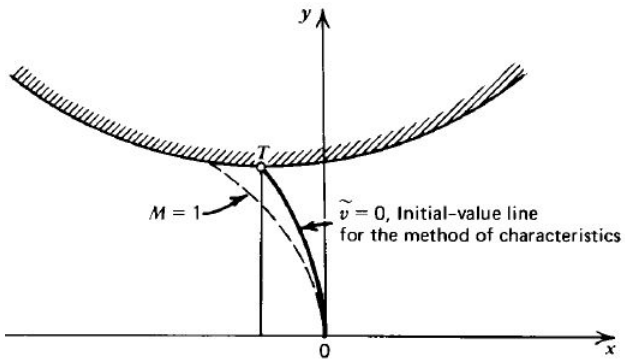

Figure 8.. Sonic line and initial-value line

Source: Zucrow and Hoffman Joe (1977) at *Gas Dynamics. Volume 2.*

This line begins in the throat and intersects the axis at the same point as the sonic line. Also, the flow velocity is parallel to the wall. Hence, the line satisfies the solid wall boundary condition exactly.

Supersonic Diverging Contour

The ideal contour of the diverging section of de Laval nozzle is designed by the method of characteristics through construction expansion waves inside the nozzle. This nozzle produces primarily axial exit of the gas flow, and its velocity field is the most uniform (Škorpík, 2018, p.8). The ideal nozzle embodies an expansion section from the sonic throat followed by an overturning or straightening section, which turns the flow of given Mach number without introducing compressive disturbance; it merely eliminates further expansion and guides the gas toward axial flow (DILLAWAY, 1957).

The length of the ideal contour of the nozzle is longer than any other contour, therefore has lower internal efficiency due to internal friction of the working gas.

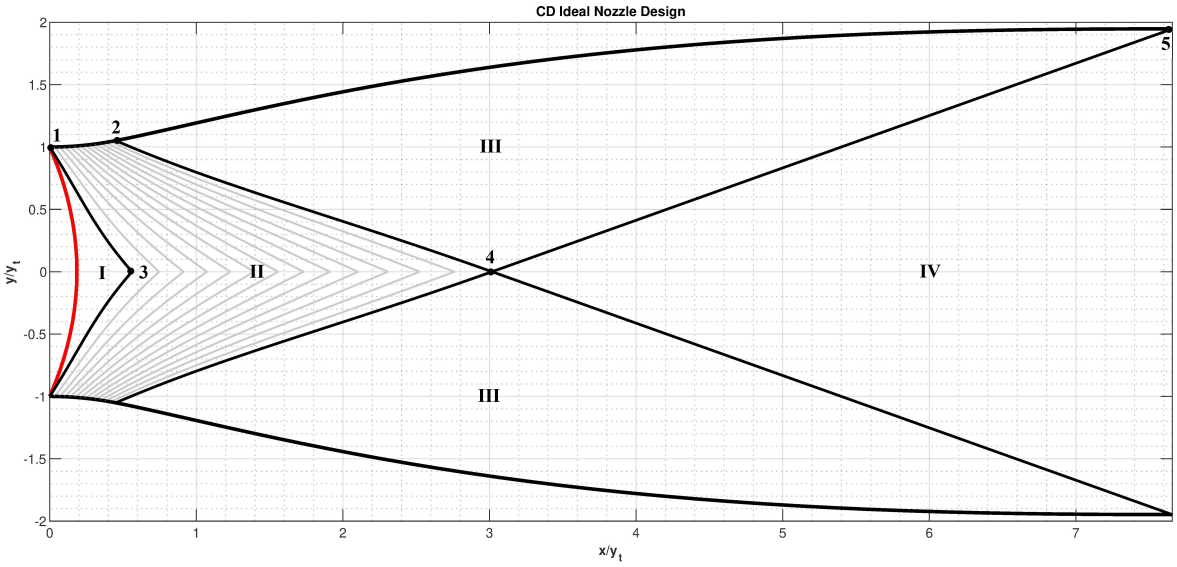

Figure 9.. Diverging supersonic nozzle contour by the MoC

If the nozzle contour is not proper, shock waves may occur inside the duct and will act as a supersonic diffuser. The MoC provides a technique for adequately designing the contour of a supersonic nozzle for shock-free, isentropic flow, considering the multidimensional flow inside the duct (John D. Anderson, 2003).

The aerodynamic design of wind-tunnel nozzles has evolved from the two-dimensional type used for supersonic testing to the axisymmetric type as the test Mach number has increased into the hypersonic regime (SIVELLS, 1970). There are analytical methods of design of contour diverging nozzle, where a polynomial approximates the contour of the nozzle.

The design of this part with de MoC is divided into some other parts specified in the figure. First, the subsonic and transonic design must already be done. The red line represents the initial-value line that is found by applying the condition of $v = 0$ in the analysis of Sauer. Then, it comes the part I between the sonic line and the line 1-3, which represents the extent of the initial-value line. After, the boundary value problem is analyzed, which represents the expansion of the upstream radius. Thus, the initial expansion is wholly determined and is called the kernel that comprises the area between points 1, 2, 3, and 4. A kernel means the central or most important part of something; this is because this part of the nozzle

makes the expansion of the gas and in the last point of the kernel, denoted by 4, the Mach number of design is established and specified. After this point is encountered, all the characteristics must be straight lines at the Mach angle of design α_D. Thus, a straight line making this angle is extended from point 4 until the exit point of the nozzle 5. The exit point of the nozzle is found by applying the continuity law to this line, i.e., a mass balance where all the mass that crosses the line 4-5 is the same amount of mass that enters through the initial-value line. The III zone is the straightening section, which turns the flow axially without creating disturbances. Finally, part IV represents the uniform flow that exits the nozzle.

All of these complicate designs will be explained with thorough detail in chapter 4, specifically, in the methodology section.

3. Framework

3.1 Method of Characteristics for Supersonic Flow

The Method of Characteristics (MoC) is essentially a numerical technique for the solution of completely supersonic, steady, and limited to inviscid flows.

Mathematically, the MoC as applied to the inviscid flow equations is a branch of absolute differential calculus, in which a system of partial differential equations (which apply to field variables in a given domain) can be reduced to one of the total differential equations or even algebraic equations that are valid along the characteristic curves (which represent the path of propagation of disturbances in such flows) (Haddad, 1988; R. J. Hartfield & Burkhalter, 2015).

The partial differential equations of motion, such as those governing irrotational supersonic flow in two dimensions and axisymmetric situations, fall into a class that the mathematician calls the elliptic type for subsonic flow, and into the hyperbolic type for supersonic flow (Rotty, 2008). The discussion here will be centered on the technique of the solution of the hyperbolic type. Solutions of hyperbolic partial differential equations may be found in terms of loci, "characteristics," on which the continuous functions of the flow properties may have discontinuous or indeterminate derivatives. The principle of characteristics involves finding directions along which the derivatives of continuous functions may be discontinuous and on which ordinary differential equations can be written (Prince, David C., 1982).

The classical foundation of the method of characteristics in the nozzle design is to achieve well-designed nozzles minimizing the loss associated with the geometric effect of the diverging zone. i.e., for shock-free nozzles, the primary loss in the high-speed, diverging section is related to the fact that for all practical nozzles, there is a non-axial component to the flow velocity at the exit plane of the nozzle. It also involves the calculation of flowfield properties at discrete points in the flow and

is predicated on the ability to expand the flowfield properties in terms of Taylor's series. Unlike traditional finite differencing schemes, this approach allows for the determination of the wall angles necessary for shock-free nozzle flow directly from the flow solution. In the theoretical limit of an infinite number of grid points (i.e., Δ_x and $\Delta_y \to 0$), the solutions are exact (John D. Anderson, 2003). If the supersonic flow properties are known at two points in a flow field, there is a third point where one and only one set of properties compatible with these. This point is determined by the intersection of characteristics, or waves, from the two original points. Usually, but not necessarily, the third point is downstream of the line between the first two (Prince, David C., 1982). These features make the method of characteristics particularly useful for nozzle design.

NOTE: For reading about the history of the method of characteristics, read the appendix A.5. Also, to check the derivation of the MoC, read the appendix B.1.

In summary, from the derivation of the MoC, two equations are given, the the first equation is the characteristic equation and gives the slope of the characteristic line, and the second equation is the compatibility equation and relates the position and the velocities.

$$\left(\frac{dy}{dx}\right)_{char} = \tan(\theta \mp \mu) \tag{3.1}$$

$$\left(\frac{d\varphi_x}{d\varphi_y}\right)_{char} = \tan(\theta \pm \mu) + \frac{\sigma \frac{v}{y}}{\left(1 - \frac{u^2}{a^2}\right)} \frac{dx}{d\varphi_y} \tag{3.2}$$

3.1.1 Discretization and Numerical Integration of the MoC

The characteristic and compatibility equations were derived for a steady two-dimensional axisymmetric irrotational supersonic flow. The discretization and integration of the MoC are generally done by using finite-differences as the equations 3.1 and 3.2 are nonlinear total differential equations. The method used within finite differences techniques is the Modified Euler predictor-corrector.

NOTE: For a better understanding of the Euler predictor-corrector method, read appendix B.2.

According to the numerical Euler method, the finite difference equations are obtained from the differential equations by replacing the total differentials by deltas such as $dx \to \Delta_x$. Thus, from equation 3.1 and **??**:

$$\frac{dy}{dx} = \tan(\theta \mp \mu) = \lambda_\pm$$

$$\Delta y_\pm = \Delta x_\pm \lambda_\pm$$

$$d\varphi_x = \left(\lambda_\pm - \frac{-2\varphi_x\varphi_y}{(c^2-\varphi_x^2)}\right) d\varphi_y + \frac{-\sigma\frac{\varphi_y}{y}}{(c^2-\varphi_x^2)} dx = 0$$

$$\left(u^2-c^2\right) du_\pm - \left[\left(u^2-c^2\right)\lambda_\pm - 2uv\right] dv_\pm - \sigma\frac{v}{y}c^2 dx_\pm = 0$$

$$\left(u^2-c^2\right) \Delta u_\pm - \left[\left(u^2-c^2\right)\lambda_\pm - 2uv\right] \Delta v_\pm - \sigma\frac{v}{y}c^2 \Delta x_\pm = 0$$

$$\left(u^2-c^2\right) \Delta u_\pm + \left[2uv - \left(u^2-c^2\right)\lambda_\pm\right] \Delta v_\pm - \sigma\frac{v}{y}c^2 \Delta x_\pm = 0$$

$$Q_\pm \Delta u_\pm + R_\pm \Delta v_\pm - S_\pm \Delta x_\pm = 0$$

In summary, it was obtained the differential equations:

$$\Delta y_\pm = \Delta x_\pm \lambda_\pm \tag{3.3}$$

$$Q_\pm \Delta u_\pm + R_\pm \Delta v_\pm - S_\pm \Delta x_\pm = 0 \tag{3.4}$$

$$Q_\pm = \left(u^2-c^2\right) \tag{3.5}$$

$$R_\pm = \left[2uv - \left(u^2-c^2\right)\lambda_\pm\right] \tag{3.6}$$

$$S_\pm = \sigma\frac{v}{y}c^2 \tag{3.7}$$

For computing these equations and apply the complete numerical integration procedure, two initial points in a supersonic flow field have to be known in conjunction with its properties. Then, there is a third point (the solution point) where only one set of properties are compatible with these. This point is determined by the intersection of characteristics, from the two original points. Generally, the third point is downstream of the line between the first two.

As a result, the coefficients Q, R, and S are then determined at the initial points for the predictor and in an average manner for the corrector for the left and right running characteristic lines.

3.2 Sauer Analysis for Transonic Flow through Nozzles

The analysis of Sauer (1947) is a methodology to determine the flow pattern at near-critical speeds in a nozzle, i.e., at the throat under flow-choked conditions. The application of any method to characterize the flow at this point is necessary as its avoiding is one of the significant sources of error in supersonic nozzle design.

In summary, the necessary equations to design the transonic contour with y_t and ρ_{up} in the Sauer reference frame are:

$$\epsilon = -\frac{(\gamma+1)\alpha}{2(3+\sigma)}y_t^2 \qquad (Origin\ of\ the\ Sauer\ reference\ frame)$$

$$\alpha = \sqrt{\frac{1+\sigma}{(\gamma+1)y_t\rho_{up}}} \qquad (Coefficient\ of\ the\ linear\ axial\ perturbation\ velocity)$$

$$u_a = \alpha x + \frac{(\gamma+1)\alpha^2}{2(1+\sigma)}y^2 \qquad (Nondimensional\ perturbation\ velocity)$$

$$v_a = \frac{(\gamma+1)\alpha^2}{(1+\sigma)}xy + \frac{(\gamma+1)^2\alpha^3}{2(3+\sigma)(1+\sigma)}y^3 \qquad (Nondimensional\ perturbation\ velocity)$$

$$u = c^*(1+u_a); \qquad v = c^*v_a \qquad (Dimensional\ velocities)$$

$$x_{sonic} = -\frac{(\gamma+1)\alpha}{2(1+\sigma)}y^2 \qquad (Critical\ curve)$$

$$x_{Cartesian} = x_{sonic} - \epsilon \qquad (Critical\ curve\ Cartesian\ reference\ frame)$$

$$x_{IV} = -\frac{(\gamma+1)\alpha}{2(3+\sigma)}y^2 \qquad (Initial-value\ line\ for\ the\ MoC)$$

NOTE: The geometrical variables are depicted in figure 7. For seeing how to derive the method of Sauer, read appendix B.2.

4. Methodological Design

In this chapter, an example of a nozzle design will be carried out in order to use all the concepts mentioned before and to create a step by step process or algorithm representing it into a flowchart. There are three levels of the flowchart, full color, yellow, and green represent the respective levels.

4.1 General Procedure

As it was already mentioned, the design of a CD nozzle implies three sub-designs. A converging or subsonic design, a transonic design, and a diverging or supersonic design. Finally, these designs will merge into one to give the shape of the CD nozzle. For depicting the general procedure, the following steps will be developed.

Step one: have the necessary input data ready.

- Necessary input data
  - Gas properties
    - T_{0T}
    - p_{0T}
    - R
    - γ
    - M_D
  - Geometric data
    - ρ_{up}
    - ρ_{down}
    - y_t
    - δ
    - y_{cham}

Step two: proceed with the transonic design. Here, the critical properties, the sonic line, the initial-value line, and the transonic contour are obtained. Also, the two-dimensional data of the initial value line is stored.

Step three: starting from the results of the transonic design, specifically the sonic line, the subsonic or converging design is carried out. The subsonic, one-dimensional properties are calculated and stored, and its contour is obtained.

Step four: starting from the results of the transonic design, specifically the initial-value line, the supersonic or diverging design is carried out. The supersonic, one-dimensional, and two-dimensional properties are calculated and stored; the free-shock supersonic contour is obtained.

Step five: Merge the results to give the final shape to the CD nozzle and transfer the stored data into a database. There have to be two databases, one for the one-dimensional analysis and the other for the two-dimensional analysis.

Step six: Read the data of the database and transform it into a scaling data to present it as graphical results; this permits to analyze them easier.

Step seven: Validate that the exit has uniform flow by calculating the complete expansion of the gas within the nozzle until de exit.

Necessary procedures are required in every stage that will be explained in the upcoming sections and chapters. All the process is presented in a flowchart, and the specific methodology is presented with an example.

For summarizing the process, it is presented into a flowchart.

The rest of the methodology is developed following the design of a CD nozzle with the initial conditions:

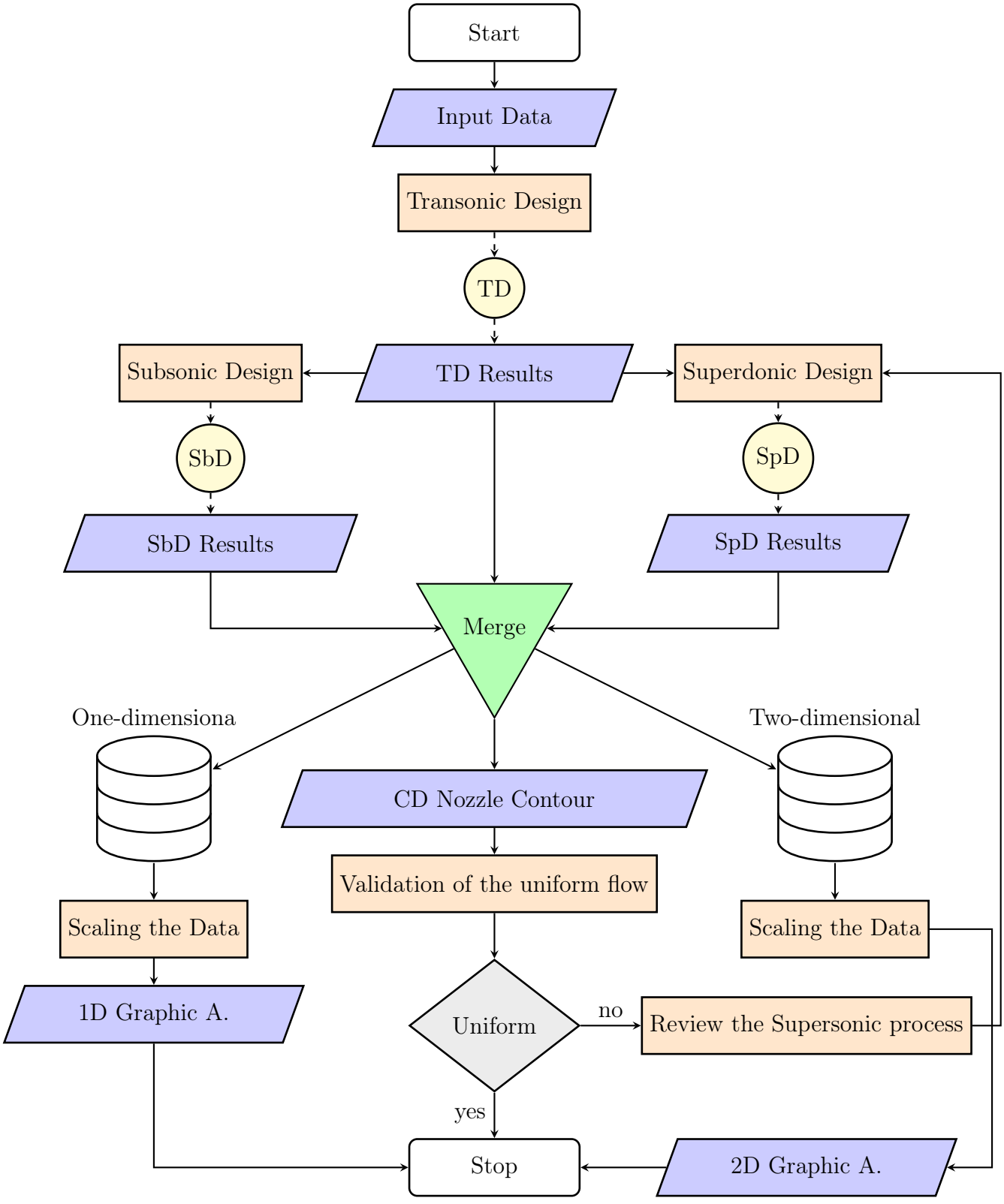

Figure 10.. General procedure flowchart

The rest of the methodology is developed following the design of a CD nozzle with the initial conditions:

$$\text{Gas properties} \begin{cases} T_{0t} = 3000[K] \\ p_{0t} = 70 * 10^5 \left[\frac{N}{m^2}\right] \\ R = 287.04 \left[\frac{J}{kg.K}\right] \\ \gamma = 1.2 \\ M_D = 2.5 \end{cases} \qquad \text{Geometric data} \begin{cases} \rho_{up} = 2[m] \\ \rho_{down} = 2[m] \\ y_t = 1[m] \\ \sigma = 1 \\ y_{cham} = 2[m] \end{cases}$$

These gas properties are typical for propulsive nozzles of rocket motors. Zucrow and Hoffman Joe (1977) and R. J. Hartfield and Burkhalter (2015) uses them in its computation. The radius of the throat was chosen in an illustrative way. The radius upstream of the throat was given taking a relation of $\rho_{up} \geq 2y_t$ and the radius downstream by taking into account a relationship between the radius of $\rho_{up}/\rho_{down} = 1$; this relation is of influence in the way that the gas is expanded.

4.2 Transonic design

As was mentioned, this is the design core since the supersonic and subsonic nozzle part depends on the results of the transonic section. For calculating this part, the Sauer analysis is used.

Step one: calculate the themodynamics critical properties. From the set of equations **??**:
For an ideal gas, from equation **??** and **??**:

$$\rho_{0T} = \frac{p_{0T}}{RT_{0T}} = \frac{70 * 10^5}{287.04 * 3000} = 8.12 \left[\frac{kg}{m^3}\right]$$

$$c_0 = \sqrt{\gamma RT} = \sqrt{1.2 * 287.04 * 3000} = 1016.5 \left[\frac{m}{s}\right]$$

Critical properties

$$T^* = \frac{2T_{0t}}{\gamma+1} = \frac{2*3000}{1.2+1} = 2727.3\ [K]$$

$$p^* = \frac{p_{0t}}{\left(\frac{\gamma+1}{2}\right)^{\frac{\gamma}{\gamma-1}}} = \frac{70*10^5}{\left(\frac{1.2+1}{2}\right)^{\frac{1.2}{1.2-1}}} = 39.5*10^5\ \left[\frac{N}{m^2}\right]$$

$$\rho^* = \frac{p^*}{RT^*} = \frac{39.5*10^5}{287.04*2727.3} = 5.05\ \left[\frac{kg}{m^3}\right]$$

$$c^* = \sqrt{\left(\frac{2}{\gamma+1}\right)c_{0t}^2} = \sqrt{\left(\frac{2}{1.2+1}\right)1016.5^2} = 969.23\ \left[\frac{m}{s}\right]$$

Step two: now, it is necessary to calculate the geometric Sauer parameters, its reference frame origin, and the coefficient of the linear axial perturbation velocity. From equation **??** y **??**:

$$\alpha = \sqrt{\frac{1+\sigma}{(\gamma+1)y_t\rho_{up}}} = \sqrt{\frac{1+1}{(1.2+1)*1*2}} = 0.6742\ [m^{-1}]$$

$$\epsilon = -\frac{(\gamma+1)\alpha}{2(3+\sigma)}y_t^2 = -\frac{(1.2+1)*0.6742}{2*(3+1)}*1^2 = -0.1854\ [m]$$

Step three: the geometry of the sonic line and the initial-value line are calculated. From equations **??** y **??**:

$$x_{sonic} = -\frac{(\gamma+1)\alpha}{2(1+\sigma)}y^2 = -\frac{(1.2+1)*0.6742}{2*(1+1)}y^2 = -0.37081y^2$$

$$x_{Initial} = -\frac{(\gamma+1)\alpha}{2(3+\sigma)}y^2 = -\frac{(1.2+1)*0.6742}{2*(3+1)}y^2 = -0.185405y^2$$

These formulae are the profile of the sonic line and the initial-value line that begins in the nozzle wall boundary and ends in the x-axis.

Step four: the two-dimensional data of the initial-value line is computed by giving an extra input parameter, N_{ponits}; this parameter means how many segments the initial-value line will be divided. The constant Mach lines mesh refinement depends upon this parameter. It can be even or odd, and of that depends on the numerical integration method applied on this line to compute the mass and the thrust. For this example:

$$N_{ponits} = 11$$

As the initial-value line analysis has to be two-dimensional in order to continue with the two-dimensional analysis in the diverging section, it is necessary to discretize the IV line.

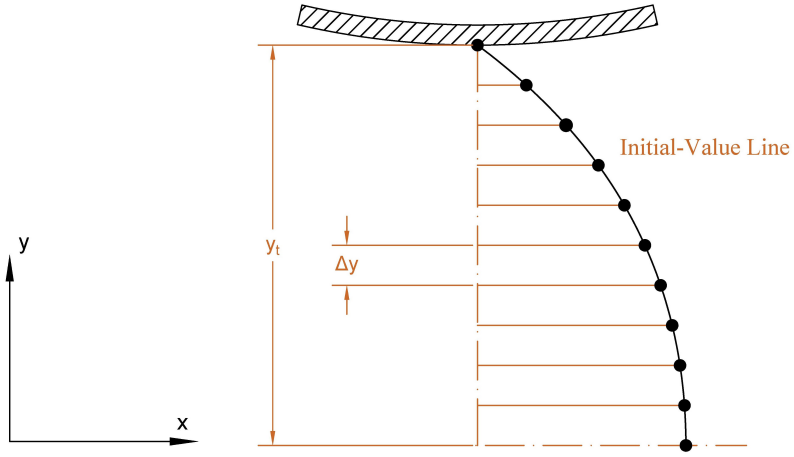

Figure 11.. Discretization of the initial-value line

Where Δy:

$$\Delta y = \frac{y_t}{N_{points} - 1} = \frac{1}{11 - 1} = 0.1$$

$$A_t = \pi y_t^2 = 3.1416 \; [m^2]$$

Once the geometry is discretized, it is necessary to compute the thermodynamics and flow field properties in every point. First, the location in the Sauer reference frame is found, and then, this location is expressed in the Cartesian coordinate system.

Example for the point $y = 0$:

$$x_{Initial}(y = 0) = -0.185405(0))^2 = 0$$

Now, in the Cartesian coordinate system:

$$x_{IV}(y = 0) = x_{Initial}(y = 0) - \epsilon = 0 - (-0.1854) = 0.1854 \; [m]$$

For calculating the dimensionless velocity, equations **??** y **??** are expressed in the Sauer reference frame. The Cartesian coordinate system is used just to see the solution from this point.

$$u_a = \alpha x + \frac{(\gamma+1)\alpha^2}{2(1+\sigma)}y^2 = (0)(0.6742) + \frac{(1.2+1)(0.6742)^2}{2(1+1)}(0)^2 = 0$$
$$v_a = \frac{(\gamma+1)\alpha^2}{(1+\sigma)}xy + \frac{(\gamma+1)^2\alpha^3}{2(3+\sigma)(1+\sigma)}y^3 = 0$$

The dimensional velocity as it was already mentioned in the derivation of the Sauer method:

$$u = c^*(1+u_a) = 969.23 * (1+0) = 969.23 \ \left[\frac{m}{s}\right]$$

Now, the local velocity of sound and the Mach number is given for equations **??** and **??**:

$$c = \sqrt{c_0^2 - \left(\frac{\gamma-1}{2}\right)u^2} = \sqrt{(1016.5)^2 - \left(\frac{1.2-1}{2}\right)969.23^2} = 969.2 \ \left[\frac{m}{s}\right]$$

$$M = \frac{V}{c} = \frac{u}{c} = \frac{969.23}{969.23} = 1$$

Once having either the Mach number or the velocity, the thermodynamic properties cam be computed. From the set of equation **??**:

$$T = \frac{T_0}{1+\left(\frac{\gamma-1}{2}\right)M^2} = \frac{3000}{1+\left(\frac{1.2-1}{2}\right)(1)^2} = 2727.3 \ [K]$$
$$p = \frac{p_0}{\left[1+\left(\frac{\gamma-1}{2}\right)M^2\right]^{\frac{\gamma}{\gamma-1}}} = \frac{70*10^5}{\left[1+\left(\frac{1.2-1}{2}\right)(1)^2\right]^{\frac{1.2}{1.2-1}}} = 39.513*10^5 \ \left[\frac{N}{m^2}\right]$$
$$\rho = \frac{p}{RT} = \frac{39.513*10^5}{287.04*2727.3} = 5.0474 \ \left[\frac{kg}{m^3}\right]$$

The mass rate of flow can be obtained by applying a numerical integration method over the extent of the initial-value line. The method to be used here is the Trapezoidal Rule, expressed as:

$$I = \sum_{i=2}^{n+1}(x_i - x_{i-1})\frac{[f(x_i) + f(x_{i-1})]}{2} \tag{4.1}$$

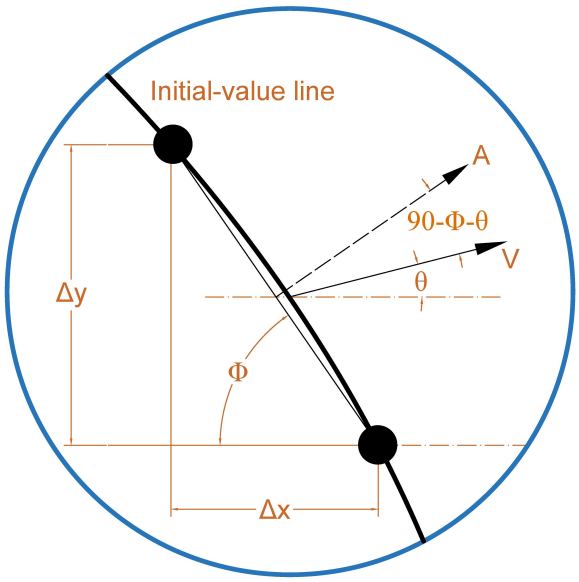

Figure 12.. Flow across an element of the control surface

To apply this formula, first, it is necessary to show graphically the parameter involved when the flow across an element of a control surface.
From the geometry:

$$\phi = \arctan\left(\frac{\Delta y}{\Delta x}\right)$$

If a ds represent the curve segment of the element of the control surface in the figure 12, then, a dA is represented by:

$$dA = 2\pi y ds$$

Where:

$$ds = \frac{dy}{\sin\phi}$$

Then, the amount of mass that pass through the control surface element, in the direction of the normal to the area, is:

$$\dot{dm_{element}} = \rho V dA cos(90 - \phi - \theta) = \rho V 2\pi y dy \frac{\sin(\phi - \theta)}{\sin\phi}$$

The total amount of mass across the initial-value line is:

$$\dot{m_{IV}} = \dot{m_{actual}} = \int_{IV} \rho V 2\pi y \frac{\sin(\phi - \theta)}{\sin\phi} dy \tag{4.2}$$

Now, the Trapezoidal Rule can be applied. From equation 4.1:

$$\dot{m_{actual}} = \sum_{i=2}^{N_{points}} \left(\frac{\Delta y}{2}\right)(2\pi)\left[\left(\rho V y \frac{\sin(\phi-\theta)}{\sin\phi}\right)_i + \left(\rho V y \frac{\sin(\phi-\theta)}{\sin\phi}\right)_{i-1}\right] \tag{4.3}$$

For calculating the gross thrust, the process made for calculating the mass is repeated. Calculate the function in an element of a control surface and integrating it over the total control surface. As it was mentioned, the thrust is sum of the pressure forces and the momentum flux. Then, for an element of control surface:

$$dF_g = 2\pi y p dy + V\dot{dm_{element}}$$

$$dF_g = 2\pi y p dy + V^2\rho 2\pi y dy \frac{\sin(\phi-\theta)}{\sin\phi}$$

$$dF_g = 2\pi y dy\left(p + V^2\rho\frac{\sin(\phi-\theta)}{\sin\phi}\right)$$

The total amount of gross thrust in the throat section is given by:

$$F_{IV} = F_{g-actual} = \int_{IV} 2\pi y\left(p + V^2\rho\frac{\sin(\phi-\theta)}{\sin\phi}\right)dy \tag{4.4}$$

Finally, applying the trapezoidal rule:

$$\dot{F_{g-actual}} = \sum_{i=2}^{N_{points}} \left(\frac{\Delta y}{2}\right)(2\pi)\left[\left(p + V^2\rho\frac{\sin(\phi-\theta)}{\sin\phi}\right)_i y_i + \left(p + V^2\rho\frac{\sin(\phi-\theta)}{\sin\phi}\right)_{i-1} y_{i-1}\right]$$

This process is repeated for every point over the initial-value line. The complete transonic design procedure is summarized in a flowchart, and the two-dimensional results are presented in a table. This table will only be shown for this line (IV line) as it represent a time consumption and is just illustrative.

Also, once the $\dot{m_{actual}}$ and the $F_{g-actual}$ is known, the ideal one-dimensional gross thrust and mass across the throat section can be computed, and with this data, the discharge coefficient C_D and the thrust coefficient C_{fg} can be calculated.

Table 1. 2D Thermodynamics and flow-field properties of the initial-value line

Thermodynamics and flow-field properties										
Position			**Flow-field**					**Thermodynamics**		
Point	$y\,[m]$	$x\,[m]$	$u\,\left[\frac{m}{s}\right]$	$v\,\left[\frac{m}{s}\right]$	M	$m\,\left[\frac{kg}{s}\right]$	$F_g * 10^5\,[N]$	$T\,[K]$	$p * 10^5\,\left[\frac{N}{m^2}\right]$	$\rho\,\left[\frac{kg}{m^3}\right]$
1	0	0.185	969.23	0	1	0	0	2727.27	39.51	5.05
2	0.1	0.184	970.44	0	1.0014	153.69	2.73	2726.59	39.45	5.04
3	0.2	0.178	974.08	0	1.0055	461.06	8.19	2724.54	39.28	5.02
4	0.3	0.169	980.13	0	1.0124	768.38	13.65	2721.10	38.98	4.99
5	0.4	0.156	988.61	0	1.0221	1075.50	19.11	2716.25	38.56	4.95
6	0.5	0.139	999.52	0	1.0345	1382.12	24.57	2709.96	38.03	4.89
7	0.6	0.119	1012.84	0	1.0498	1687.74	30.01	2702.18	37.38	4.82
8	0.7	0.095	1028.59	0	1.0680	1991.56	35.44	2692.84	36.61	4.74
9	0.8	0.067	1046.77	0	1.0891	2292.47	40.83	2681.89	35.73	4.64
10	0.9	0.035	1067.36	0	1.1132	2589	46.18	2669.25	34.73	4.53
11	1	0	1090.38	0	1.1402	2879.24	51.46	2654.83	33.62	4.41

It is the process that is necessary to do with every point in order to know the complete flow-field and be able to analyze it. The highlighted row represents the first point that was calculated as an example.

Now that all the mass and thrust was computed over the IV line, equations 4.3 and 4.4:

$$m_{actual} = 15280.8 \left[\frac{kg}{s}\right]$$

$$F_{g-actual} = 2.72 * 10^7 \ [N]$$

Then, the one-dimensional rate of mass flow and the 1D gross thrust need to be calculate, to obtain the discharge and thrust coefficients.

$$m_{1D} = \rho(1) * u(1) * A_t = (5.05)(969.23)(3.1416) = 15369.04 \left[\frac{kg}{s}\right]$$

$$F_{g-1D} = p(1)*A_t+m_{1D}*u(1) = (39.51*10^5)(3.1416)+(15369.04)(969.23) = 2.73*10^7 \ [N]$$

And the coefficients:

$$C_D = \frac{m_{actual}}{m_{1D}} = \frac{15280.8}{15369.04} = 0.9943$$

$$C_{fg} = \frac{F_{g-actual}}{F_{g-1D}} = \frac{2.72 * 10^7}{2.73 * 10^7} = 0.9967$$

Finally, the last date that is necessary to know is the point where the sonic line touches the wall upstream of the throat; for this is necessary to solve a system of two equations, the first, the equation of the sonic line, and the second, the equation of the arc. From equation **??** in the Cartesian coordinate system:

$$x = -\frac{(\gamma + 1)\alpha}{2(1 + \sigma)} y^2 - \epsilon$$

$$x^2 + (y - 3)^2 = 2^2$$

Clearing for the negative part of x, the result is $x = -0.1923$ and $y = 1.0093$. At that point, the critical curve will touch the wall.

With these results, the transonic design is completed, and the solution can be plotted. Figure 13 shows the solution for the example mentioned. Also, this

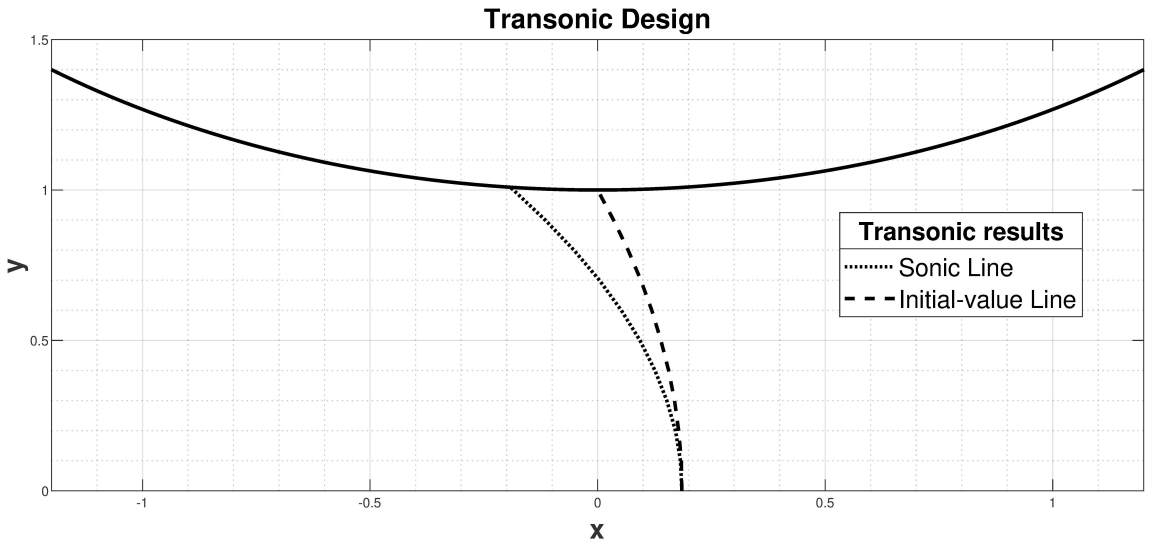

Figure 13.. Transonic design example

figure shows the difference between the sonic line and the initial-value line for a real example graphically.

For summarizing the process of the transonic design, a flowchart is presented following one by one the mentioned steps for carrying out a transonic design. The final results in the flowchart will converge with the mentioned results in the general procedure flowchart to give the shape to the complete nozzle.

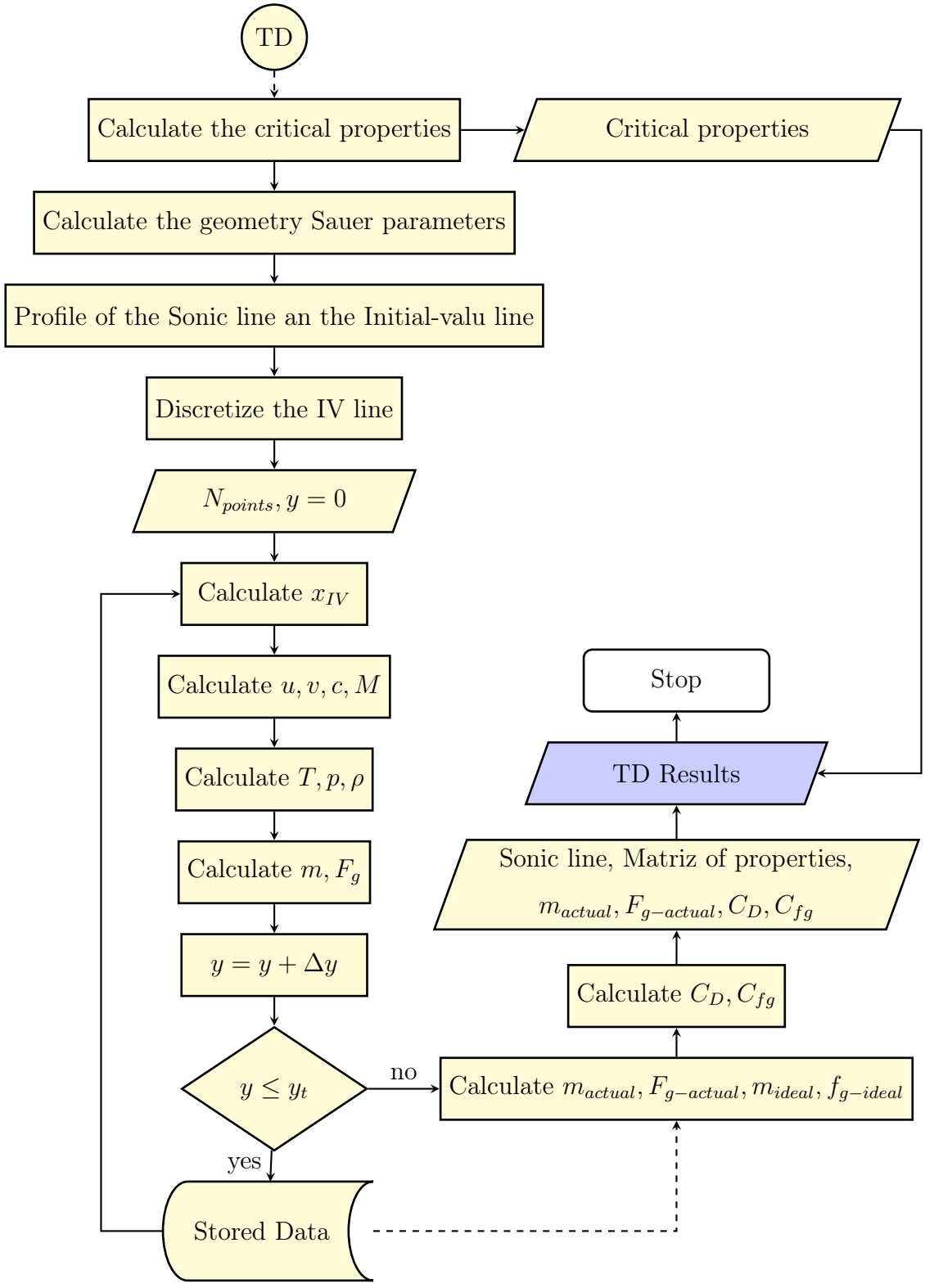

Figure 14.. Transonic design flowchart

4.3 Subsonic or converging design

This part of the nozzle is the most straightforward. Here, it is only needed the Vitoshinsky formula and the location where the sonic line touches the wall upstream of the throat.

Vitoshinsky Formula from equation 2.22

$$y = \frac{y_t}{\sqrt{1 - \left[1 - \left(\frac{y_t}{y_{cham}}\right)^2\right] \frac{\left(1 - \frac{x^2}{L^2}\right)^2}{\left(1 + \frac{x^2}{3L^2}\right)^3}}}$$

The parameters of the formula are illustrated in figure 6.

In order to apply this formula, extra data is necessary, and this extra data is the locus obtained from the transonic design where the critical curve touches the wall. Replacing this position in the Vitoshinsky formula will result in obtaining the total length of the converging part, and of course, a contour that will converge in the necessary point for developing the transonic flow. Then:

Step one: calculate the total length of the converging section by replacing in the Vitoshinsky formula the locus where the sonic line touch the wall.

$$1.0093 = \frac{1}{\sqrt{1 - \left[1 - \left(\frac{1}{2}\right)^2\right] \frac{\left(1 - \frac{(-0.1923)^2}{L^2}\right)^2}{\left(1 + \frac{(-0.1923)^2}{3L^2}\right)^3}}}$$

Solving for L:

$$L = 1.64\ [m]$$

Step two: replace L into the formula and divide the nozzle length in a desired number of elements. In this example, the length was divided into 100 equidistant elements. The reason for the division is to discretize the problem and be able to know the one-dimensional flow field over these 100 points.

$$\Delta x = \frac{L}{100}$$

Step three: calculate the location and the one-dimensional thermodynamics and flow-field properties of every one of the 100 points. The one-dimensional

computation is done by calculating the properties at the wall and take them as a constant through the y-axis.

NOTE: As henceforth, there will be lots of points, and hence lots of data, the data is obtained through a Matlab code and stored for its subsequent analysis.

The procedure is to calculate the position y from the Vitoshinsky formula for every value of x. Then, the area y calculated, and the equation **??** is used to calculate the Mach number.

$$A = \pi y^2$$

$$\frac{A(x)}{A_t} = \frac{1}{M(x)} \left[\frac{1 + \left(\frac{\gamma-1}{2}\right) M(x)^2}{1 + \left(\frac{\gamma-1}{2}\right)} \right]^{\frac{\gamma}{\gamma-1}}$$

There will be two solutions, as the equations are quadratic. One of them is subsonic, and another one is supersonic, it is necessary to get the subsonic solution.

Once the Mach number is obtained, the thermodynamic properties can be calculated with the isentropic equations expressed in terms of the Mach number.

From the set of equations **??**:

$$T = \frac{T_0}{1 + \left(\frac{\gamma-1}{2}\right) M^2} \, [K]$$

$$p = \frac{p_0}{\left[1 + \left(\frac{\gamma-1}{2}\right) M^2\right]^{\frac{\gamma}{\gamma-1}}} \, \left[\frac{N}{m^2}\right]$$

$$\rho = \frac{p}{RT} \, \left[\frac{kg}{m^3}\right]$$

Step four: graphic the converging contour and store the calculated data for its analysis.

The figure was plotted the Subsonic contour by the Vitoshinsky equation, and as mentioned before, this part is not critical in achieving high performance as the subsonic flow can easily be turned at a very low-pressure drop, i.e., any wall contour curve is usually satisfactory. However, this contour is smooth, and the exit flow is approximately uniform.

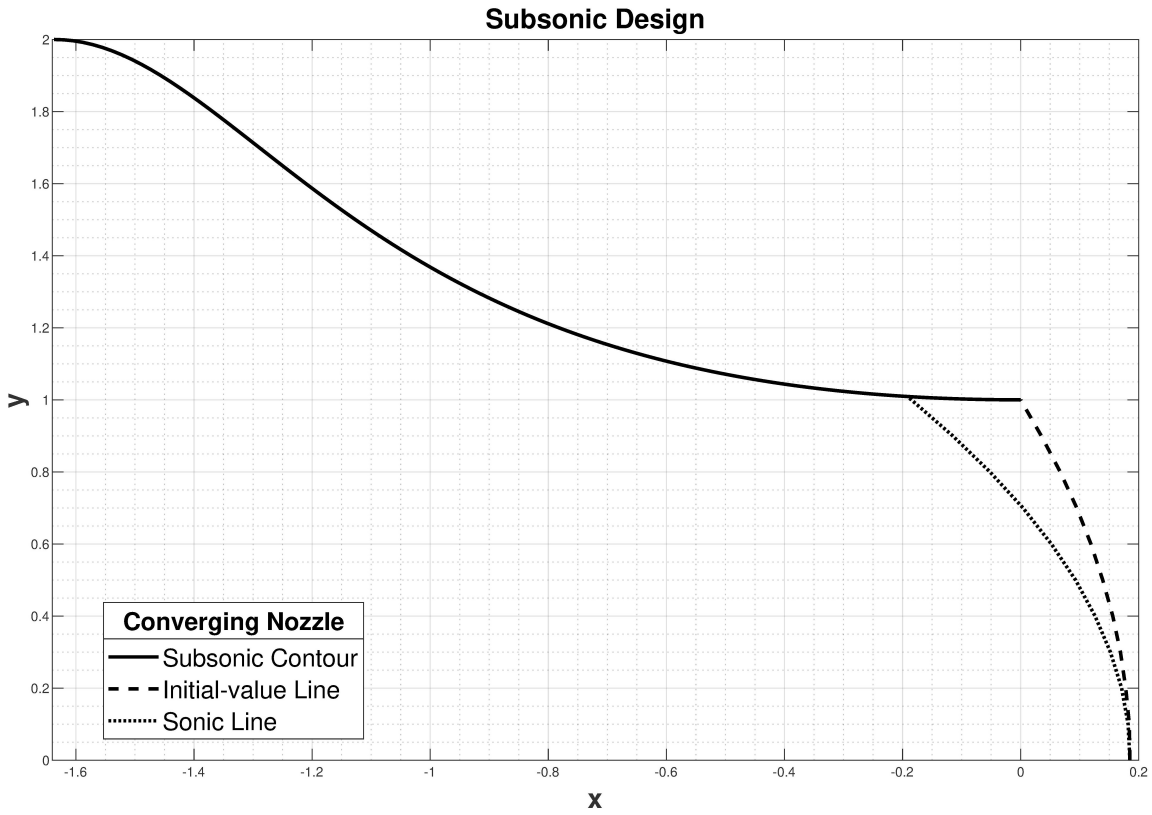

Figure 15.. Subsonic design of the example

The analysis was assumed to be one-dimensional because the behavior of the flow is almost constant in the y direction; the most famous line of flow is the sonic line, and this is already computed. The converging nozzle is mixed with the upstream transonic design, and the sonic and initial-value lines are showed to see how these interact with the contour.

The subsonic nozzle is achieved by obtaining its contour and its one-dimensional properties stored. After this, the process can be summarized graphically through a flowchart.

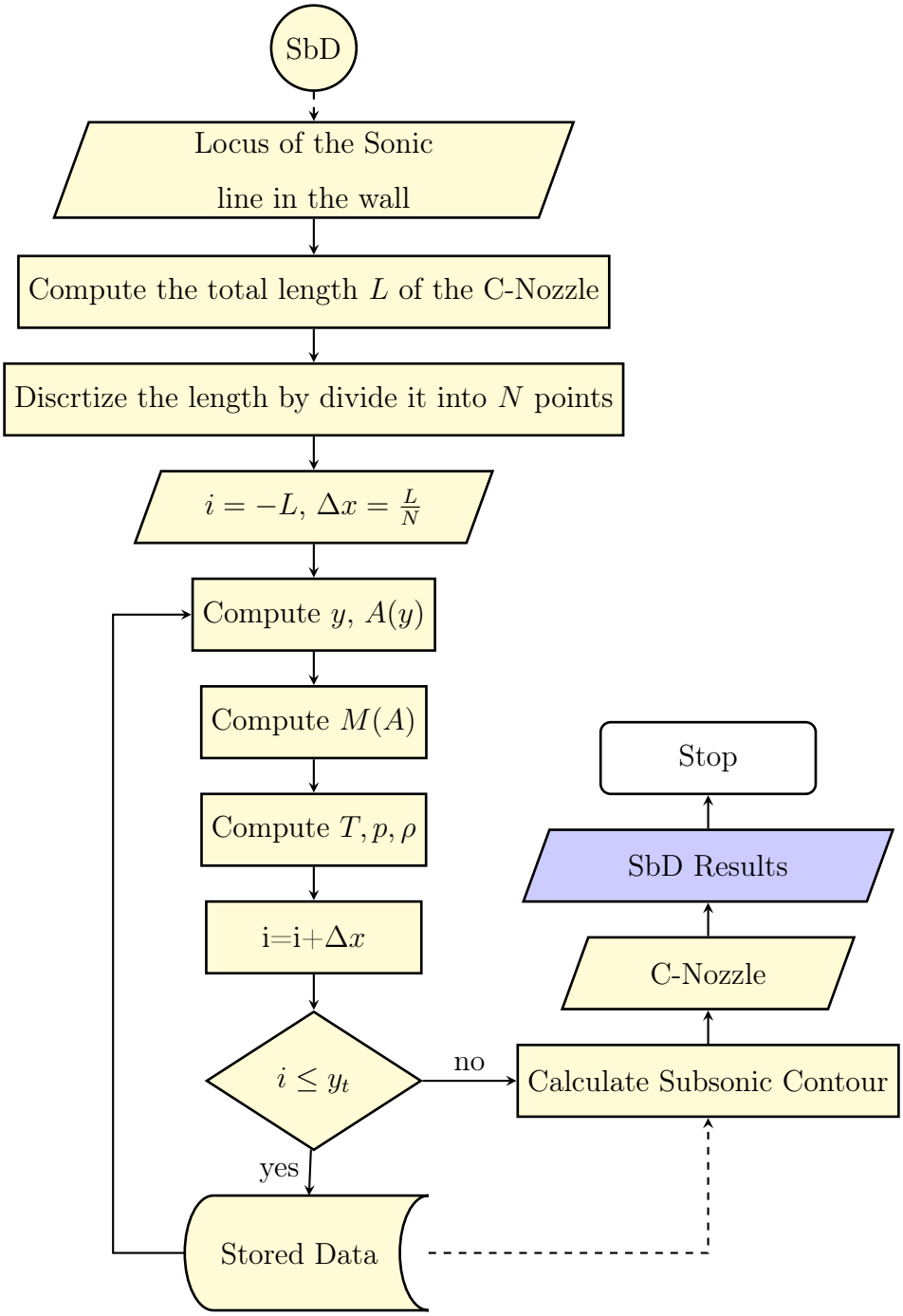

Figure 16.. Transonic design flowchart

4.4 Supersonic or diverging design

The Supersonic design is divided into four parts that converge to complete the supersonic nozzle. Every part of it contains its flowchart and its procedure. The general procedure of the supersonic design is described with a few steps, as it is shown in the flowchart.

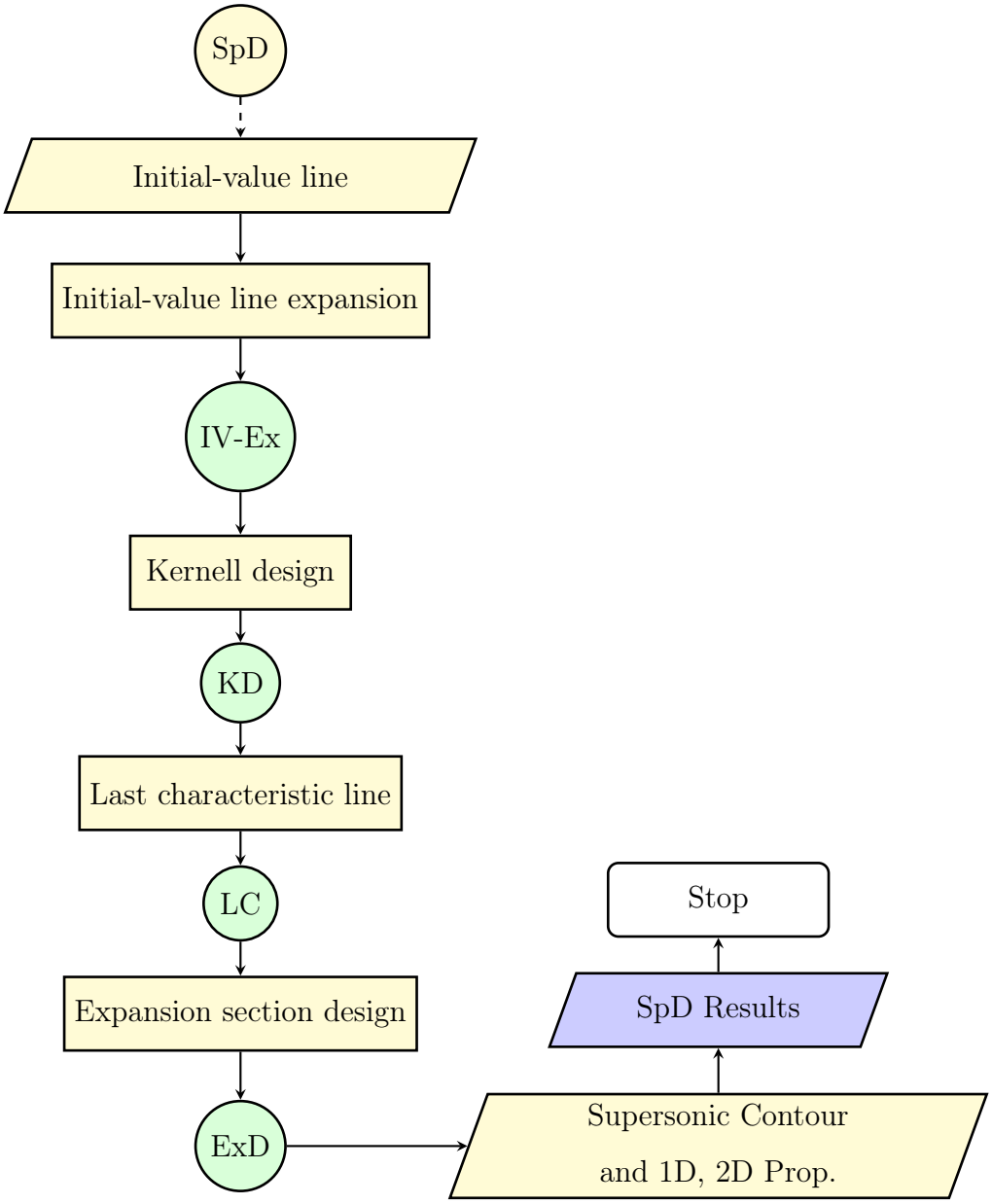

Figure 17.. General procedure of the supersonic design

4.4.1 Initial-value line expansion

Initiating the calculation of the downstream supersonic flow-field requires an initial-value line to be established that is everywhere supersonic; this line is the $v = 0$ line from the flow-field in the throat region.

The unit process of the MoC may then be applied to the flow downstream from the initial-value line. However, the unit process of the MoC has not been mentioned and explained.

Unit process of the MoC for the extent of the Initial-value line

Up to this point, it is already known that the IV line was divided into N_{points} through which in every point pass two characteristics lines, the left running characteristic C_+ and the right running characteristic C_-.

The application of the MoC can include several cases, though, for this specific part of the design, only two cases are necessary:

- Interior point (General case)
- Axis-symmetrical point

Figures 18 and 19 show graphically the two cases. For the first case, for two interior points, it was already mentioned that if the supersonic flow properties are known at these two points in a flow field, there is a third point where one and only one set of properties compatible with these. This point is determined by the intersection of a right-running and left-running characteristics that pass through the two original points.

In the second case, an axisymmetric flow, the x-axis is a line of symmetry, and the solution point (point 4) is located over the axis. Point 2 is a mirror image of point 1.

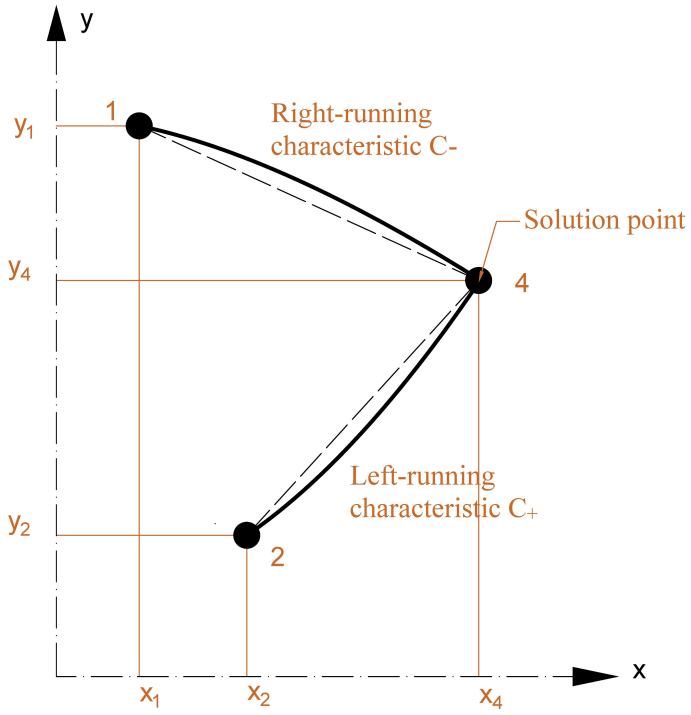

Figure 18.. Unit process of an interior point

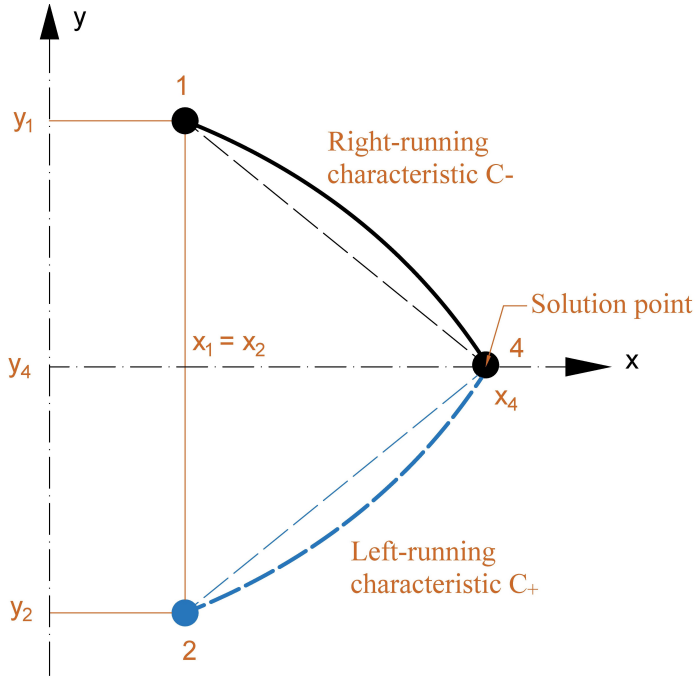

Figure 19.. Unit process of an axisymmectric point

The unit process of the Moc consists of applying the modified Euler predictor-corrector method to the discretized equations of the MoC, the set of equations 4.18 - 4.22. Examples of the Euler method applied to the cases presented are shown, and the procedure is summarized in a flowchart.

In general, as the Euler predictor-corrector method is a finite differential method for integrating total differential equations, the characteristics connecting two points of the grid, are replaced by the dashed straight lines.

For showing the procedure of integrating the total differential equations of the MoC, the initial-value line is located in the space, then, as it was divided in N_{pints}, the process for obtaining a solution for the first two points are carried out.

From the table 1 the initial data of the first two, points 1 and 2 (from figure 18) for a ***interior point*** are:

$$\text{Point 2} \begin{cases} x_2 = 0.185\ [m] \\ y_2 = 0\ [m] \\ u_2 = 969.23\ \left[\frac{m}{s}\right] \\ v_2 = 0\ \left[\frac{m}{s}\right] \end{cases} \qquad \text{Point 1} \begin{cases} x_1 = 0.184\ [m] \\ y_1 = 0.1\ [m] \\ u_1 = 970.44\ \left[\frac{m}{s}\right] \\ v_1 = 0\ \left[\frac{m}{s}\right] \end{cases}$$

NOTE: As it is seen in figure 18, the point 1 and 2 of the figure are interspersed.

For applying the Euler predictor-corrector method, from the discretized equations of the MoC, a new set of algebraic equations are obtained from the figures **??** and 18:

Equations from the figure **??**:

$$\begin{aligned} \theta_{\pm} &= \arctan\left(\frac{v_{\pm}^2}{u_{\pm}^2}\right) \\ \alpha_{\pm} &= \arcsin\left(\frac{a_{\pm}}{V_{\pm}}\right) \\ \lambda_{\pm} &= \tan\left(\theta_{\pm} \pm \alpha_{\pm}\right) \end{aligned} \tag{4.5}$$

Equations from the discretized equations of the MoC and the figure 18:

$$\begin{aligned} y_4 - \lambda_+ x_4 &= y_2 - \lambda_+ x_2 \\ y_4 - \lambda_- x_4 &= y_1 - \lambda_- x_1 \\ Q_+ u_4 + R_+ v_4 &= T_+ \\ Q_- u_4 + R_- v_4 &= T_- \\ T_+ &= S_+(x_4 - x_2) + Q_+ u_2 + R_+ v_2 \\ T_- &= S_-(x_4 - x_1) + Q_- u_1 + R_- v_1 \end{aligned} \tag{4.6}$$

Variables for the Euler predictor algorithm:

$$u_+ = u_2; \qquad v_+ = v_2 \qquad y_+ = y_2$$
$$u_- = u_1; \qquad v_- = v_1 \qquad y_- = y_1$$

Variables for the Euler corrector algorithm:

$$u_+ = \frac{u_2 + u_4}{2}; \qquad v_+ = \frac{v_2 + v_4}{2} \qquad y_+ = \frac{y_2 + y_4}{2}$$
$$u_- = \frac{u_1 + u_4}{2}; \qquad v_- = \frac{v_1 + v_4}{2} \qquad y_- = \frac{y_1 + y_4}{2}$$

The process is to calculate the slope of the running characteristic ($\lambda_\pm$); this represents the first equation of the MoC. For computing $\lambda_\pm$, the set of equations 4.5 are used.

Euler predictor algorithm

Positive Characteristic

$$V_+ = \sqrt{u_2^2 + v_2^2} = \sqrt{969.23^2 + 0^2} = 969.23 \ \left[\frac{m}{s}\right]$$
$$\theta_+ = \arctan\left(\frac{v_2^2}{u_2^2}\right) = \arctan\left(\frac{0^2}{969.23^2}\right) = 0$$
$$c_+ = \sqrt{c_0^2 - \frac{(\gamma - 1)}{2} V_+^2} = \sqrt{1016.5^2 - \frac{(1.2 - 1)}{2} * 963.23^2} = 969.23 \ \left[\frac{m}{s}\right]$$
$$\alpha_+ = \arcsin\left(\frac{c_+}{V_+}\right) = \arcsin\left(\frac{969.23}{969.23}\right) = 90^o$$
$$\lambda_+ = \tan\left(\theta_+ + \alpha_+\right) = \tan\left(0 + 90\right) = +\infty$$

Negative Characteristic

$$V_- = \sqrt{u_1^2 + v_1^2} = \sqrt{970.44^2 + 0^2} = 970.44 \ \left[\frac{m}{s}\right]$$
$$\theta_- = \arctan\left(\frac{v_1^2}{u_1^2}\right) = \arctan\left(\frac{0^2}{970.44^2}\right) = 0$$
$$c_- = \sqrt{c_0^2 - \frac{(\gamma-1)}{2}V_-^2} = \sqrt{1016.5^2 - \frac{(1.2-1)}{2} * 970.44^2} = 969.11 \ \left[\frac{m}{s}\right]$$
$$\alpha_- = \arcsin\left(\frac{c_-}{V_-}\right) = \arcsin\left(\frac{969.17}{970.44}\right) = 87^o$$
$$\lambda_- = \tan\left(\theta_- - \alpha_-\right) = \tan\left(0 - 87\right) = -19.08$$

Once having these data, the equations 4.6 can be used in order to obtain the location and the velocity of the solution point. Usually, there will be two systems of equations 2x2, one system for the position, and one for the velocities. However, there are three special cases for an interior point; two of them are when $\lambda_\pm = \pm\infty$, and the other is when $y = 0$. Some approximations need to be taken into account to avoid any discontinuity and error.

Next step in a normal process is to obtain the compatibility equations coefficients $Q_\pm, R_\pm$ and $S_\pm$. From equations 4.20 to 4.22:

Positive running characteristic:

$$Q_+ = \left(u_2^2 - c_+^2\right)$$
$$R_+ = \left[2u_2v_2 - \left(u_2^2 - c_+^2\right)\lambda_+\right]$$
$$S_+ = \sigma\frac{v_2}{y_2}c_+^2$$

Negative running characteristic:

$$Q_- = \left(u_1^2 - c_-^2\right)$$
$$R_- = \left[2u_1v_1 - \left(u_1^2 - c_-^2\right)\lambda_-\right]$$
$$S_- = \sigma\frac{v_1}{y_1}c_-^2$$

After this is done, the location of the solution point is obtained through solving the following system of equations:

$$y_4 - \lambda_+x_4 = y_2 - \lambda_+x_2$$
$$y_4 - \lambda_-x_4 = y_1 - \lambda_-x_1$$

Once the location is got, the $T_{\pm}$ coefficients are computed:

$$T_+ = S_+(x_4 - x_2) + Q_+u_2 + R_+v_2$$

$$T_- = S_-(x_4 - x_1) + Q_-u_1 + R_-v_1$$

The last step of the predictor algorithm in a normal process is to solve the system of equations for getting the velocities of the solution point:

$$Q_+u_4 + R_+v_4 = T_+$$

$$Q_-u_4 + R_-v_4 = T_-$$

However, this example is an special case because it fulfilled that $\lambda_+ = \infty$ and $y_2 = 0$. Then, as mentioned before, some approximations need to be taken in order to avoid discontinuities.

When $y_2 = 0$, the coefficient S_+ are calculated replacing $y_2 = y_1$ and $v_2 = v_1$, then:

$$S_+ = \sigma\frac{v_2}{y_1}c_+^2 = \sigma\frac{v_1}{y_1}c_+^2$$

If $\lambda_+ = \infty$, there is not necessity to calculate Q_+, R_+, S_+ and T_+, as x_4 and u_4 are set equal to x_2 and u_2 respectively.

Thus, for the example:

$$Q_- = \left(u_1^2 - c_-^2\right) = (970.44^2 - 969.11^2) = 2579.6 \left[\frac{m^2}{s^2}\right]$$

$$R_- = [2u_1v_1 - Q_-\lambda_-] = [2(970.44)(0) - (2579.6)(-19.08)] = 49222 \left[\frac{m^2}{s^2}\right]$$

$$S_- = \sigma\frac{v_1}{y_1}c_-^2 = (1)\left(\frac{0}{0.1}\right)969.11^2 = 0$$

From the approximation when $\lambda_+ = \infty$:

$$x_4 = x_2 = 0.185[m]$$

$$u_4 = u_2 = 969.23 \left[\frac{m}{s}\right]$$

The location of the solution point is given by:

$$y_4 - (-19.08)(0.185) = 0.1 - (-19.08)(0.184)$$

$$y_4 = 0.080919\ [m]$$

The T_- coefficient is giving by:

$$T_- = S_-(x_4 - x_1) + Q_- u_1 + R_- v_1$$
$$= (0)(0.185 - 0.184) + (2579.6)(970.44) + (49222)(0) = 2.5033 * 10^6 \left[\frac{m^3}{s^3}\right]$$

Finally, the velocity is defined by:

$$Q_- u_4 + R_- v_4 = T_-$$
$$(2579.6)(969.23) + (49222)(v_4) = 2.5033 * 10^6$$
$$v_4 = 0.063413 \left[\frac{m}{s}\right]$$

Although the results would seem to deviate from the real solution because of the taken approximations, the Euler corrector algorithm will correct this error.

Euler corrector algorithm

Variables for the Euler corrector algorithm:

$$u_{1*} = \frac{u_1 + u_4}{2} = \frac{970.44 + 969.23}{2} = 969.835 \left[\frac{m}{s}\right]$$
$$v_{1*} = \frac{v_1 + v_4}{2} = \frac{0 + 0.063413}{2} = 0.0317 \left[\frac{m}{s}\right]$$
$$y_{1*} = \frac{y_1 + y_4}{2} = \frac{0.1 + 0.080919}{2} = 0.0905 \, [m]$$

With these new variables, all the process is repeated for the angles, and the coefficients.

$$V_{-*} = \sqrt{u_{1*}^2 + v_{1*}^2} = 969.84 \ \left[\frac{m}{s}\right]$$
$$\theta_{-*} = \arctan\left(\frac{v_{1*}^2}{u_{1*}^2}\right) = 0.002^o$$
$$c_{-*} = \sqrt{c_0^2 - \frac{(\gamma-1)}{2}V_{-*}^2} = 969.17 \ \left[\frac{m}{s}\right]$$
$$\alpha_{-*} = \arcsin\left(\frac{c_{-*}}{V_{-*}}\right) = 87.87^o$$
$$\lambda_{-*} = \tan\left(\theta_{-*} - \alpha_{-*}\right) = -26.86$$
$$Q_{-*} = \left(u_{1*}^2 - c_{-*}^2\right) = 1289.4 \ \left[\frac{m^2}{s^2}\right]$$
$$R_{-*} = \left[2u_{1*}v_{1*} - Q_{-*}\lambda_{-*}\right] = 34698 \ \left[\frac{m^2}{s^2}\right]$$
$$S_{-*} = \sigma\frac{v_{1*}}{y_{1*}}c_{-*}^2 = 3.29 * 10^5 \ \left[\frac{m^2}{s^2}\right]$$

For the location:

$$y_4 - \lambda_{-*}x_4 = y_1 - \lambda_{-*}x_1$$
$$y_4 - (-26.86)(0.185) = 0.1 - (-26.86)(0.184)$$
$$y_4 = 0.073138 \ [m]$$

The T_{-*} coefficient:

$$T_{-*} = S_{-*}(x_4 - x_1) + Q_{-*}u_1 + R_{-*}v_1$$
$$= (3.29 * 10^5)(0.185 - 0.184) + (1289.4)(970.44) + (34698)(0) = 1.2517 * 10^6 \ \left[\frac{m^3}{s^3}\right]$$

Finally, the velocity:

$$Q_{-*}u_4 + R_{-*}v_4 = T_{-*}$$
$$(1289.4)(969.23) + (34698)(v_4) = 1.2517 * 10^6$$
$$v_4 = 0.054454 \ \left[\frac{m}{s}\right]$$

By applying the corrector a couple more times, a better accuracy can be obtained. That is called the *Modified Euler Predictor-Corrector Algorithm*. Since

the corrector works with iterations, a limit in the amount of iterations is necessary, this limitation is a tolerance between the results of the corrector. For distances, Zucrow and Hoffman Joe (1977) establish a tolerance of $|x_i - x_{i-1}| = T_1 = 0.1$ and $|y_i - y_{i-1}| = T_1 = 0.1$. For velocities, he establish a tolerance of $|u_i - u_{i-1}| = T_2 = 0.001$ and $|v_i - v_{i-1}| = T_2 = 0.001$.

For this specific example, results are presented in a table and graphically, and the procedure is showed in a flowchart.

Table 2. Modified Euler predictor-corrector results

Modified Euler predictor-corrector			
Variable	*Predictor*	$Corrector_1$	$Corrector_2$
λ_+	∞	∞	∞
λ_-	-19.08	-26.86	-26.86
$Q_+ \ [m^2/s^2]$	N/A	N/A	N/A
$R_+ \ [m^2/s^2]$	N/A	N/A	N/A
$S_+ \ [m^2/s^2]$	N/A	N/A	N/A
$T_+ \ [m^3/s^3]$	N/A	N/A	N/A
$Q_- \ [m^2/s^2]$	2579.60	1289.44	1289.44
$R_- \ [m^2/s^2]$	49221.73	34698.12	34689.43
$S_- \ [m^2/s^2]$	0	329228.33	295417.46
$T_- \ [m^3/s^3]$	$2.5 * 10^6$	$1.25 * 10^6$	$1.25 * 10^6$
$x_4 \ [m]$	0.185	0.185	0.185
$y_4 \ [m]$	0.0809	0.0731	0.0731
$u_4 \ [m/s]$	969.23	969.23	969.23
$v_4 \ [m/s]$	0.0634	0.0544	0.0534

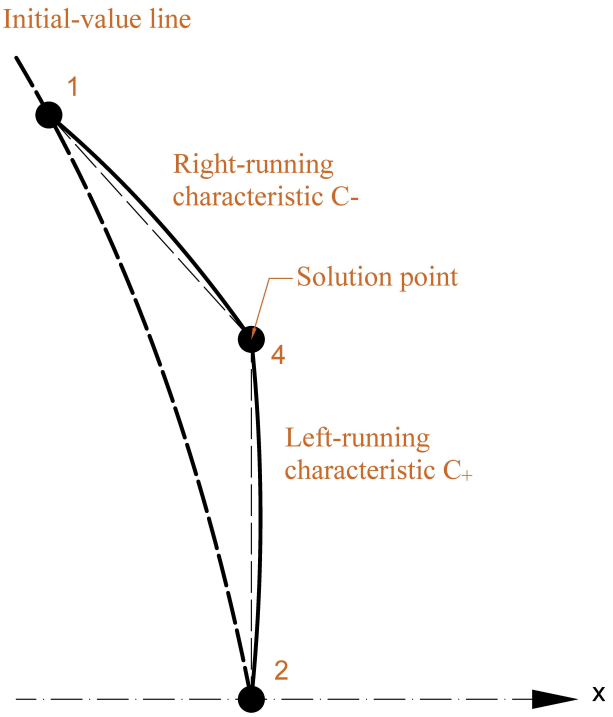

Figure 20.. The first interior point in the IV line

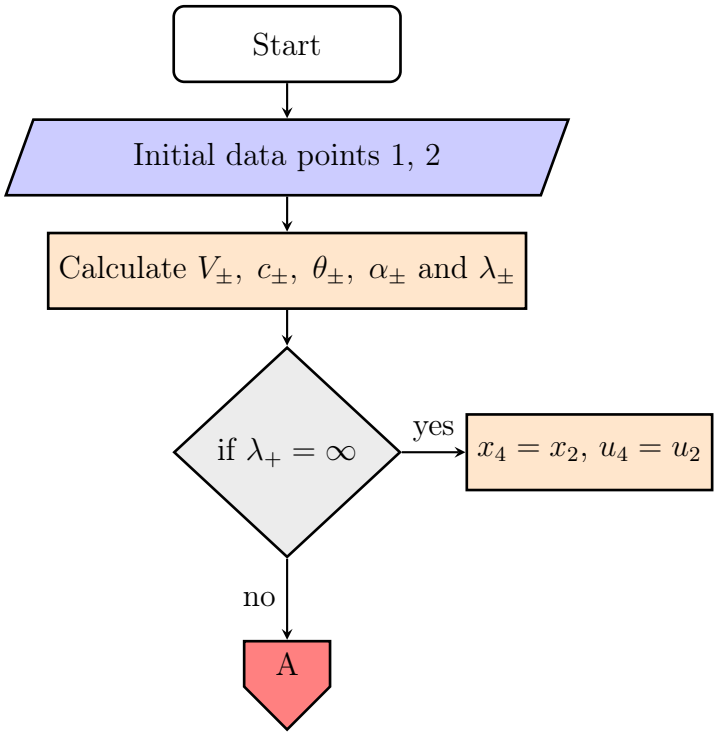

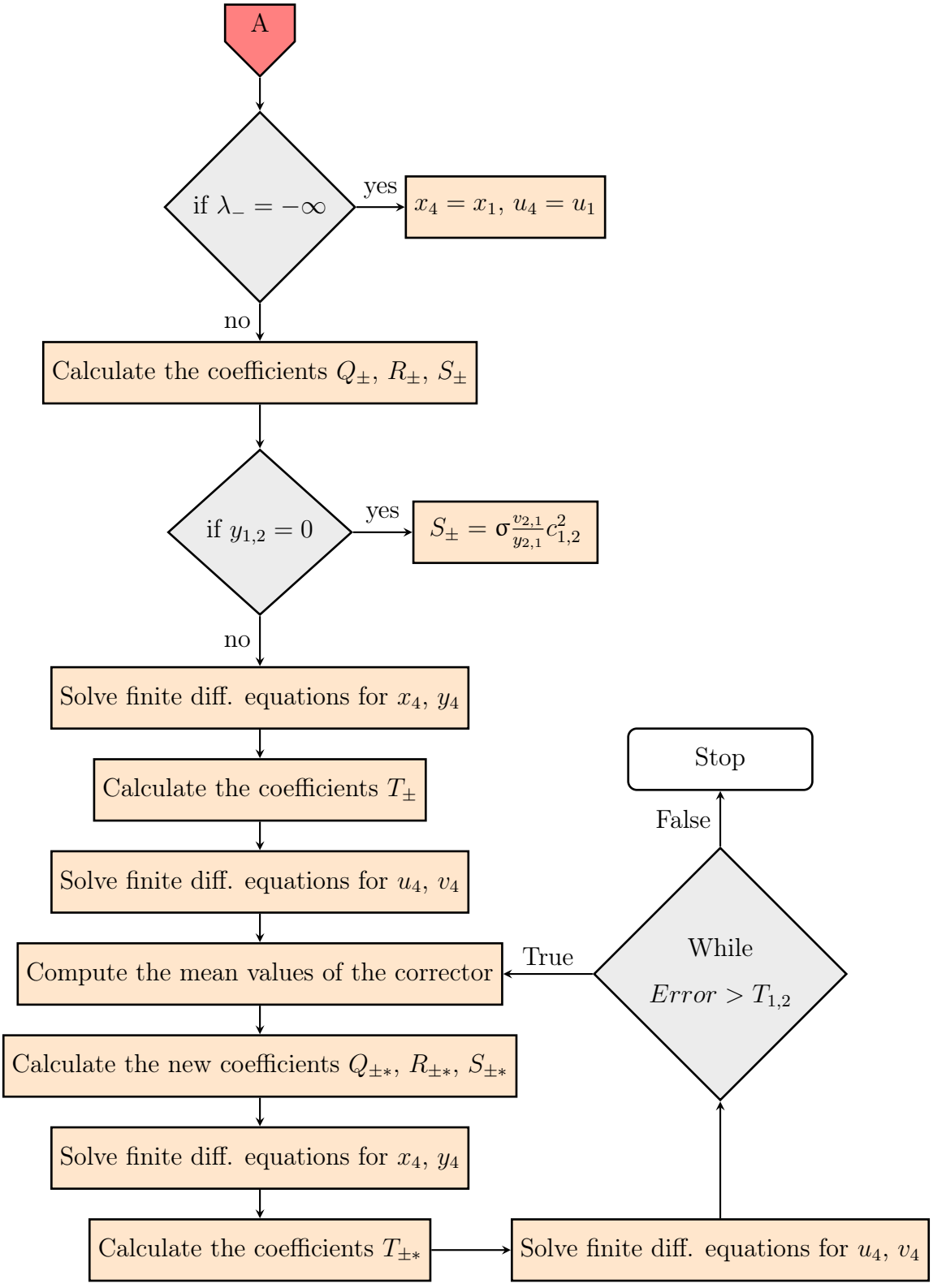

Figure 21.. Unit process of the Euler predictor-corrector algorithm for an interior point

For a ***axisymmetric point***, the initial data of the initial point is taken of the solution point of the just solved example (point 4 from figure 20). From the last corrector applied in table 2:

$$\text{Point 1} \begin{cases} x_1 = 0.185\ [m] \\ y_1 = 0.0731\ [m] \\ u_1 = 969.23\ \left[\frac{m}{s}\right] \\ v_1 = 0.0534\ \left[\frac{m}{s}\right] \end{cases} \qquad \text{Point 4} \begin{cases} y_4 = 0\ [m] \\ v_4 = 0\ \left[\frac{m}{s}\right] \\ \theta_4 = 0 \end{cases}$$

Since enough data from the solution point is already known, only the right-running characteristic (line 1-4 from figure 19) is used. Therefore, the finite differential equations are solved with this data to obtain x_4 and u_4.

Euler predictor algorithm

Calculation of the direction λ_- of the negative characteristic

$$V_- = \sqrt{u_1^2 + v_1^2} = \sqrt{969.23^2 + 0.0534^2} = 969.230001471\ \left[\frac{m}{s}\right]$$

$$\theta_- = \arctan\left(\frac{v_1^2}{u_1^2}\right) = \arctan\left(\frac{0.0534^2}{969.33^2}\right) = 0.0032^o$$

$$c_- = \sqrt{c_0^2 - \frac{(\gamma-1)}{2}V_-^2} = \sqrt{1016.5^2 - \frac{(1.2-1)}{2} * 969.23^2} = 969.2282\ \left[\frac{m}{s}\right]$$

$$\alpha_- = \arcsin\left(\frac{c_-}{V_-}\right) = \arcsin\left(\frac{969.2282}{969.23}\right) = 89.88^o$$

$$\lambda_- = \tan\left(\theta_- - \alpha_-\right) = \tan\left(0 - 87\right) = -505.43$$

Following the same procedure for an interior point, the next steps would be to calculate the coefficients of the compatible equations, compute the position, obtain the coefficient of the finite difference equations for getting the velocities.

Coefficients of the negative characteristic compatible equation to obtain the position:

$$Q_- = \left(u_1^2 - c_-^2\right) = (969.23^2 - 969.2282^2) = 3.4725 \ \left[\frac{m^2}{s^2}\right]$$

$$R_- = [2u_1v_1 - Q_-\lambda_-] = [2(969.23)(0.0534) - (3.4725)(-505.43)] = 1858.6 \ \left[\frac{m^2}{s^2}\right]$$

$$S_- = \sigma\frac{v_1}{y_1}c_-^2 = (1)\left(\frac{0.0534}{0.0731}\right)969.2282^2 = 6.86 * 10^5 \ \left[\frac{m^2}{s^2}\right]$$

Location of the solution point:

$$y_4 - \lambda_- x_4 = y_1 - \lambda_- x_1$$

$$(0) - (-505.43)x_4 = 0.0731 - (-505.43)(0.185)$$

$$x_4 = 0.18514 \ [m]$$

Once the location is got, the $T_\pm$ coefficients are computed:

$$T_- = S_-(x_4 - x_1) + Q_-u_1 + R_-v_1$$

$$T_- = (6.86 * 10^5)(0.18514 - 0.185) + (3.4725)(969.23) + (1858.6)(0) = 3564.1 \ \left[\frac{m^3}{s^3}\right]$$

Finally the velocity is computed:

$$Q_-u_4 + R_-v_4 = T_-$$

$$(3.4725)u_4 + (1858.6)(0) = 3564.1$$

$$u_4 = 1026.4 \ \left[\frac{m}{s}\right]$$

The results show that the solution deviates from the real solution as the coefficients usually powers of 10^5 and 10^6. For correcting that error, enough number of iterations must be done in the corrector algorithm to achieve the desired tolerance or error range.

Euler corrector algorithm

Variables for the Euler corrector algorithm:

$$u_{1*} = \frac{u_1 + u_4}{2} = \frac{969.23 + 1026.4}{2} = 997.812 \ \left[\frac{m}{s}\right]$$
$$v_{1*} = \frac{v_1 + v_4}{2} = \frac{0.0534 + 0}{2} = 0.0267 \ \left[\frac{m}{s}\right]$$
$$y_{1*} = \frac{y_1 + y_4}{2} = \frac{0.1 + 0}{2} = 0.0366 \ [m]$$

With these new variables, all the process is repeated for the angles, and the coefficients.

$$V_{-*} = \sqrt{u_{1*}^2 + v_{1*}^2} = 997.8 \ \left[\frac{m}{s}\right]$$
$$\theta_{-*} = \arctan\left(\frac{v_{1*}^2}{u_{1*}^2}\right) = 0.002^o$$
$$c_{-*} = \sqrt{c_0^2 - \frac{(\gamma - 1)}{2} V_{-*}^2} = 966.32 \ \left[\frac{m}{s}\right]$$
$$\alpha_{-*} = \arcsin\left(\frac{c_{-*}}{V_{-*}}\right) = 75.56^o$$
$$\lambda_{-*} = \tan\left(\theta_{-*} - \alpha_{-*}\right) = -3.88$$
$$Q_{-*} = \left(u_{1*}^2 - c_{-*}^2\right) = 61854.28 \ \left[\frac{m^2}{s^2}\right]$$
$$R_{-*} = \left[2u_{1*}v_{1*} - Q_{-*}\lambda_{-*}\right] = 2.4 * 10^5 \ \left[\frac{m^2}{s^2}\right]$$
$$S_{-*} = \sigma\frac{v_{1*}}{y_{1*}} c_{-*}^2 = 6.82 * 10^5 \ \left[\frac{m^2}{s^2}\right]$$

For the location:

$$y_4 - \lambda_{-*} x_4 = y_1 - \lambda_{-*} x_1$$
$$(0) - (-3.88)x_4 = 0.0731 - (-3.88)(0.185)$$
$$x_4 = 0.2038 \ [m]$$

The T_{-*} coefficient:

$$T_{-*} = S_{-*}(x_4 - x_1) + Q_{-*}u_1 + R_{-*}v_1$$
$$= (6.82 * 10^5)(0.2038 - 0.185) + (61854.28)(969.23) + (2.4 * 10^5)(0.0534) = 5.9977 * 10^7 \ \left[\frac{m^3}{s^3}\right]$$

Finally, the velocity:

$$Q_{-*}u_4 + R_{-*}v_4 = T_{-*}$$
$$(61854.28)u_4 + (2.4 * 10^5)(0) = 5.9977 * 10^7$$
$$u_4 = 969.645 \ \left[\frac{m}{s}\right]$$

NOTE: For achieving the desired tolerance of error, eight iterations of the corrector algorithm were necessary.

For the axisymmetric point, the results are shown in a table and graphically as well as, the procedure is summarized in a flowchart.

Table 3. Modified Euler predictor-corrector results

Modified Euler predictor-corrector			
$Variable$	$Predictor$	$Corrector_7$	$Corrector_8$
λ_-	-505.43	-19.36	-20.24
$Q_-\ [m^2/s^2]$	3.47	2437.99	2247.29
$R_-\ [m^2/s^2]$	1858.61	47249.23	45545.29
$S_-\ [m^2/s^2]$	$6.86 * 10^5$	$6.86 * 10^5$	$6.86 * 10^6$
$T_-\ [m^3/s^3]$	3564.13	$2.368 * 10^6$	$2.183 * 10^6$
$x_4\ [m]$	0.18514	0.18878	0.18861
$y_4\ [m]$	0	0	0
$u_4\ [m/s]$	1026.39	971.33	971.41
$v_4\ [m/s]$	0	0	0

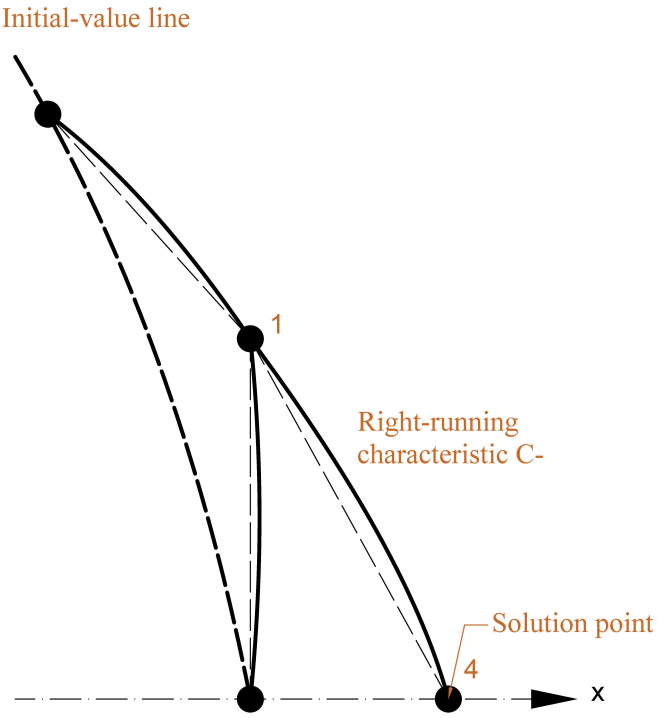

Figure 22.. The first axially symmetric point in the IV line

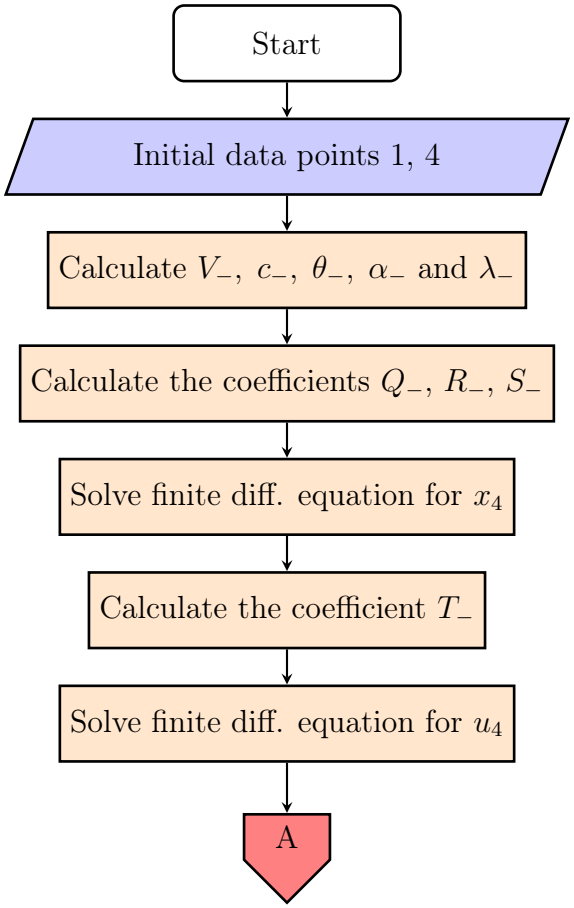

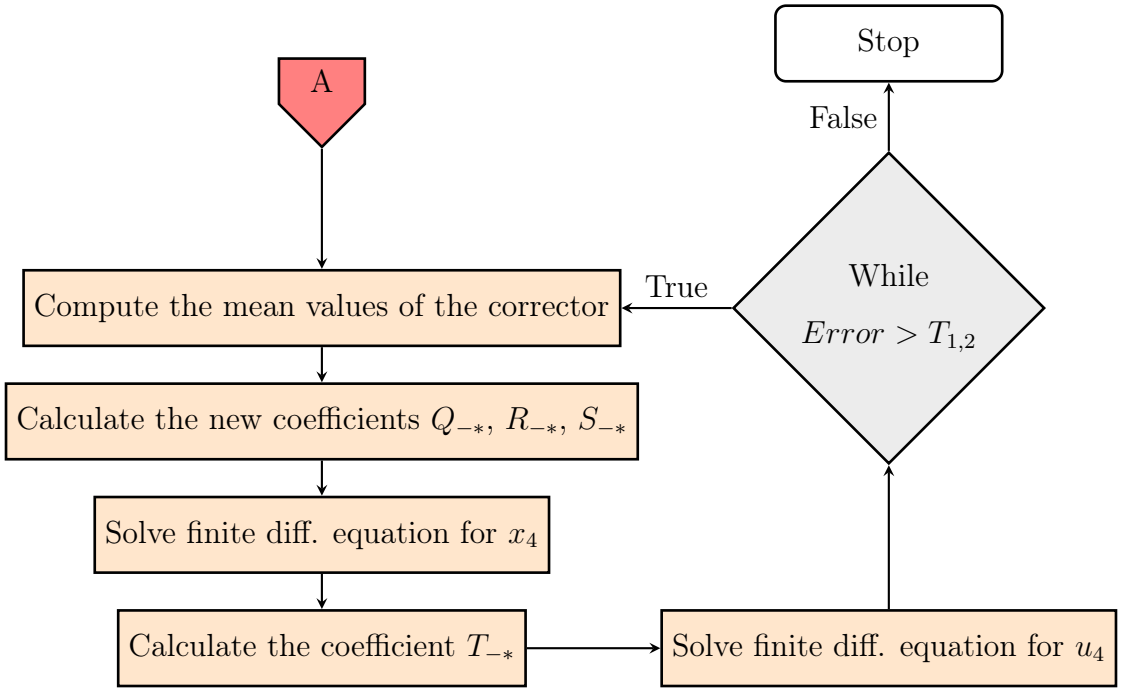

Figure 23.. Unit process of Euler predictor-corrector algorithm for an axisymmetric point

Once the computation procedure for the two cases (interior-point and axisymmetric point) necessary for the extend of the initial value line, this part of the design can be carried out.

In order to construct the algorithm of the initial-value line extend, an idea is planted. If the extension of the first four points of the IV line is carried out, it will look like the figure 4.24(a). Then, for programming in any language, it is necessary to go through the IV points in pairs, i.e., points $1-2$, points $2-3$ and points $3-4$ will represent the diagonal rows of the extension. However, every time that a pair of points are caught, the unit process of an interior and axisymmetric points are utilized a determined number of times. That number of times is cleared by finding a relation between the IV pair of points upper number and how many solutions points are encountered by the MoC.

Analyzing the figure 4.24(a), the relation can be cleared, if we stand at the first upper point of the first pair, i.e., point 2 (this upper point represents the point $No1$), there will be 2 solutions points, if we stand at the upper point of the second pair, there will be 4 solutions points and the relation will be constant if the process

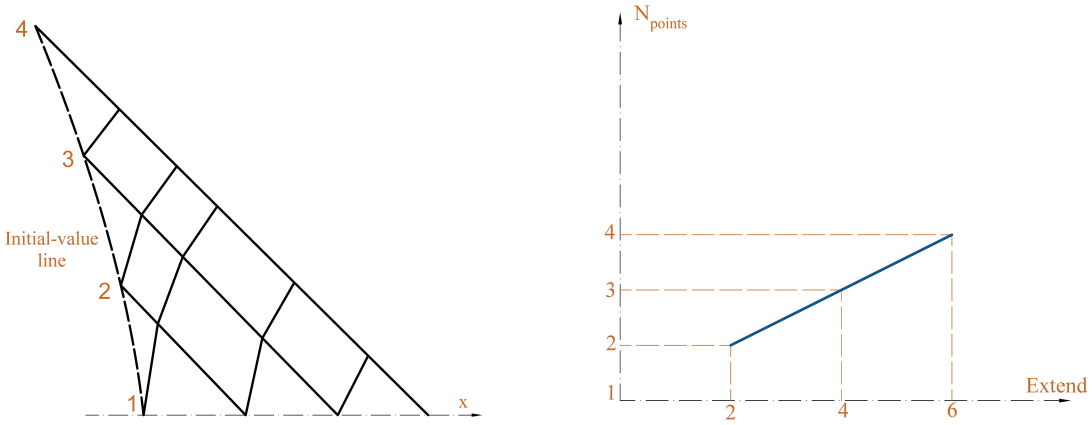

(a) Extend - first four points of the IV line

(b) Direct relation between the IV points and its expansion

Figure 24.. Idea of the IV line expansion

is continued. Therefore, plotting that relation, figure 4.24(b) is encountered and the relation is cleared by doing an equation of a straight line with two known points. From the figure 4.24(b):

$$Extend = 3i - 1$$

Flowchart of the IV line extend:

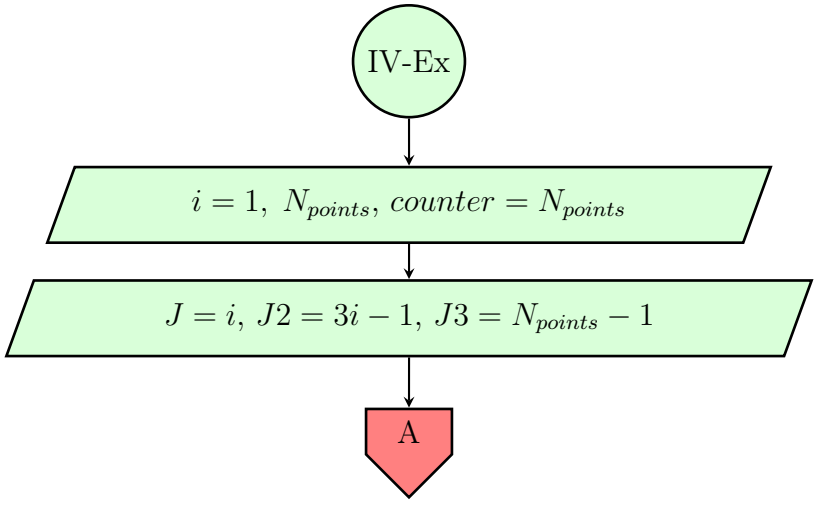

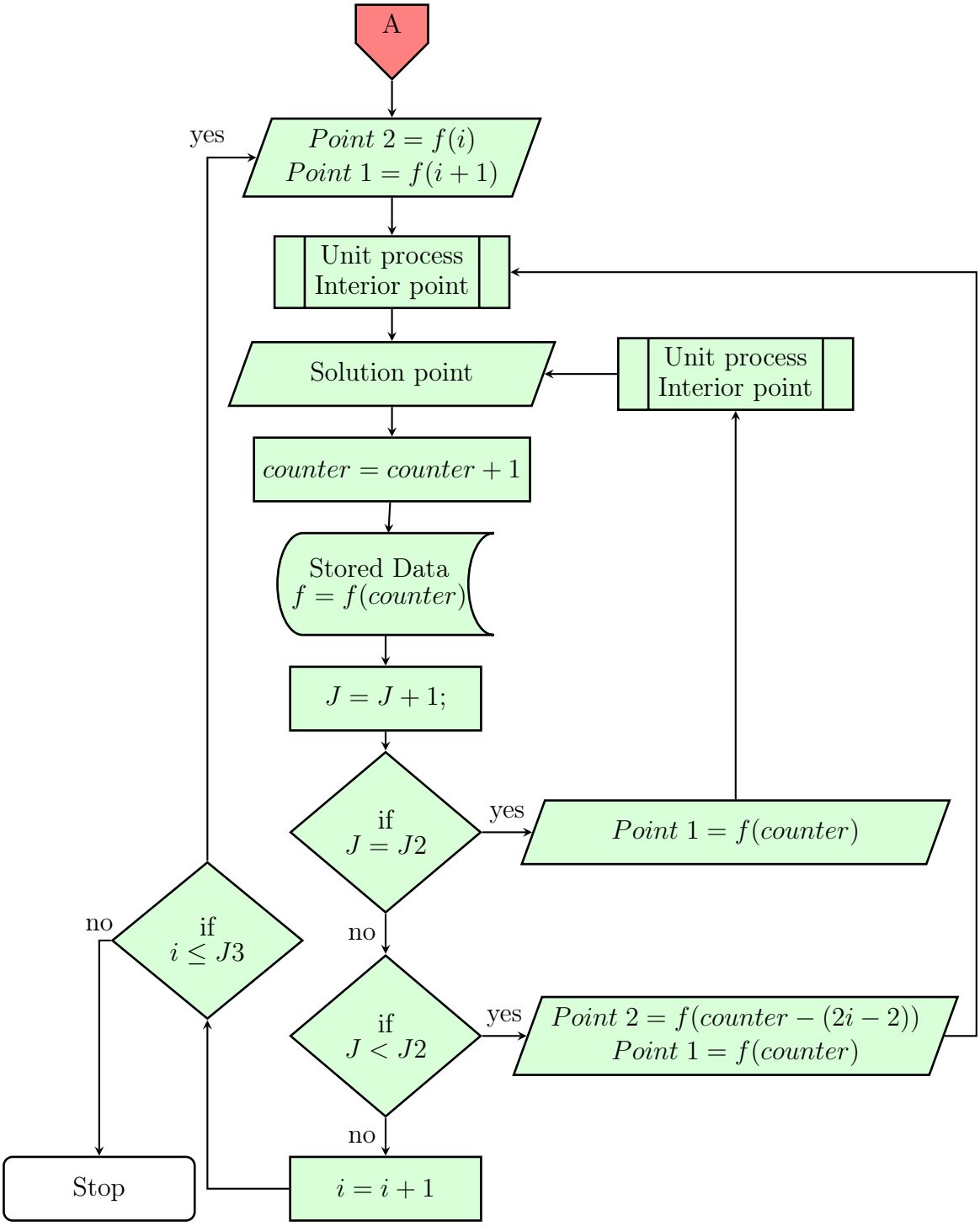

Figure 25.. Initial-value line extend procedure

For the proposed example, the initial-value line is:

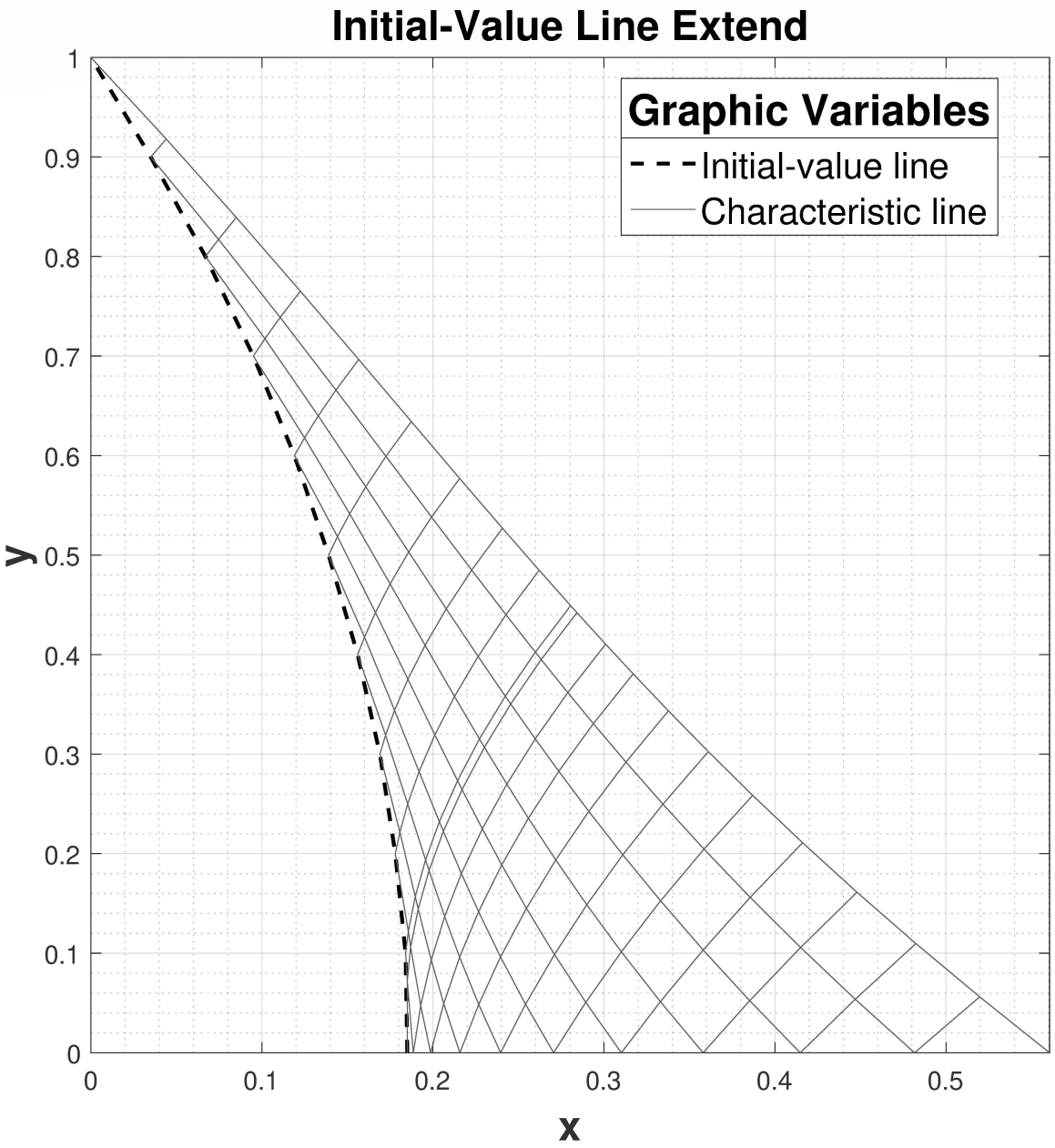

Figure 26.. Initial-value line extend

The line that goes from point 11 to the axis will receive a name in this thesis of a *Total characteristic line* and correspond to the sum of all the right-running characteristics from point 11 to the axis.

4.4.2 Kernel design

The kernel is an essential part of a design, in a nozzle design, the last point of the kernel over the axis will give us the Mach of design. The design can be conservative or exact; in this example, the process will be conservative.

The important things that the kernel needs are, the Mach number that we want in the jet of the nozzle, the radius downstream of the throat, the unit process for an interior and axisymmetric points, and a extra procedure is needed and is another case of the application of the MoC, the unit process for an inverse wall point.

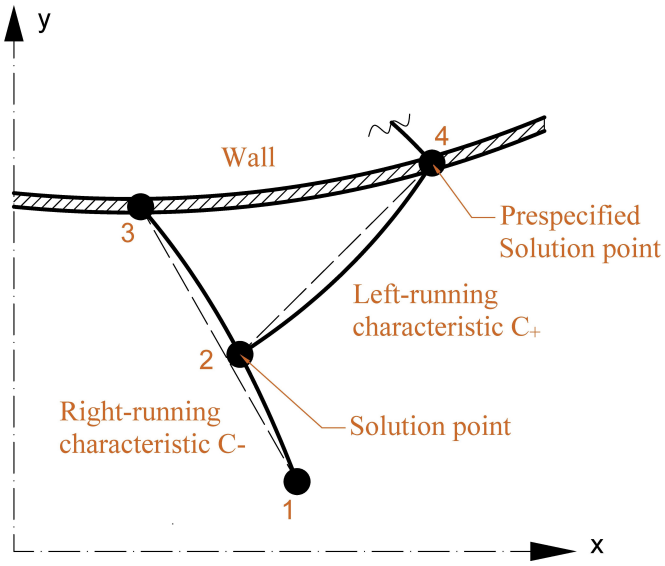

Figure 27.. Inverse wall point

In the figure, a predefined wall boundary point is showed; this predefined point is due to the division of the downstream radius. The reason for dividing the throat radius downstream path is that near the wall, the properties gradients are substantial, and a direct method (from a point to the wall) will result in too large a spacing of the solution points along the wall. Moreover, as it is desired a refined grid near the wall, then it is better to employ spaced solutions point by beforehand along the wall and then use the MoC for determining the flow properties.

As the wall boundary path is known until some unknown point, this path can be divided, and all of its points have a known location by geometry. Every point over the wall will result in a *Total characteristic line* that goes from the wall to the x-axis, just like the extent of the IV line. Every characteristic line ends in an axisymmetric point that gives us the velocity or Mach number over the axis at that specific point. When that Mach number has reached the Mach number of design, the kernel will be completed, and the point over the wall of the last total characteristic line corresponds to the final point of the upstream radius path.

Reaching this Mach number in the x-axis requires to walk along the wall boundary in equidistant steps, in this project that distant will be 1^o in the radius (every 1^o there will be a predefined point). The process is then to obtain the location x_4 and y_4 by geometry and get the flow and thermodynamics properties by applying the MoC through the unit process of an inverse wall point.

The procedure for the kernel is to save the total last characteristic line previously calculated (the line from point 11 at $y = 1$ to the x-axis from figure 26) in a vector and this will be the line of departure for the kernel, i.e., the initial data of the kernel.

Once this vector is got, the next step is to apply the unit process of an inverse wall point, and after the location and flow properties are encountered, from the predefined point over the wall, a new total characteristic line will unfold until it touches the x-axis. At that point, over the x-axis, the Mach number (M_{Axis}) is compared with the Mach number of design (M_D). If $M_{Axis} < M_D$, then another total characteristic need to be created from a new predefined point over the downstream radius wall until the x-axis. One more time, the M_{Axis} is compared with the M_D, and the process is repeated until M_{Axis} reaches a value immediately higher than M_D. If the design is stooped here, the design will be conservative, and the velocity will be a little higher than what it was defined at the beginning as a M_D. However, if the design requires to be very exact, bisection or interpolation can be used to find the exact point where the last total characteristic of the kernel will reach the M_D.

As it was done with the interior point and the axisymmetric point, an example for this case, the inverse wall point, will be carried out. The initial data of points 3 and 1 (figure 27) are taken from the vector of initial data for the kernel; they are the first two points. The data saved in the vector is taken from the previously saved data in every process.

$$\text{Point 3} \begin{cases} x_3 = 0\ [m] \\ y_3 = 1\ [m] \\ u_3 = 1090.4\ \left[\frac{m}{s}\right] \\ v_3 = 0\ \left[\frac{m}{s}\right] \end{cases} \qquad \text{Point 1} \begin{cases} x_1 = 0.0441\ [m] \\ y_1 = 0.9181\ [m] \\ u_1 = 1079.4\ \left[\frac{m}{s}\right] \\ v_1 = 6.0734\ \left[\frac{m}{s}\right] \end{cases}$$

Finding the location of point four (x_4 y_4) requires to analyze the involved angles in the geometry.

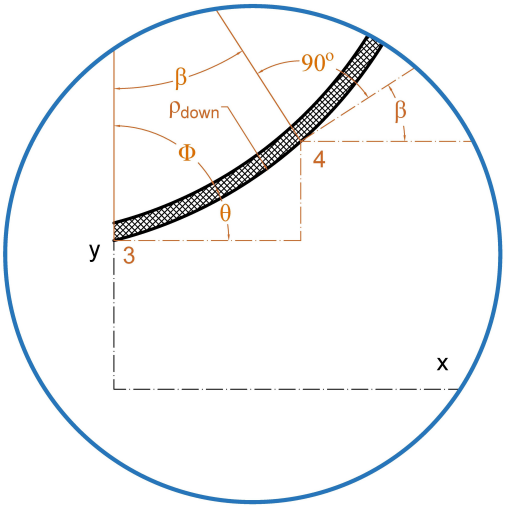

Figure 28.. Involved angles in an inverse wall point

From the figure, it is seem that the point 3 represent the throat and the point 4 is the first point over the downstream throat radius. Then, for finding the location of the point 4, the linear distance between both points (here, this distance is denoted by hte letter b) and the angle θ. Also the angle of the velocity at the

point 4 is necessary, but by geometry, this angle is equal to the angle β. Thus, the following relations are obtained by geometry:

$$b^2 = 2\rho_{down}^2 - 2\rho_{down}^2 \cos\beta \qquad From\ the\ cosenos\ law$$
$$b = \sqrt{2\rho_{down}^2 - 2\rho_{down}^2 \cos\beta} \tag{4.7}$$

Since the triangle is isosceles:

$$\phi = \frac{180^o - \beta}{2} \tag{4.8}$$
$$\theta_4 = 90^o - \phi \tag{4.9}$$
$$x_4 = b\cos\theta_4 \tag{4.10}$$
$$y_4 = y_t + b\sin\theta_4 \tag{4.11}$$

The location of the first point in the downstream radius for a $\beta = 1^o$:

$$b = 0.0349\ [m]$$
$$\phi = 89.5^o$$
$$\text{Point 4} \begin{cases} x_4 = 0.0349\ [m] \\ y_4 = 1.0003\ [m] \\ \theta_4 = 1^o \end{cases}$$

The process is the same as the interior-point or axisymmetric point process. Calculation of λ_+, the position of point 2, velocities of point 2, and thermodynamics properties, for the point 4, only is necessary to find the flow properties. However, there are some little changes, the velocities of point 2 are supposed to be equal to the velocities of point 3.

$$u_2 = u_3$$
$$v_2 = v_3$$

Euler predictor algorithm

Positive Characteristic

$$V_+ = \sqrt{u_2^2 + v_2^2} = \sqrt{1090.4^2 + 0^2} = 1090.4 \ \left[\frac{m}{s}\right]$$
$$\theta_+ = \arctan\left(\frac{v_2^2}{u_2^2}\right) = \arctan\left(\frac{0^2}{1090.4^2}\right) = 0$$
$$c_+ = \sqrt{c_0^2 - \frac{(\gamma-1)}{2}V_+^2} = \sqrt{1016.5^2 - \frac{(1.2-1)}{2} * 1090.4^2} = 956.2671 \ \left[\frac{m}{s}\right]$$
$$\alpha_+ = \arcsin\left(\frac{c_+}{V_+}\right) = \arcsin\left(\frac{956.2671}{1090.4}\right) = 61.3^o$$
$$\lambda_+ = \tan\left(\theta_+ + \alpha_+\right) = \tan\left(0 + 61.3\right) = 1.8251$$

Now, the equation of line 1-3:

$$\frac{y - y_1}{x - x_1} = \frac{y_3 - y_1}{x_3 - x_1}$$
$$\frac{y - 0.9181}{x - 0.0441} = \frac{1 - 0.9181}{0 - 0.0441}$$
$$\frac{y - 0.9181}{x - 0.0441} = -1.857$$

Thus, for point 2:

$$(y_2 - 0.9181) = (-1.857)(x_2 - 0.0441)$$

Now the equation for line 2-4:

$$(y_2 - y_4) = \lambda_+(x_2 - x_4)$$

$$(y_2 - 1.0003) = \lambda_+(x_2 - 0.0349)$$

Solving the system of equations for x_2 and y_2:

$$x_2 = 0.0172 \ [m]$$

$$y_2 = 0.968 \ [m]$$

Interpolating between the points 3 and 1:

$$u_2 = u_1 + \left(\frac{x_2 - x_1}{x_3 - x_1}\right)(u_3 - u_1)$$
$$v_2 = v_1 + \left(\frac{x_2 - x_1}{x_3 - x_1}\right)(v_3 - v_1)$$

Solving the equations:

$$u_2 = 1086.1 \left[\frac{m}{s}\right]$$
$$v_2 = 2.3711 \left[\frac{m}{s}\right]$$

After these velocities are encountered, the process is repeated until the difference between the results of the velocities has the desired grade of error.

After three more iterations the results have a better accuracy giving:

$$x_2 = 0.0174\ [m] \qquad u_2 = 1086.1 \left[\frac{m}{s}\right]$$
$$y_2 = 0.9676\ [m] \qquad v_2 = 2.4014 \left[\frac{m}{s}\right]$$

Recalculating λ_+ and the coefficients of the finite differential equations:

$$V_+ = 1096.1 \left[\frac{m}{s}\right] \qquad Q_+ = 2.6411 * 10^5 \left[\frac{m^2}{s^2}\right]$$
$$\theta_+ = 0.1267^o \qquad R_+ = -4.891 * 10^5 \left[\frac{m^2}{s^2}\right]$$
$$c_+ = 956.76 \left[\frac{m}{s}\right] \qquad S_+ = 2.2718 * 10^6 \left[\frac{m^2}{s^2}\right]$$
$$\alpha_+ = 61.75^o \qquad T_+ = 2.8571 * 10^8 \left[\frac{m^3}{s^3}\right]$$
$$\lambda_+ = 1.8716$$

For computing the flow properties of point 4, there will be a system of 2*2 equations. The first equations are the equations of the direction of the flow θ_4 and the second equation will be the finite difference compatibility equation of the MoC, then:

$$\tan\theta_4 = \frac{v_4}{u_4} \qquad Q_+u_4 + R_+v_4 = T_+$$
$$u_4 \tan 1 = v_4 \qquad 2.6411 * 10^5 u_4 - 4.891 * 10^5 v_4 = 2.8571 * 10^8$$

Solving the system, the velocities are:

$$u_4 = 1117.9 \left[\frac{m}{s}\right]$$
$$v_4 = 19.513 \left[\frac{m}{s}\right]$$

Now, once the predictor is completed, the corrector algorithm can be employed for all the process using the variables for the corrector previously mentioned in the unit process of an interior and axisymmetric point. The results are shown in a table with only the results at the points 2 and 4 (four application of the corrector were enough), and the procedure is summarized in a flowchart.

Table 4. Modified Euler predictor-corrector results

Modified Euler predictor-corrector			
$Variable$	$Predictor$	$Corrector_3$	$Corrector_4$
$x_2\ [m]$	0.0174	0.0170	0.0170
$y_2\ [m]$	0.9676	0.9684	0.9684
$u_2\ [m]$	1086.05	1086.16	1086.16
$v_2\ [m]$	2.401	2.343	2.343
$u_4\ [m/s]$	1117.89	1115.95	1115.95
$v_4\ [m/s]$	19.51	19.48	19.48

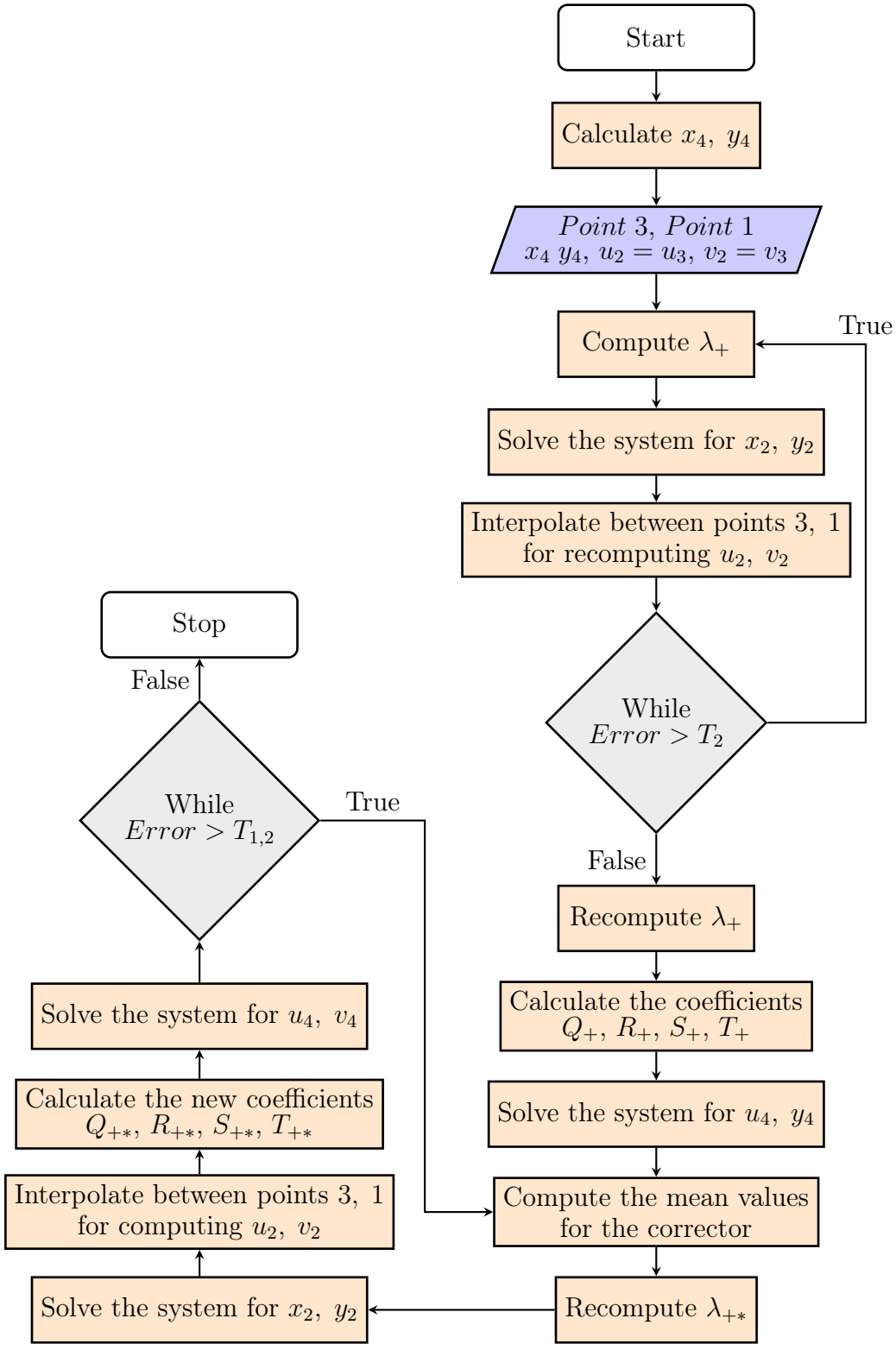

Figure 29.. Unit process of Euler predictor-corrector algorithm for an inverse wall point

The process to complete the kernel was already explained, though a particular case has to be taken into account. In the previous example of the unit process, y_2 is a point between the points 3 and 1; usually, the location of that solution point 2 is in that way, but some times the solution point is out of this range and will be below of the point 1. As mentioned before, after the unit process of an inverse wall point is applied and its solutions are obtained, the following step is to apply the unit process for an interior to the pair of points 1 (left-running char) and 4 (right-running char) of the figure 27. When the particular case happens, if the unit process is applied to the points 1 and 4, an error in the computation will happen, and the characteristics lines will intersect each other, and some solution points will be out of the wall. In order to avoid that error, the unit process for an interior point is applied to the points 4, and it continues being the right-running characteristic and to the point immediately below the point 2. After this first interior point is calculated, the process continues until it reaches the Mach of design.

The kernel process is summarized in a flowchart, and the graphic results are presented for the current example.

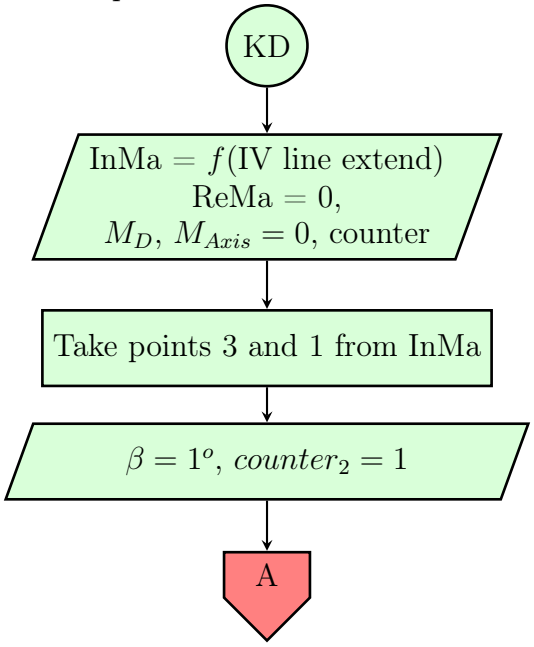

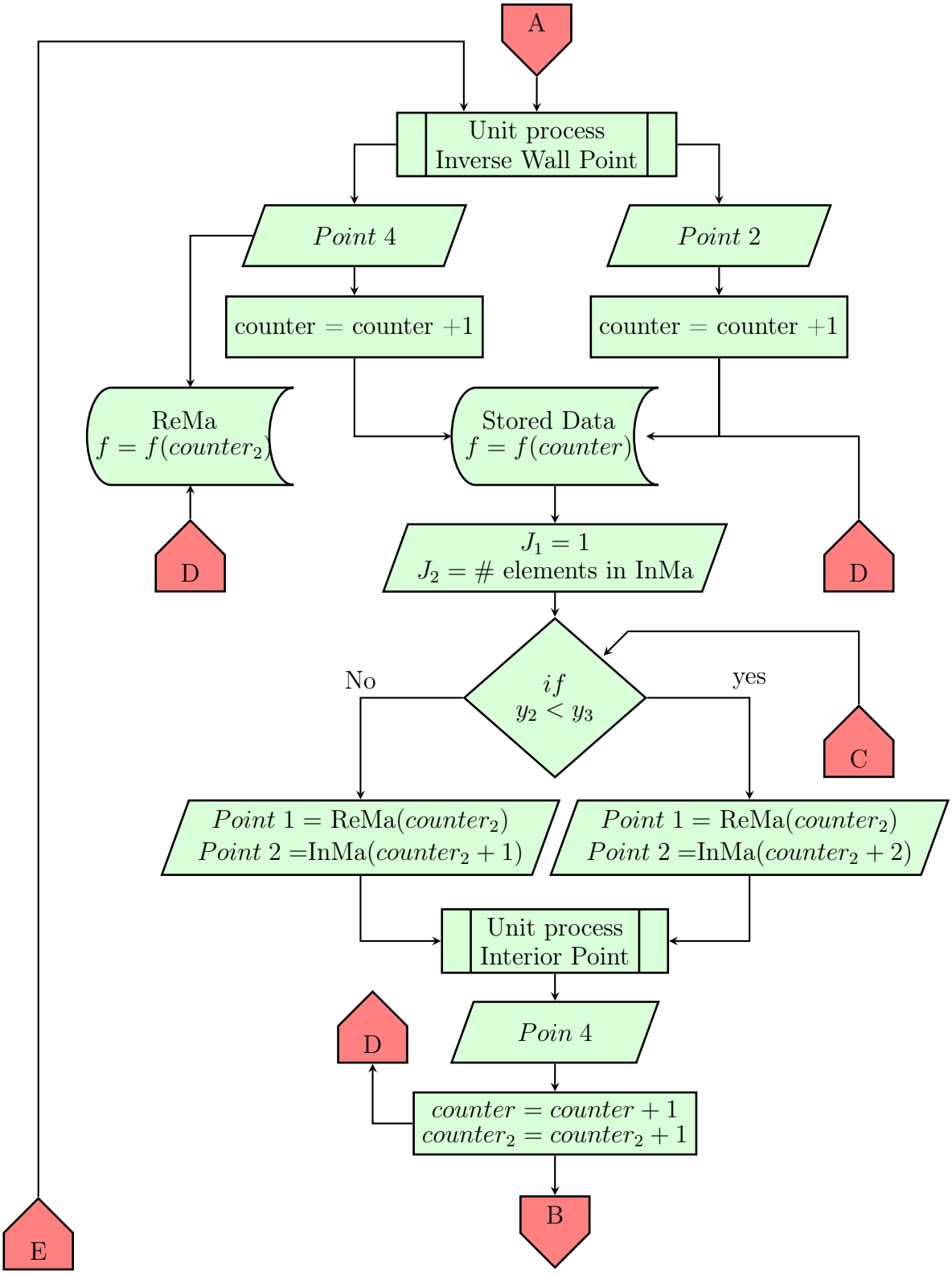
A
Unit process
Inverse Wall Point
Point 4
Point 2
counter = counter +1
counter = counter +1
ReMa
$f = f(counter_2)$
Stored Data
$f = f(counter)$
D
$J_1 = 1$
$J_2 = \#$ elements in InMa
D
No
if
$y_2 < y_3$
yes
C
Point 1 = ReMa($counter_2$)
Point 2 =InMa($counter_2 + 1$)
Point 1 = ReMa($counter_2$)
Point 2 =InMa($counter_2 + 2$)
Unit process
Interior Point
D
Poin 4
$counter = counter + 1$
$counter_2 = counter_2 + 1$
B
E

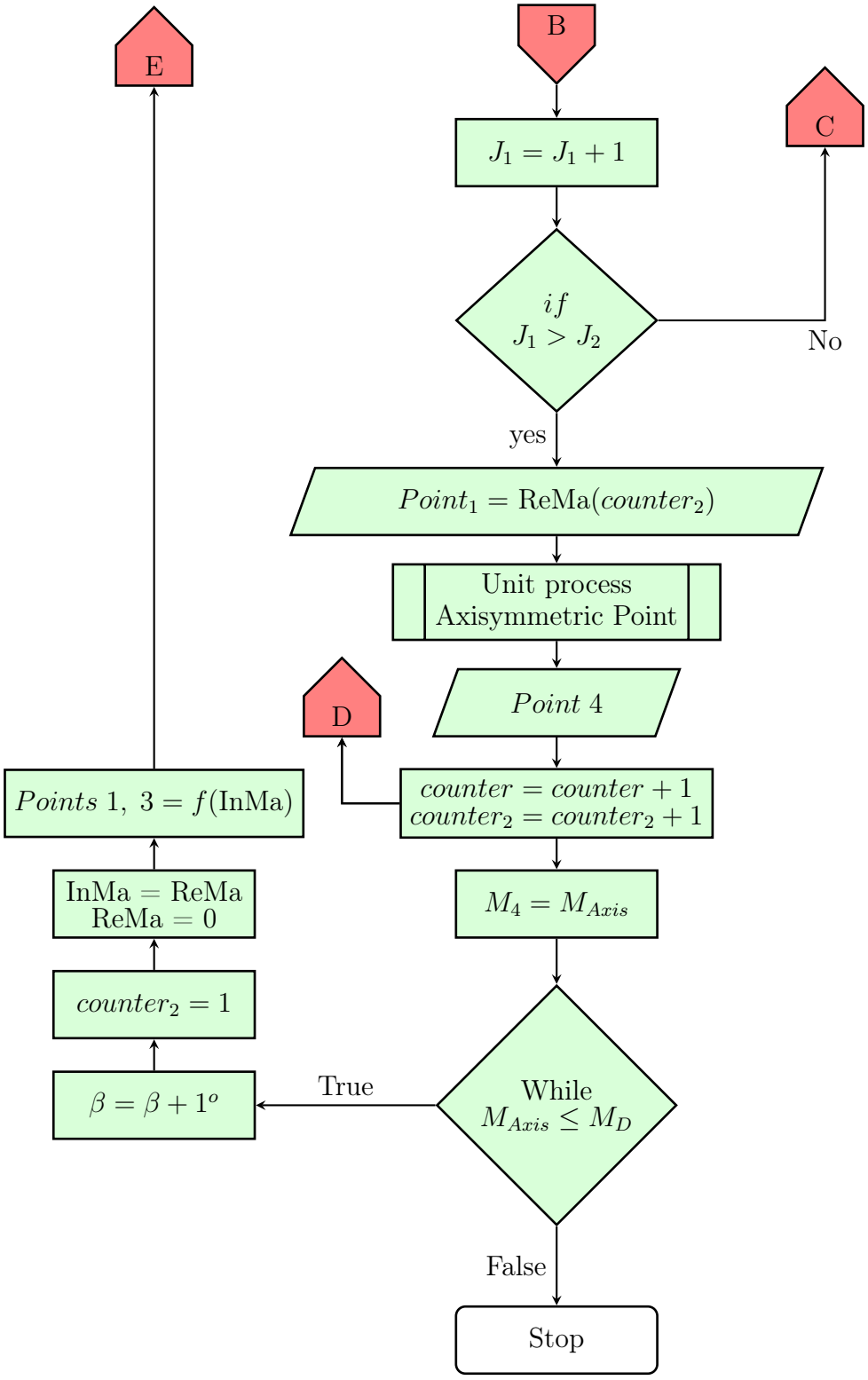

Figure 30.. Kernel design procedure

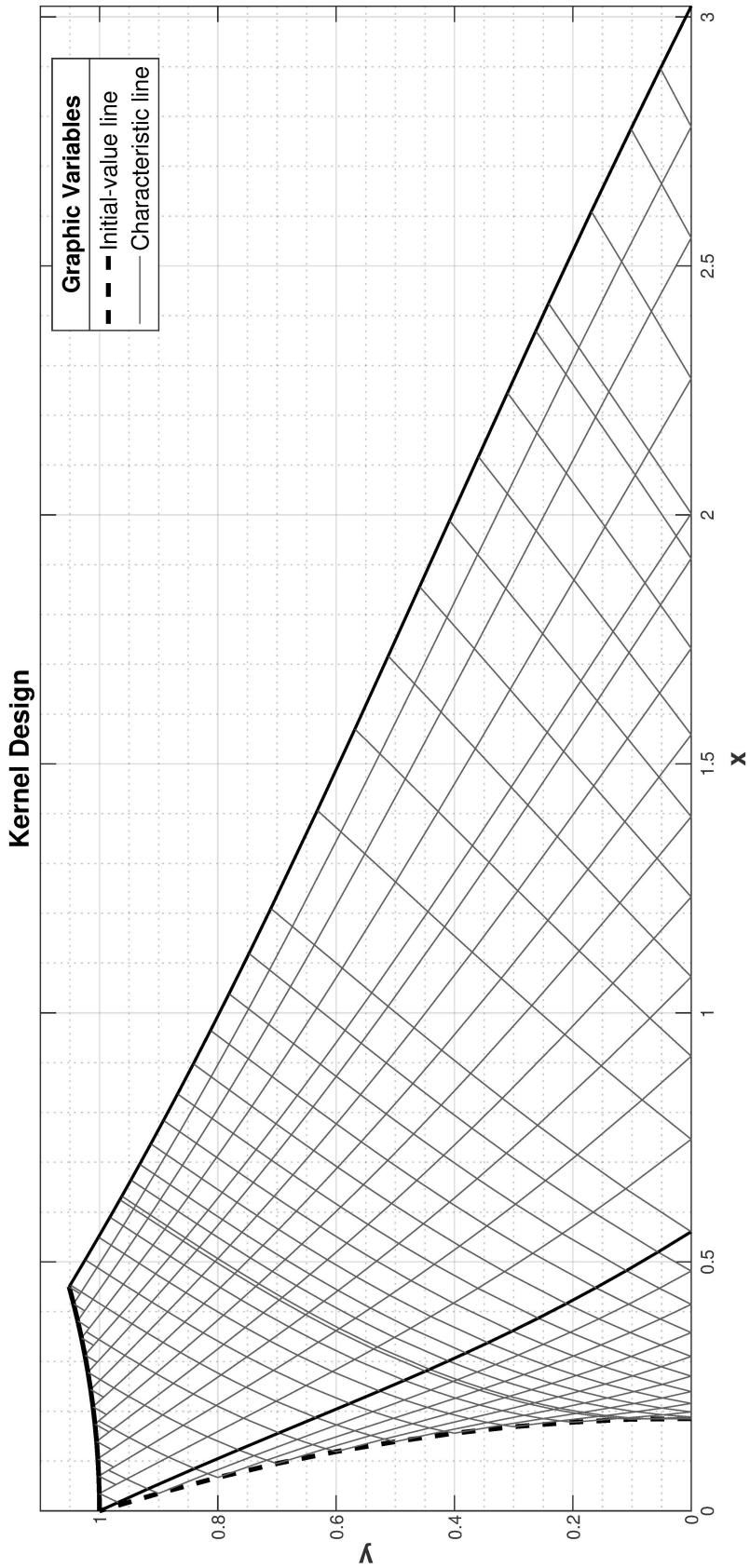

Figure 31.. Kernel design and initial-value line extend

Summarizing the results, the Mach number over the axis (M_{Axis}) reached a value of 2.58, and the Mach number of design (M_D) is 2.5; then, as predicted before, for conservative design,n the out velocity is a little higher than the velocity of design. β reached 13^o, i.e., there are thirteen new total characteristics lines in the kernel. The figure also shows the beginning of the supersonic contour, which is an arc with a radius of ρ_{down} and an opening angle of 13^o.

4.4.3 Final characteristic

As the exit flow field must be uniform, once being at the final point of the kernel over the axis, all the left-running characteristics from this point must be straight lines at the Mach angle of design ($\alpha_D = 1/M_{Axis}$) concerning the x-axis.

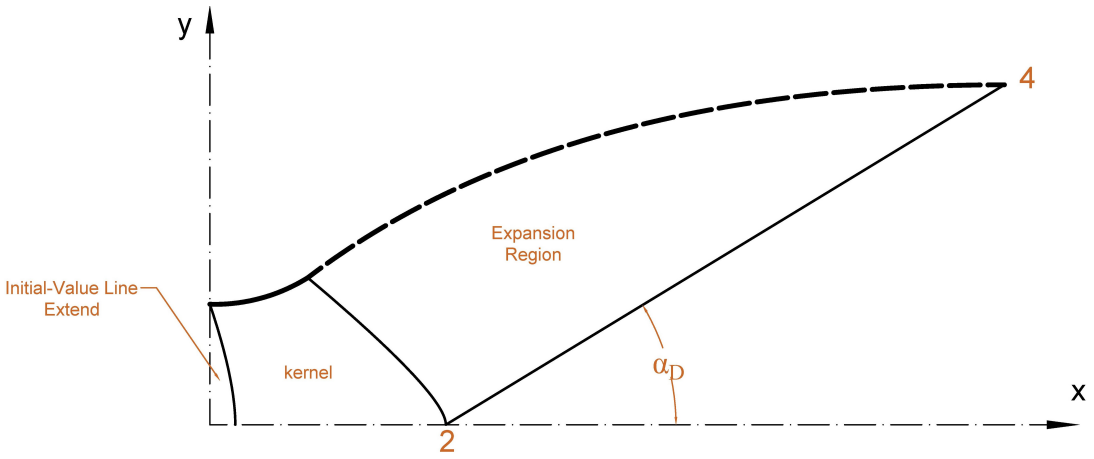

Figure 32.. Last characteristic line

In the figure 32, the last left-running characteristic can be seen, it makes an the angle α_D with the x-axis. It extend from point 2 to point 4. The point 4 is found by applying the conservation of mass to the line $2-4$. Then, the mass crossing this line, must be equal to the known mass crossing the IV line. From this line all the exit flow is parallel with the x-axis with $v = 0$ at a constant velocity and thermodynamics properties. This flow properties are known from the last point of

the kernel, i.e., the flow properties of the line $2-4$ are the same properties of point 2. Then, from point 2:

$$M_{Axis} = 2.5848 \qquad u_{last} = 2034.4\left[\frac{m}{s}\right]$$

Thermodynamic properties at 2:

$$T_2 = 1798.4\ [K]$$
$$p_2 = 324886.7\left[\frac{N}{m^2}\right]$$
$$rho_2 = 0.629\left[\frac{kg}{m^3}\right]$$

Applying the conservation of mass:

$$mass_{IV-line} = 15280.8[kg]$$
$$mass_{IV-line} = (\rho_2)(u_{last})(\pi y_{last}^2)$$
$$y_{last} = \left[\frac{mass_{IV-line}}{(\rho_2)(u_{last})(\pi)}\right]^{\frac{1}{2}} = \left[\frac{15280.8}{(0.629)(2034.4)(\pi)}\right]^{\frac{1}{2}} = 1.9491[m]$$

Then, the line 2-4 from figure 32 extends until y_{last} making the angle $\alpha_D = 22.76^o$ with the x-axis. Until here, the design has its last point but is not completed. This line need to be discretized for being able to analyze it in an axisymmetric 2D way.

The line is divided into a determined number of elements. A considerable measure of division is the high of the point before the last point of the kernel; with the high of that point, the mesh will continue refined, with small spaces between characteristics. From the saved data, the high of the necessary point is $Y = 0.052\ [m]$. Thus, the number of division of the line should be:

$$N_{Dy} = \frac{y_{last}}{Y} = \frac{1.9491}{0.052} = 37.48$$

The nearest integer of the division is 37, therefore, $N_{Dy} = 37$. The high of the points are giving by:

$$Dy = \frac{y_{last}}{N_{Dy} - 1} = \frac{1.9491}{36} = 0.0541\ [m]$$

For the new 37 points, the thermodynamic properties are computed and stored, and the design of the last characteristic is done.

4.4.4 Expansion section design

Determining the flow field of the expansion region and the contour of the dashed line in figure 32 is the remaining problem. Solving this problem requires to apply the Moc differently, although the problem continues being a problem of two families of characteristics, one right and one left. The procedure is explained following the solution of the example.

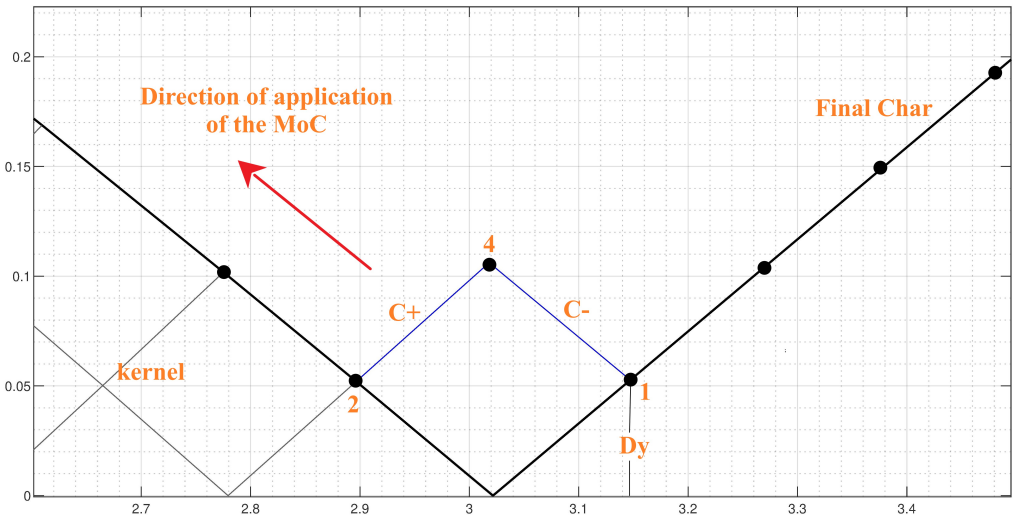

Figure 33.. First application of the unit process for a interior point in the expansion region

The figure above shows the way that the MoC has to be applied. If the image is analyzed, it is easy to determine that the location of points $1-2-4$ has changed and that the unit process for an interior point has to be applied upstream along the total right-running characteristic C_- of the kernel.

Near the contour, the final point computed along the C_- total characteristic occurs when the total mass flow crossing this line is higher than the mass flow crossing the known IV line. When the program stops, it happens that the solution point lies outside of the flowfield. Figure 34 shows that situation.

That new point can be the solution of the penultimate point, as the case of the figure, of the last point. It also must be a surface point and contribute to the contour. That situation is recognized by the Matlab software when it cannot find

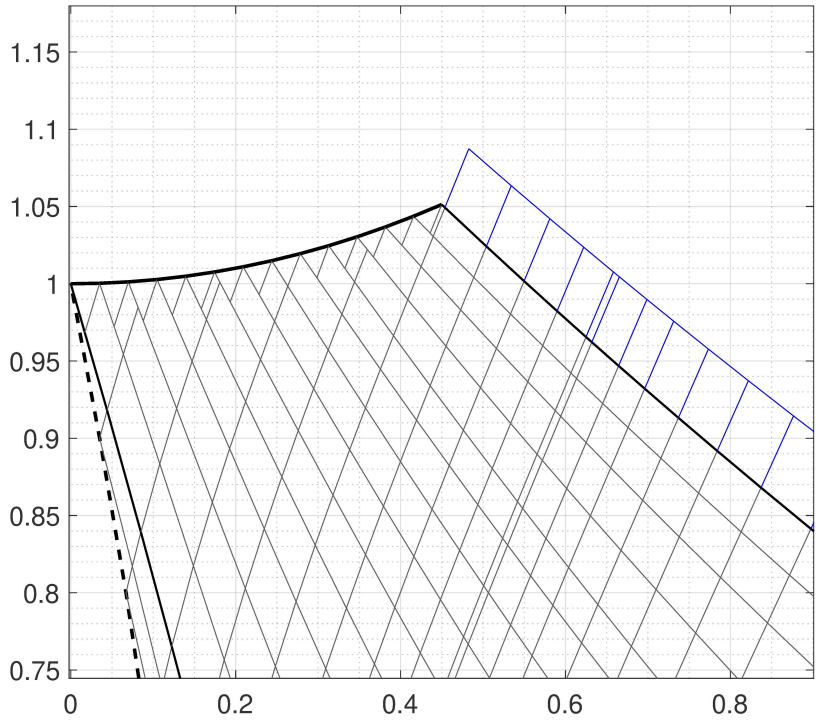

Figure 34.. First application of the unit process for a interior point in the expansion region

any points on a streamline upstream of the new point and or the mass crossing that total characteristic line is greater than the known mass flow in the throat section.

Now, the problem is to find the exact point of the boundary wall; for this, the masses need to be equaled. For equaling the masses, an algorithm for programming is utilized. That algorithm is called bisection, and the process is described in a few steps for a global variable.

General process of Bisection algorithm

1. Declare the function $f = f(variable)$, e.g., $mas_{C-} = f(position)$.
2. Declare the boundary condition, e.g., $m_{IV-line}$.
3. Declare a range of error or tolerance.

4. Declare a *minimum* and a *maximum* value, e.g., y_1, y_4 respectively.

5. Find the mean value of the *minimum* and *maximum*, e.g., y_{mean}.

6. Compute $f = f(mean\ value)$, e.g., $mas_{C-} = f(y_{mean})$.

7. If $f(mean\ value) >$ boundary condition, then, $mean\ value = maximum$, else, $mean\ value = minimum$.

8. While $|f(variable) - Boundary\ condition| >$ Tolerance, repeat steps 5 to 6.

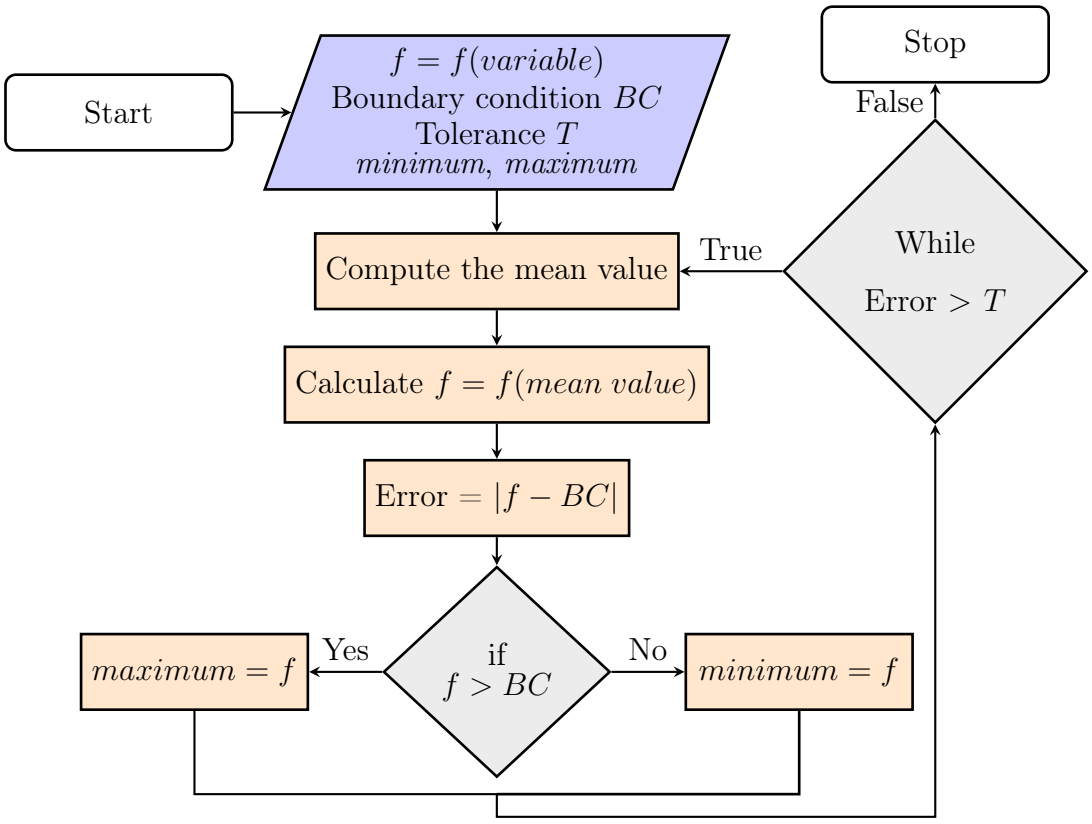

Figure 35.. General bisection algorithm

Once the variables are defined, the bisection algorithm can be applied to the problem presented in figure 34, and the mass is computed using the general trapezoidal rule because the points are no equally spaced each other. Equaling the masses leads us to find the most accurate point for the nozzle contour. Figure 36 shows the solution.

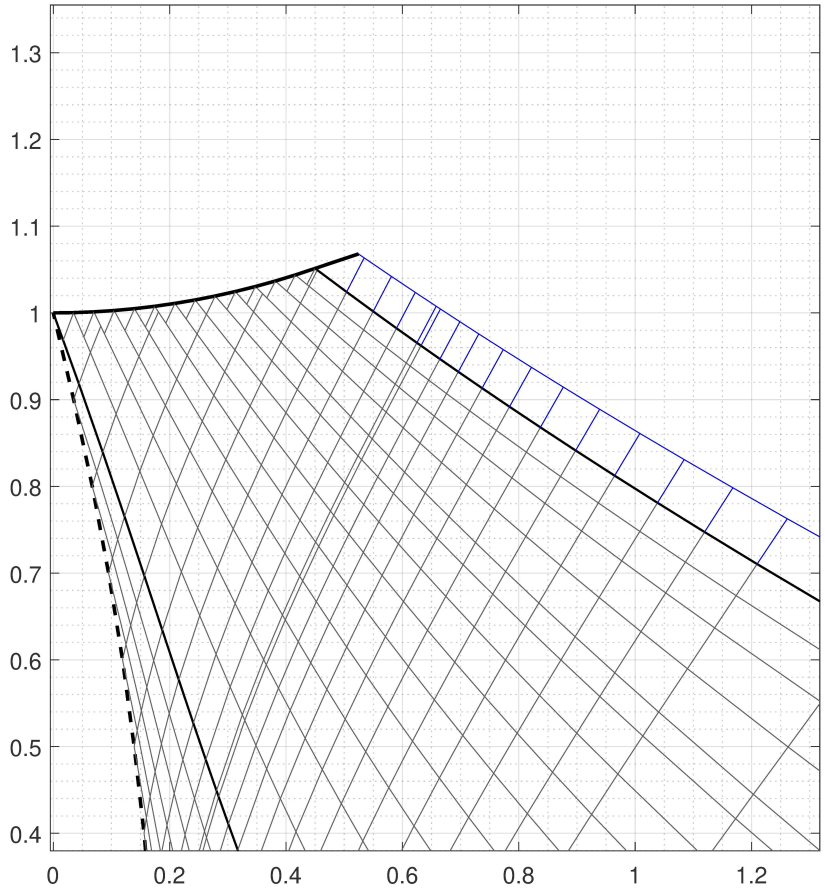

Figure 36.. Surface nozzle point

The process is applied iteratively from the last point of the kernel until the last point of the penultimate point of the last right-running characteristic.

The procedure is summarized in a flowchart and the results are showed graphically as it was done with the complete process until this point.

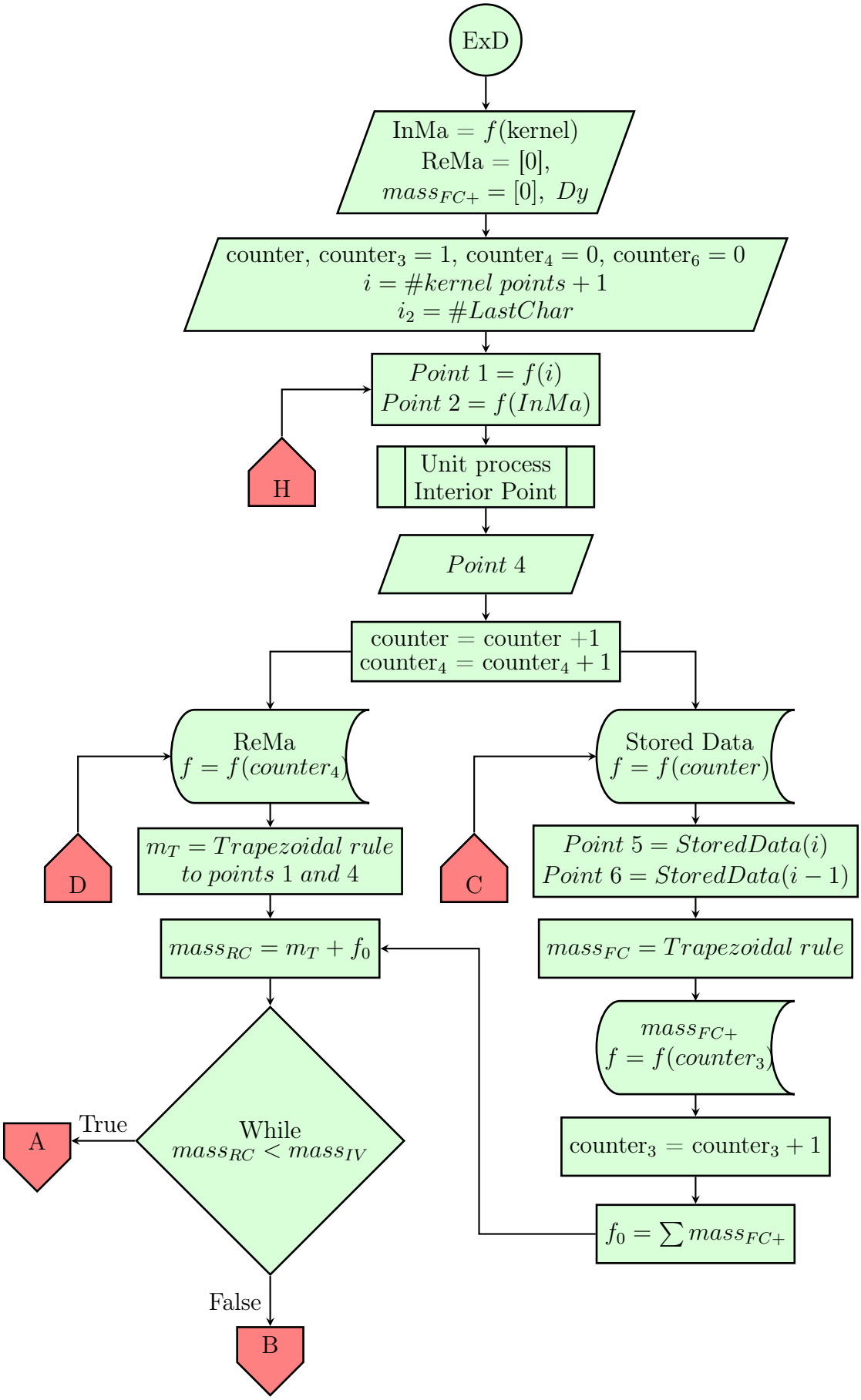
ExD
InMa = f(kernel)
ReMa = [0],
$mass_{FC+}$ = [0], Dy
counter, counter$_3$ = 1, counter$_4$ = 0, counter$_6$ = 0
i = #$kernel\ points + 1$
i_2 = #$LastChar$
$Point\ 1 = f(i)$
$Point\ 2 = f(InMa)$
H
Unit process
Interior Point
$Point\ 4$
counter = counter +1
counter$_4$ = counter$_4$ + 1
ReMa
$f = f(counter_4)$
Stored Data
$f = f(counter)$
D
$m_T = Trapezoidal\ rule$
$to\ points\ 1\ and\ 4$
C
$Point\ 5 = StoredData(i)$
$Point\ 6 = StoredData(i-1)$
$mass_{RC} = m_T + f_0$
$mass_{FC} = Trapezoidal\ rule$
$mass_{FC+}$
$f = f(counter_3)$
A
True
While
$mass_{RC} < mass_{IV}$
counter$_3$ = counter$_3$ + 1
$f_0 = \sum mass_{FC+}$
False
B

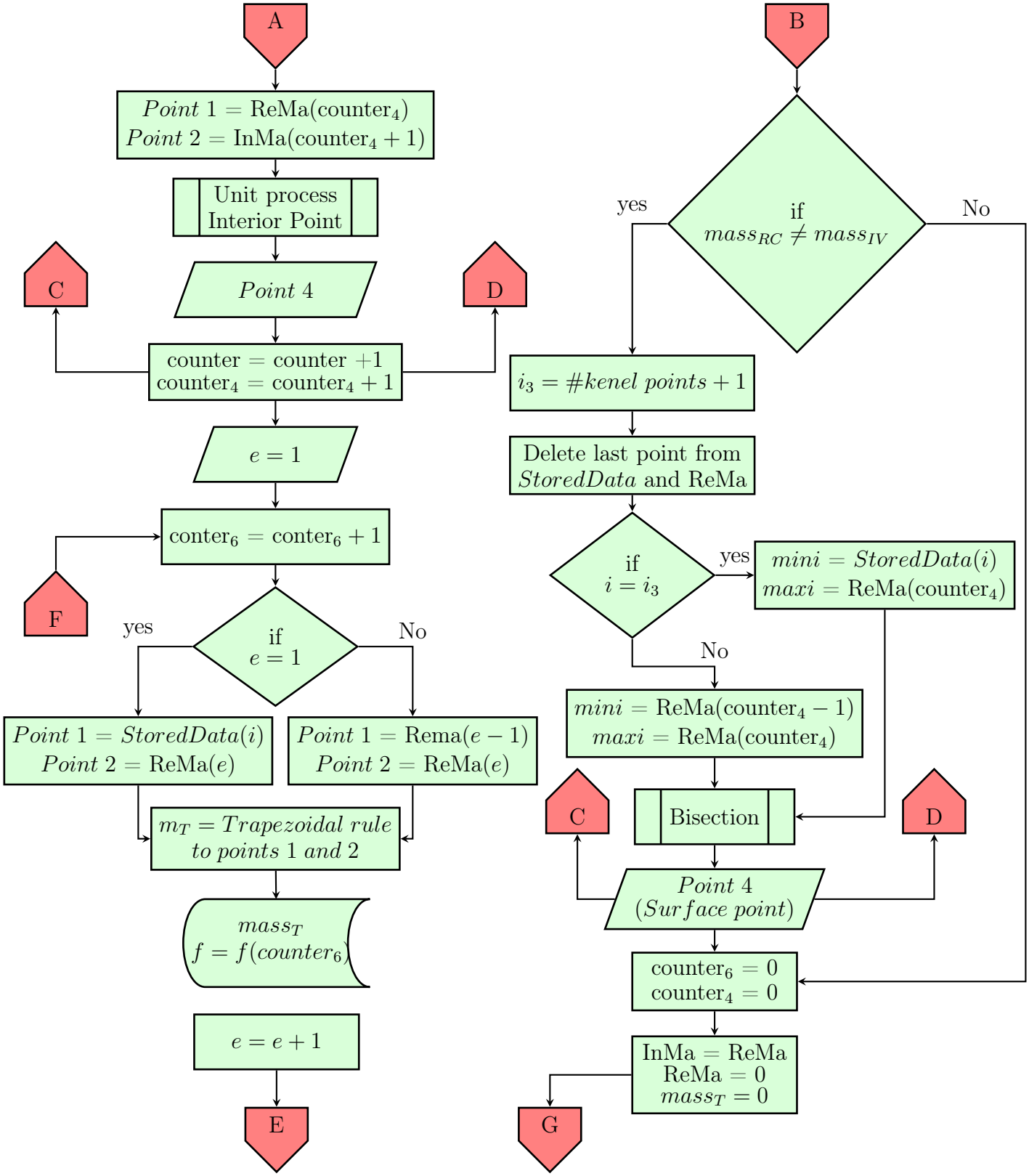
A
$Point\ 1 = \text{ReMa}(\text{counter}_4)$
$Point\ 2 = \text{InMa}(\text{counter}_4 + 1)$
Unit process
Interior Point
$Point\ 4$
C
D
counter = counter +1
$\text{counter}_4 = \text{counter}_4 + 1$
$e = 1$
F
$\text{conter}_6 = \text{conter}_6 + 1$
yes
if
$e = 1$
No
$Point\ 1 = StoredData(i)$
$Point\ 2 = \text{ReMa}(e)$
$Point\ 1 = \text{Rema}(e-1)$
$Point\ 2 = \text{ReMa}(e)$
$m_T = Trapezoidal\ rule$
$to\ points\ 1\ and\ 2$
$mass_T$
$f = f(counter_6)$
$e = e + 1$
E
B
yes
if
$mass_{RC} \neq mass_{IV}$
No
$i_3 = \#kenel\ points + 1$
Delete last point from
$StoredData$ and ReMa
if
$i = i_3$
yes
$mini = StoredData(i)$
$maxi = \text{ReMa}(\text{counter}_4)$
No
$mini = \text{ReMa}(\text{counter}_4 - 1)$
$maxi = \text{ReMa}(\text{counter}_4)$
C
Bisection
D
$Point\ 4$
$(Surface\ point)$
$\text{counter}_6 = 0$
$\text{counter}_4 = 0$
InMa = ReMa
ReMa = 0
$mass_T = 0$
G

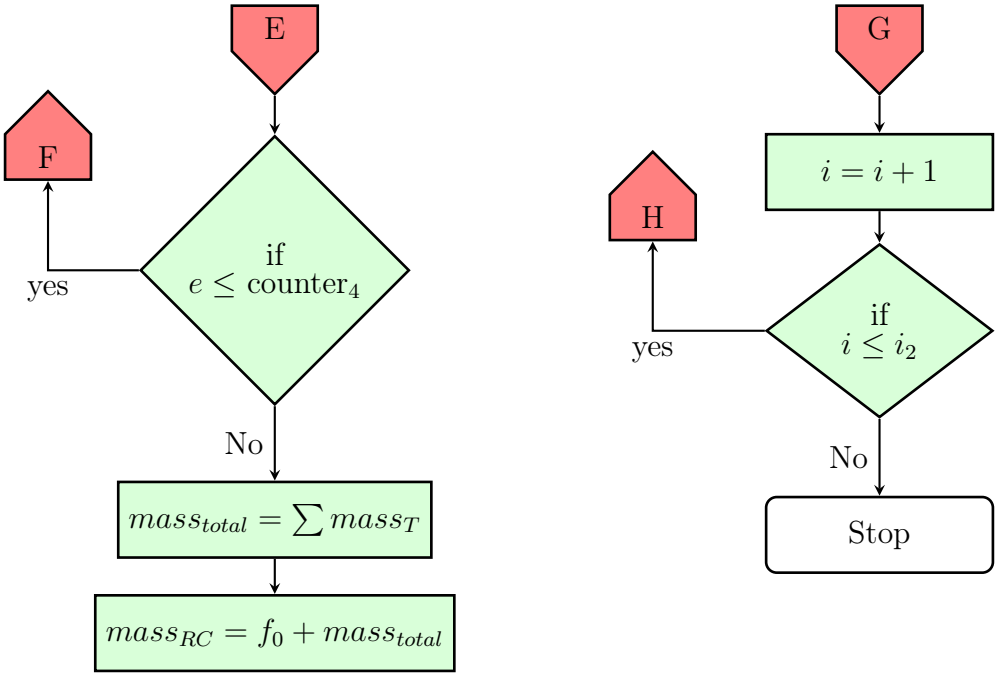

Figure 37.. Expansion region desing procedure

As it is seen in the flowchart, the design of the diverging nozzle is the most meticulous, and it is necessary to be careful in order to avoid any mistake. Some hints are:

- Divide the design into four parts, as presented in this thesis.
- Use the same technique of integration in all the characteristics to avoid any discrepancy between methods; and is recommendable to use the method in its general form as the division between points is not constant.
- Divide the process into functions as it will reduce the time of computation and hence the memory RAM.
- Create a function to calculate the thermodynamic properties as a function of the velocity for applying every time a point is computed.
- Save the data in a matrix and have in mind the number of points created in every procedure because these numbers are necessary for al the design.

For ending the process, the result is presented graphically.

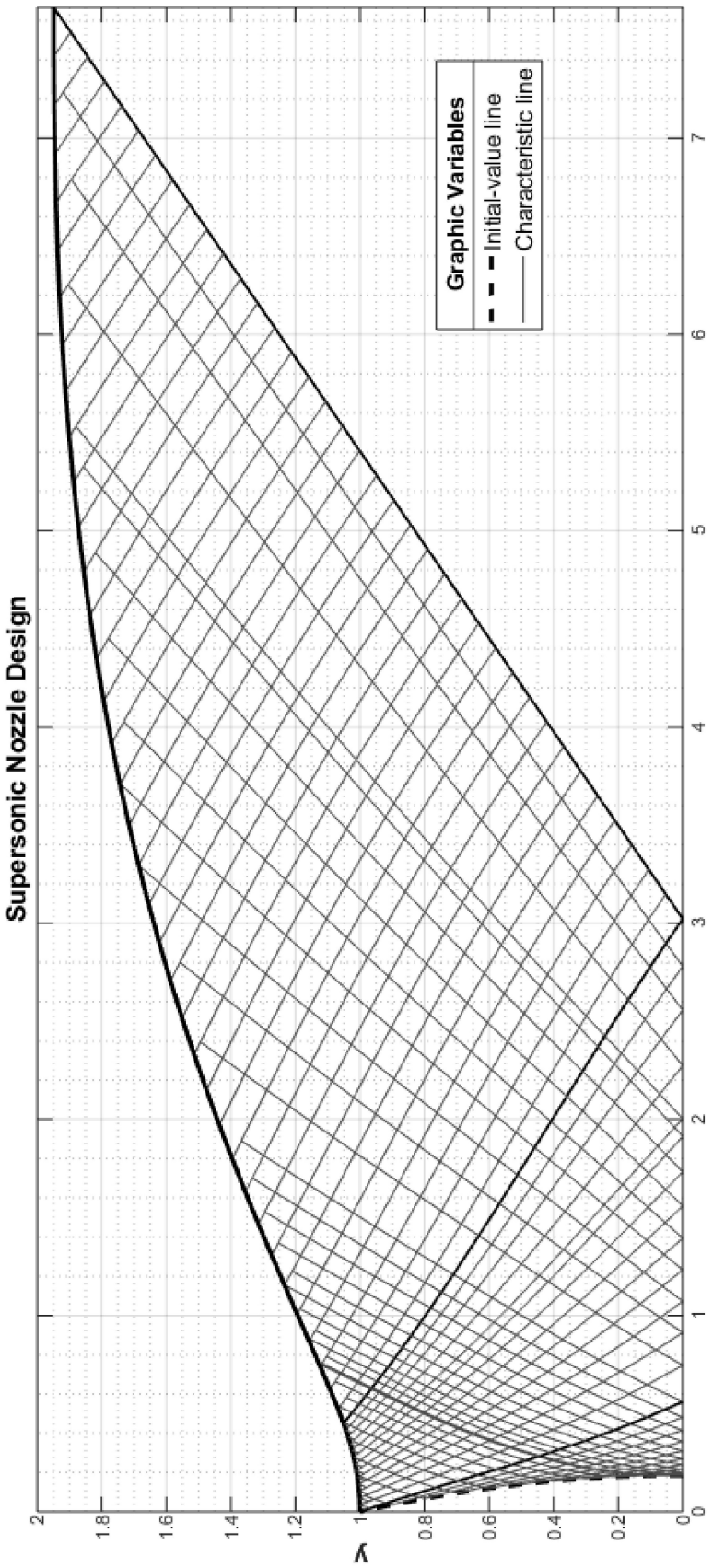

Figure 38.. Diverging nozzle design

4.5 Final results

For the final results, it is convenient to scale all the dimensions by the throat radius; in this way, the resulting flow-field is applicable for similar nozzles with the same area throat. The thermodynamics properties scale directly with the stagnation state, and therefore, the results that will be shown are scaled. Figure 45 shows the coordinates in terms of the nozzle throat.

Figure 45 also shows all the stages of the nozzle design and how they converge to give the shape to the convergent-divergent supersonic nozzle.

There are different types of results that will be shown, the nozzle contour, the total expansion inside the supersonic part and its two-dimensional analysis, the one-dimensional analysis of the nozzle, and a table with the essential parameters.

4.5.1 Validation of the Uniform Flow-field and Two-dimensional Analysis

Analyzing the tow-dimensional nozzle requires to compute the entire flow-field inside the diverging nozzle. For the two-dimensional analysis, only the supersonic part is analyzed, as this analysis does not have a significant contribution to the study.

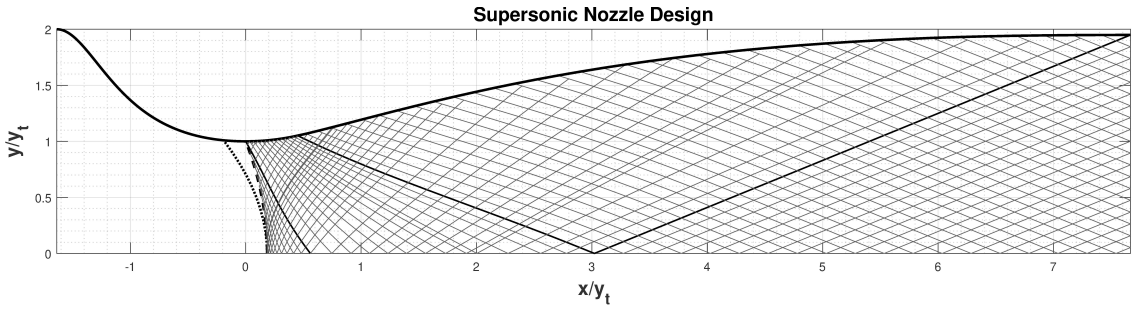

Figure 39.. Complete flow-field inside the diverging nozzle.

The figure above shows the complete expansion of the gas in the limits of the nozzle surface. Analyzing the picture, it is easily seen that the flow after the last

left-running characteristic, is constant, all the exit flow field after this line has the same characteristics as the last point in the kernel over the axis. The space between characteristics is also constant, which gives us an idea of uniformity.

A better understanding of uniformity flow at the exit in a two-dimensional analysis is contributed by plotting all the stored data following two paths, the wall, and the axis. Also, if this two-dimensional data is compared with the one-dimensional, it will be seen that the flow and thermodynamics properties converge in the same point at the exit; this can be checked in figures 40, 41, 42 and 43.

Scaling and plotting the stored data in the diverging section, the graphics for the pressure, temperature, and density are obtained; these properties scale with the stagnation properties. The same way, the Mach number is plotted and scaling with the Mach number of design.

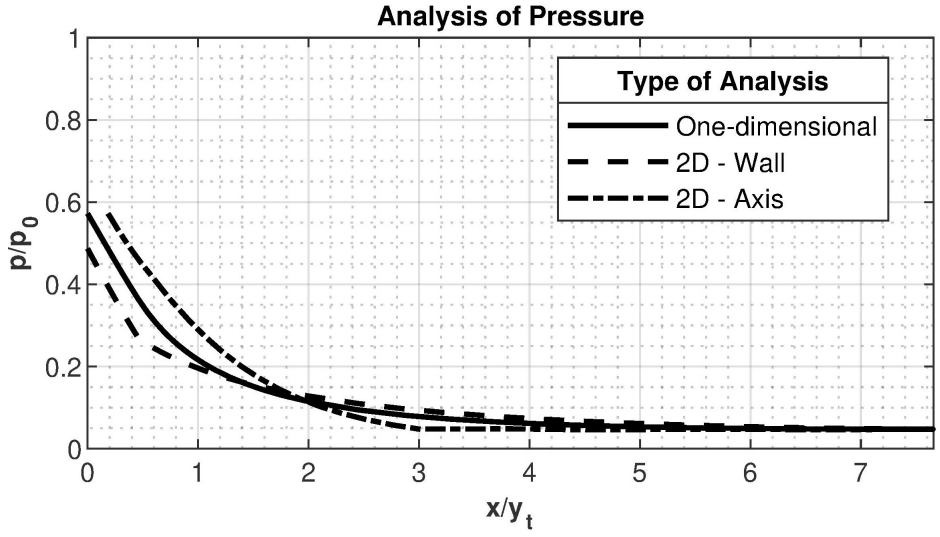

Figure 40.. Two-dimensional analysis of pressure in the supersonic region.

The rest of the values of the flow and thermodynamics properties will be between the wall and axis values, and all of them will converge to produce a uniform flow field in the exit.

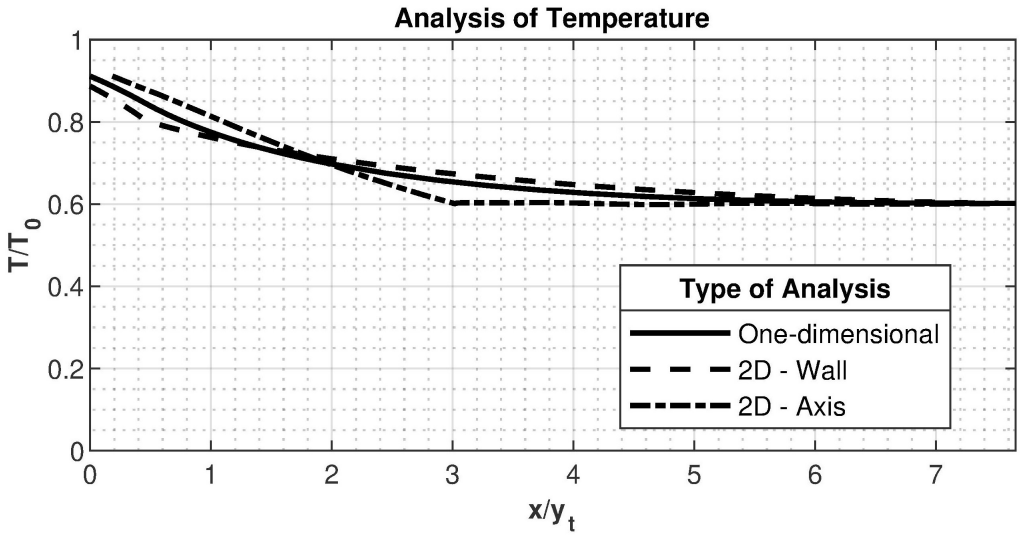

Figure 41.. Two-dimensional analysis of temperature in the supersonic region.

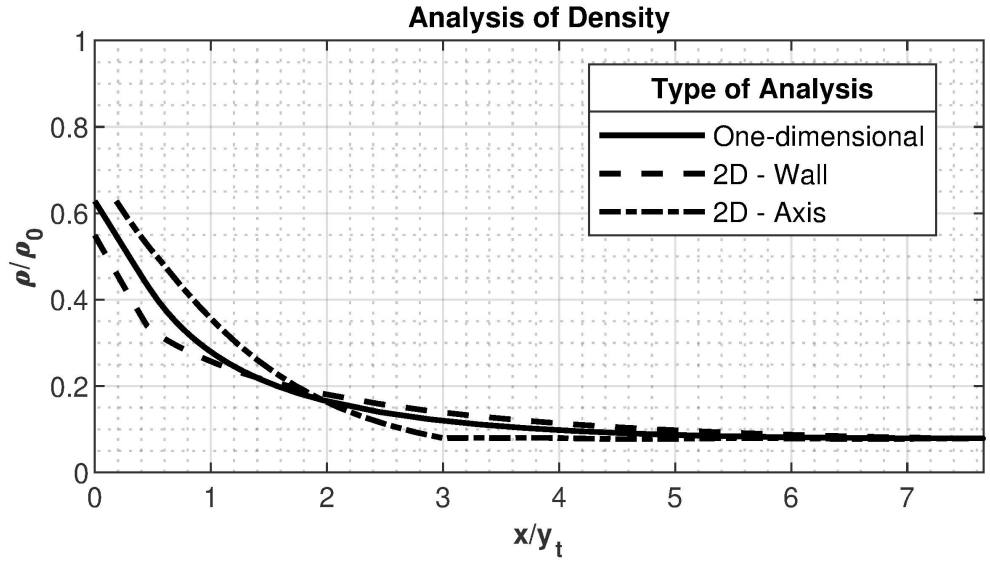

Figure 42.. Two-dimensional analysis of density in the supersonic region.

Another critical analysis is the one-dimensional analysis over all the nozzle contour; this analysis contains the subsonic and the transonic analysis. As both parts were designed separately, the throat values in the subsonic design need to be equal to the values of the throat in the supersonic design.

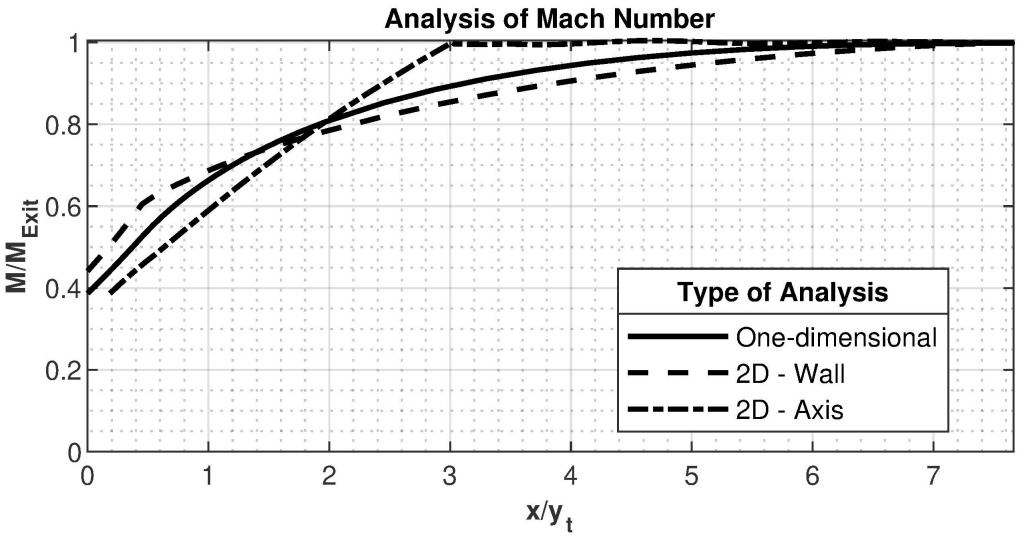

Figure 43.. Two-dimensional analysis of Mach number in the supersonic region.

In figure 44, we see that the solution converges when the subsonic and the supersonic, along with the transonic design, are united as the flow does not have discontinuities.

After the throat section, the flow has two solutions, one subsonic and the another supersonic. How the flow develops after this point depends upon the NPR. The NPR will determinate if the flow exit is subsonic or supersonic. The NPR, of design, is the value present in the supersonic solution; any other value will cause the flow to works either underexpanded or overexpanded.

Other results are:

$$C_D = 0.9943 \qquad C_{fg} = 0.9967$$

$$C_A = 1 \qquad C_v = 1$$

$$\pi_n = 1$$

These overall nozzle results are presented above; the table shows that the property that most easily expands is the pressure, followed by the density and temperature, respectively. Also, it shows that the gross thrust grew up a 28.43% from the throat to the exit. Also, the NPR of design is 21.55, and the NPR critic is

Table 5. General results of the complete design

Results of the general design			
$x\ [m]$	-1.637	0	7.667
$r\ [m]$	2	1	1.9491
$A\ [m^2]$	12.57	3.14	11.93
A/A^*	4	1	3.8
M	0.1498	1	2.58
T/T_{0T}	0.997	0.909	0.599
p/p_{0T}	0.986	0.564	0.046
ρ/ρ_{0T}	0.989	0.62	0.077
NPR		1.016	21.55
$F_{g-actual}[N]$		$2.722 * 10^7$	$3.496 * 10^7$

1.016; values between these NPR, make the nozzle works in an over-expanded mode, values up to the NPR of design makes the nozzle be in an under-expanded mode, for values equal to the NPR critic or smaller will make the nozzle to works as an intake.

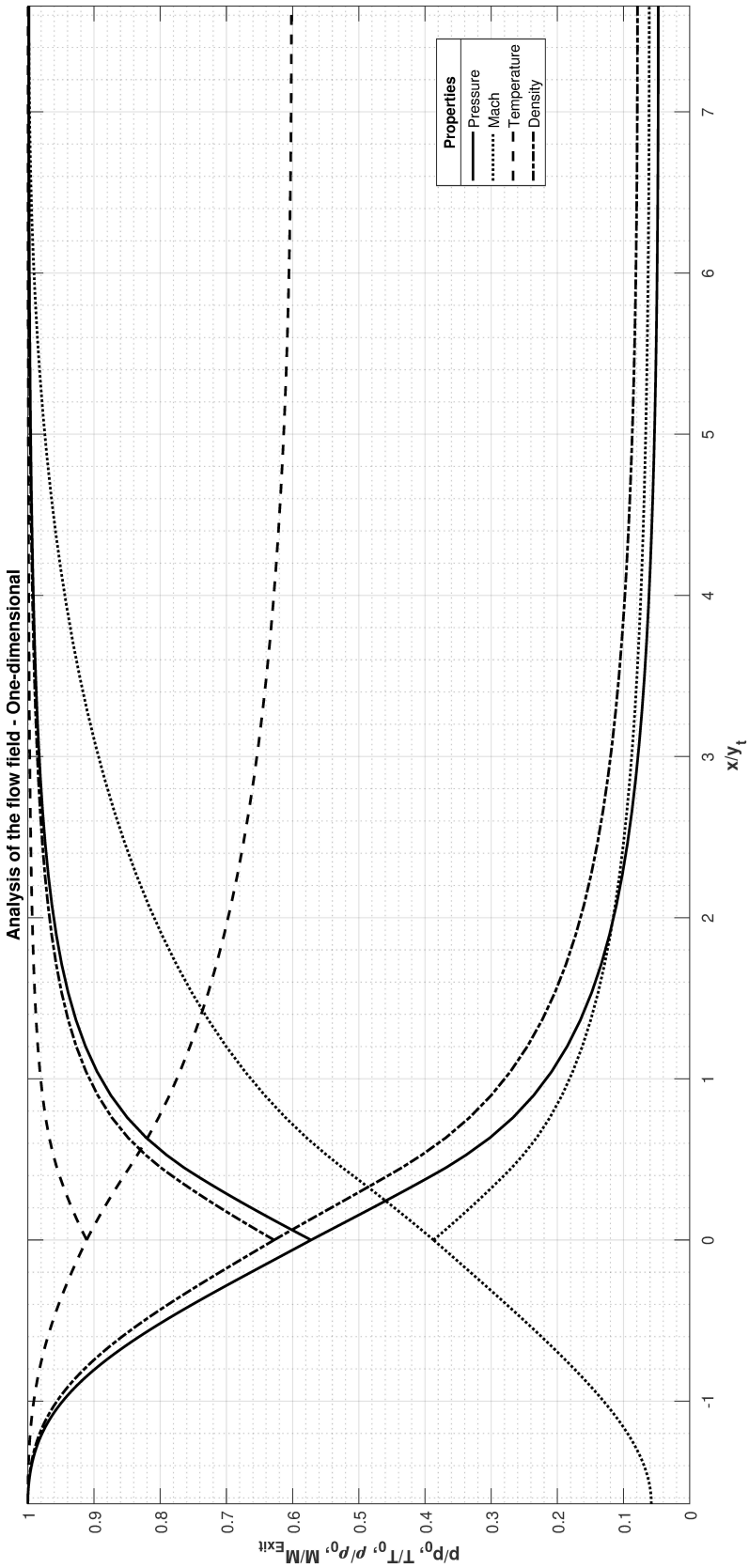

Figure 44.. One-dimensional analysis of the flow field

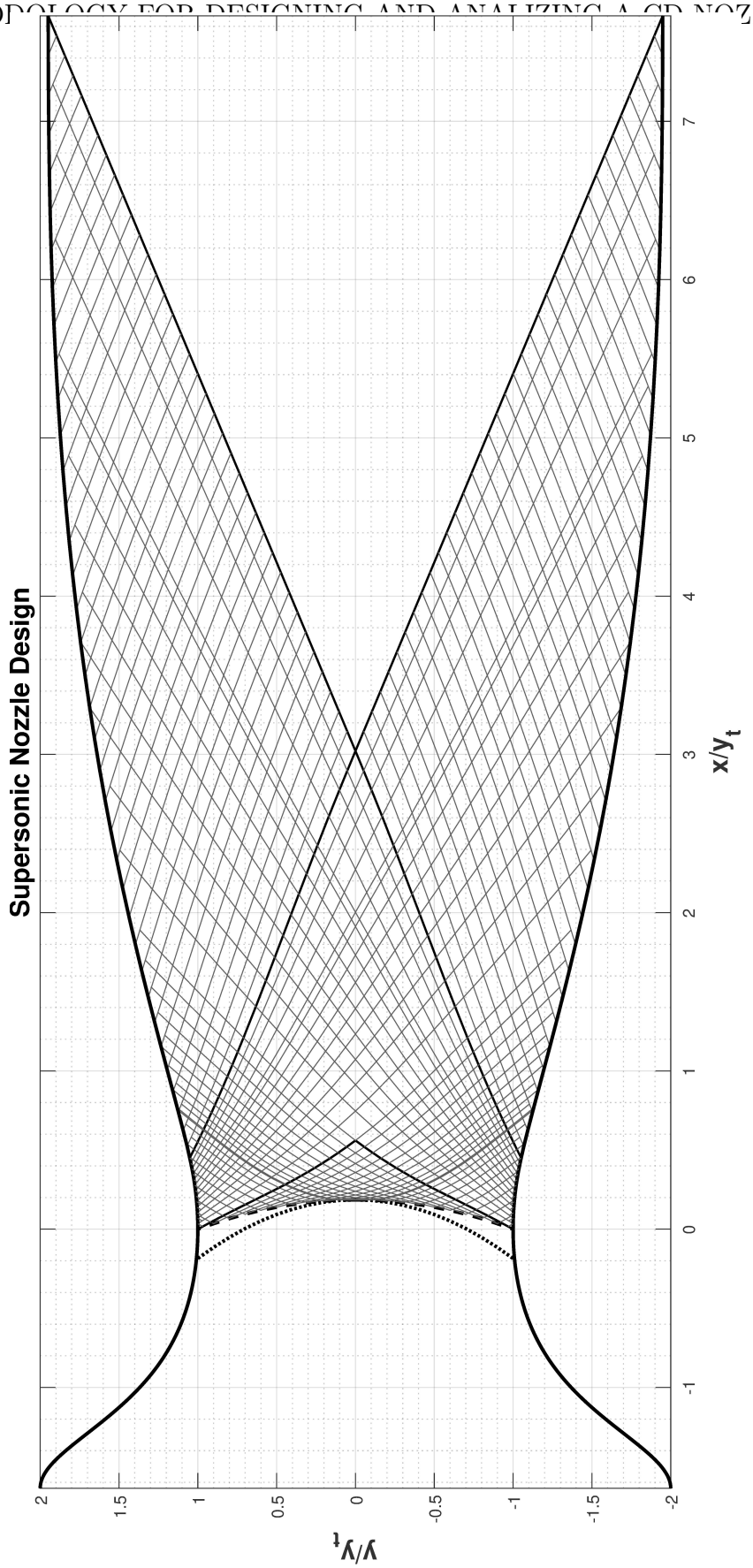

Figure 45.. Convergent-divergent nozzle final design

5. Numerical Simulation in ANSYS-Fluent

A numerical simulation is carried out to compare the methods, the uniformity flow at the exit and the complete expansion. It is hoped that the error between the method does not overcome a 5%.

NOTE: For reading about the governing equations, its discretization, and the ANSYS-Fluent solver techniques, read the appendix D.

5.0.1 Geometry Importation

This is the first step in a CFD simulation, consist of preparing the geometry and create the fluid domain for the CFD simulation. The objective here is to ensure that the geometry is as clean as possible before we create the fluid domain either in or around the body.

However, as the geometry is already created in Matlab, it is just imported. The process consists of printing a .txt file with all the surface points enumerating them and with the z-coordinate matched in zero.

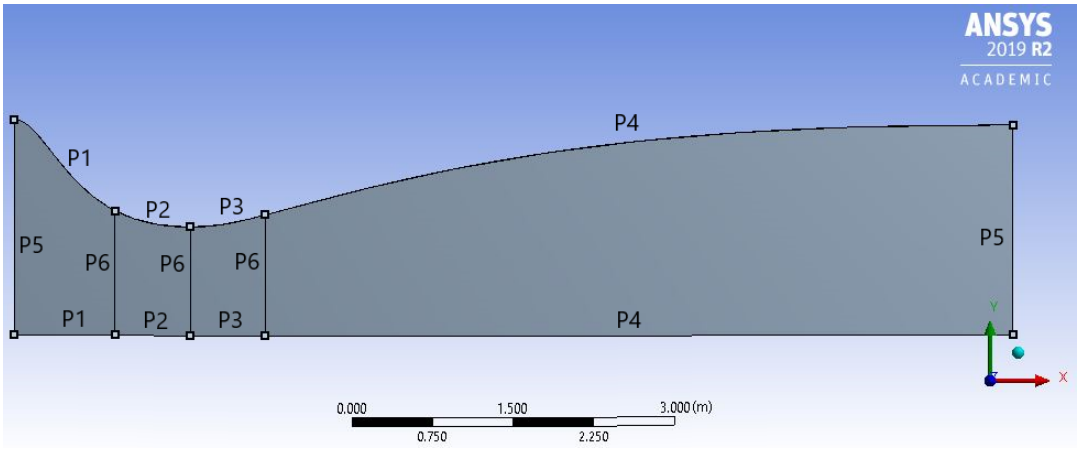

Figure 46.. Geometry and domain for the CFD simulation

Once the geometry is imported, the fluid domain is created inside this contour, with the x-axis as a boundary condition. In the geometry, some FaceSplit and NamedSection can be created for developing the grid, in this geometry, there are three FaceSplit, specifically in the throat, and the others near the throat in the converging and diverging sections respectively in order to refine the grid in the transonic section.

5.0.2 Grid Generation

A numerical simulation requires the subdivision of the domain into several smaller subdomains in order to solve the flow physics within the domain geometry that has been created; this results in the generation of a grid of cells (elements or control volumes) overlaying the whole domain geometry (Tu, Yeoh, & Liu, 2018, pg. 48). The mesh generation constitutes one of the most important steps during the preprocessing stage after the definition of the domain geometry.

It is essential to create a well-constructed mesh because it will have a significant influence on the solution, as the essential fluid flow equations are solved numerically for each of the cells, and hence the discrete values of the flow properties are determined.

The mesh can be structured, unstructured, or hybrid. A single block-structured mesh usually may comprise square elements or hexahedral elements and follow a uniform pattern. The connectivity on this type of mesh is straightforward because cells adjacent to a given elemental face are identified by the indices, and the cell edges form continuous mesh lines that begin and end on opposite elemental faces. An unstructured mesh does not follow a uniform pattern. It is usually comprised of triangle elements or tetrahedron. The cells are allowed to be assembled freely within the computational domain. The connectivity information for each face thus requires appropriate storage in the form of a table. Compared to structured meshes, the storage requirements for an unstructured mesh can be substantially larger. A hybrid mesh is a mesh that contains structured and unstructured portions. The term "mixed" is usually applied to meshes that contain

both elements associated with structured meshes and elements associated with unstructured meshes.

This thesis will carry out a structured grid. For creating the mesh, the geometry was discretized in son SplitFaces covering the subsonic, the transonic and supersonic parts. Edge sizing was created along all the contour; the vertical lines (P5, P6) from subsonic to supersonic have an Edge sizing of 100 elements each. The diverging portion has horizontal Edge sizing of 200 elements (P4), and the other parts, subsonic and transonic has Edge sizing of 50 (P1, P2, P3); thus, generating the mesh in ANSYS:

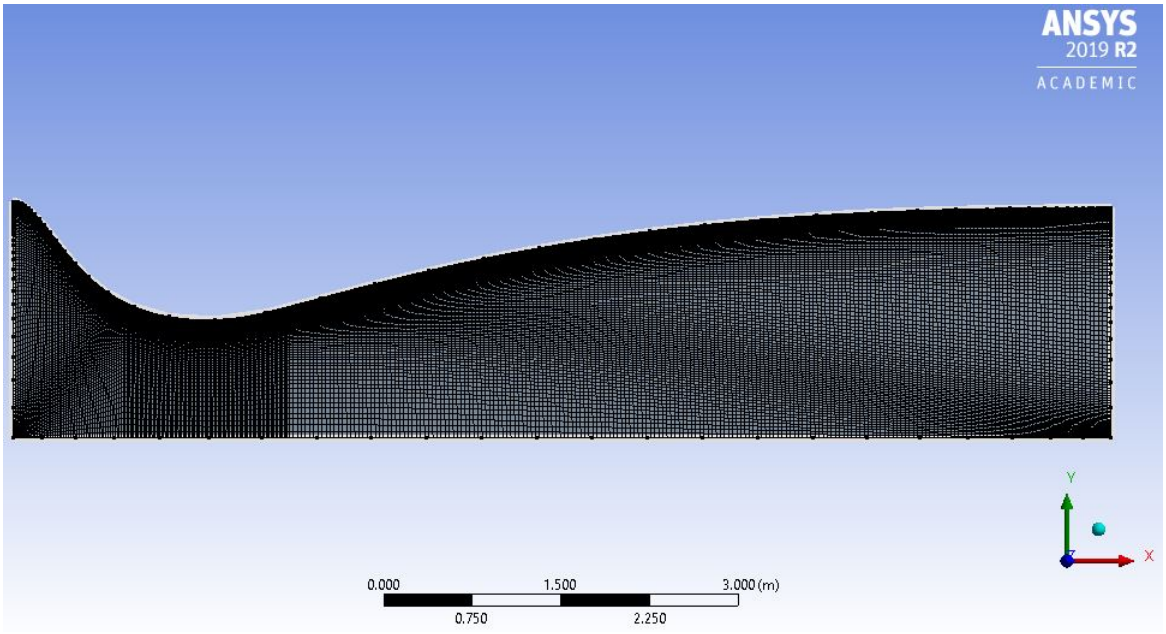

Figure 47.. Structural grid in the domain

5.0.3 Fluent Setup

Once the grid is generated, the input setup in the Fluent software can be put. The general setup includes declaring the type of problem. For this part, the problem is said to be a steady axisymmetric two-dimensional problem, the velocity formulation is absolute, and the solver is pressure-based. The model is isentropic, i.e., adiabatic and inviscid in a static reference frame. In all CFD simulations, the

continuity and momentum equations are solved, however as this problem treats with the compressible flow, the energy equation needs to be solved, and hence the calculation of energy is turned on. Likewise, the fluid is set to be air and an ideal gas with:

$$C_p = 1722.24 \left[\frac{J}{kg}\right]$$
$$Molecular\ weight = 28 \left[\frac{kg}{kmol}\right]$$

The boundary conditions were create in the meshing section and include the x-axis, an inlet, an outlet and the walls.

Inlet The inlet boundary condition is based on the mass flow entering the nozzle with the following boundary conditions:

$$mass_{actual} = 15280.8 \left[\frac{kg}{s}\right]$$
$$p = 6906400 \left[\frac{N}{m^2}\right]$$
$$T = 2993.3\ [K]$$

Outlet The outlet boundary condition is based on the pressure in the exit of the nozzle; the backflow pressure specification is set to be static pressure.

$$p = 324886.7 \left[\frac{N}{m^2}\right] \qquad T = 1798.43\ [K]$$

The operating pressure is set to zero because it is irrelevant for flows at high Mach numbers.

The reference values used for computing normalized flow field variables are match in the outlet section. It also allows to specify the reference zone for postprocessing relative velocities in moving-zone problems; this reference zone will be the flow inside the domain predefined.

$$\rho = 0.6294 \left[\frac{kg}{m^3}\right] \qquad p = 324886.7 \left[\frac{N}{m^2}\right]$$
$$T = 1798.43\ [K] \qquad V = 2034.41 \left[\frac{m}{s}\right]$$
$$\gamma = 1.2$$

The solutions method, as mentioned before, is for solving the discretized equations, a second-order upwind, and a coupled scheme for the pressure-velocity coupling.

The method of initialization is standard and it is computed from the inlet with the variables:

$$\rho = 0.6294 \left[\frac{kg}{m^3}\right] \qquad p = 6906400 \left[\frac{N}{m^2}\right]$$

$$T = 1798.43 \, [K] \qquad V = 152.1 \left[\frac{m}{s}\right]$$

$$\gamma = 1.2$$

After all of these data are matched in the input setup of ANSYS-Fluent, the calculation can be initialized for a determinate number of iterations; for this simulation, this number will be 500.

5.0.4 Results

For the numerical simulation, it is necessary to focus on getting from the post-processing the same results obtained from the Matlab code in order to compare both methods. Consequently, the results obtained from the simulation CFD are the two-dimensional analysis of the flow and thermodynamic properties and its contour that is a plot with color bands that represents discrete colored regions of the plotted variable.

Pressure

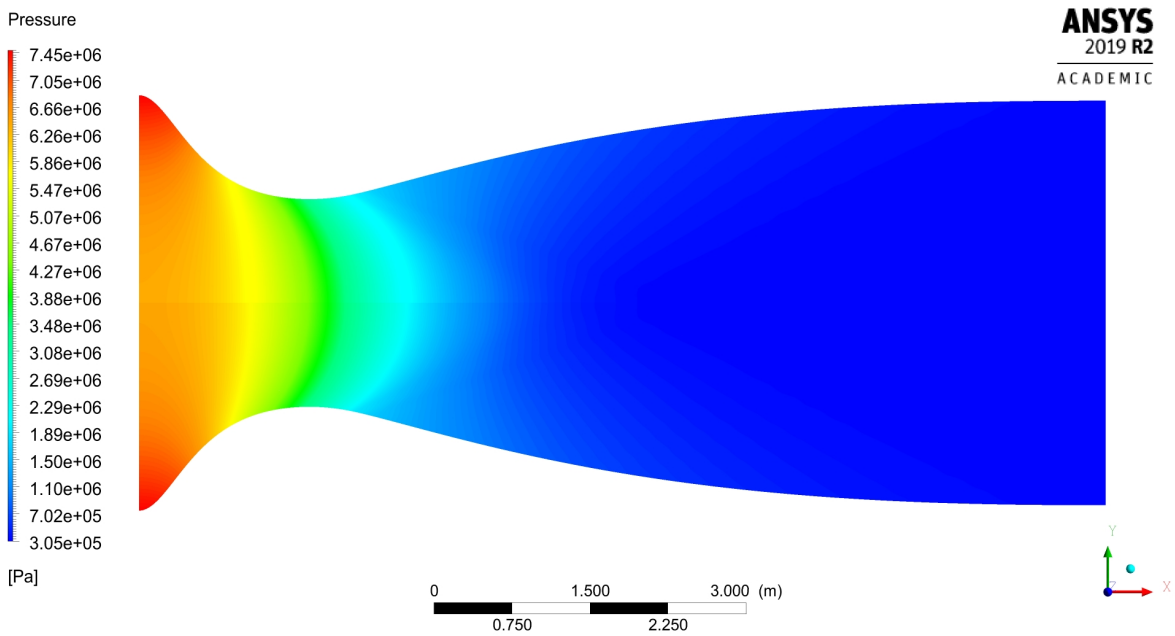

Figure 48.. Contour of the pressure distribution

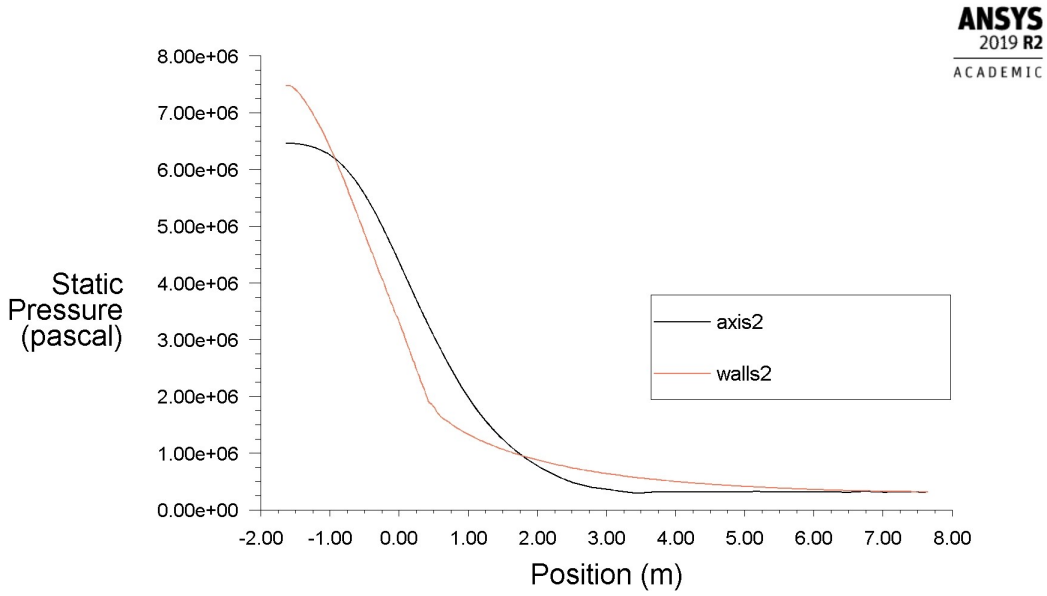

Figure 49.. Pressure distribution on the CD nozzle

Temperature

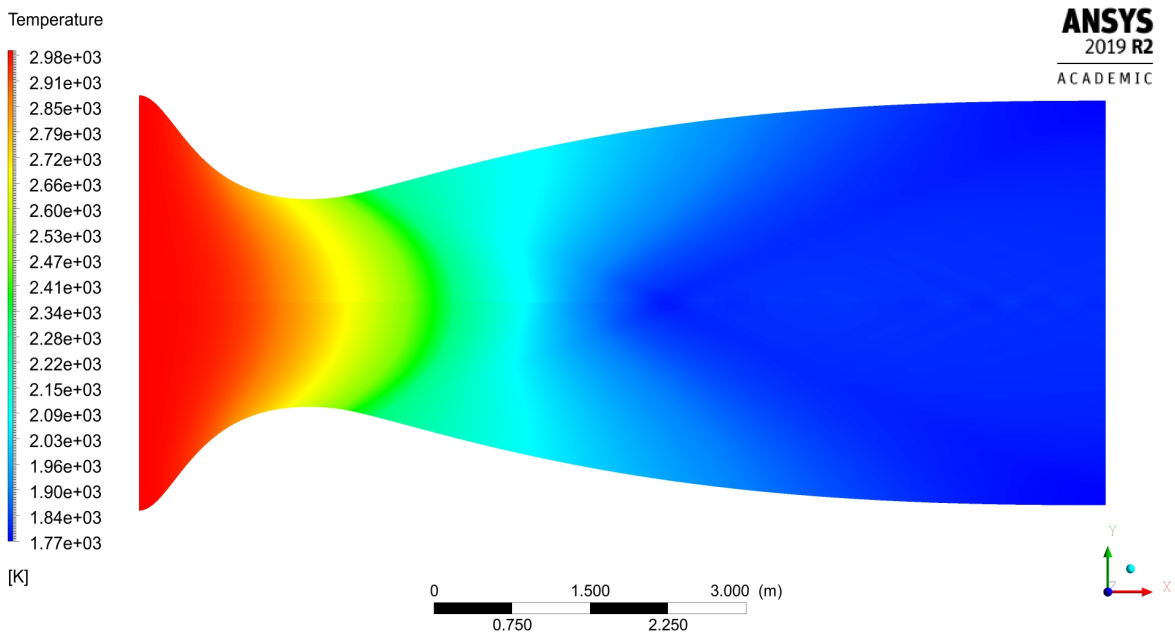

Figure 50.. Contour of the pressure distribution

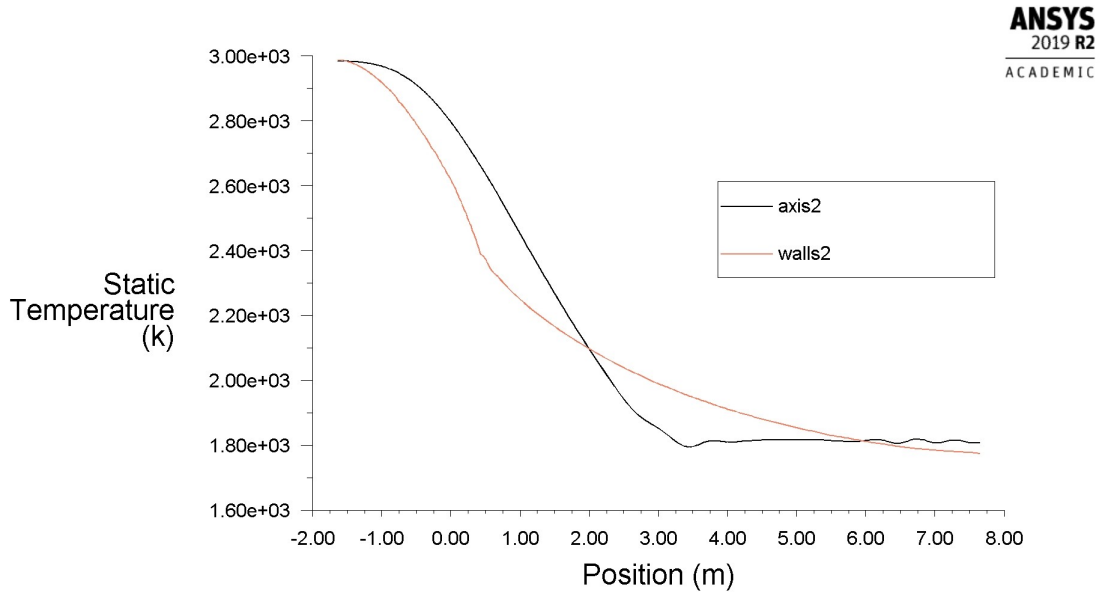

Figure 51.. Pressure distribution on the CD nozzle

Density

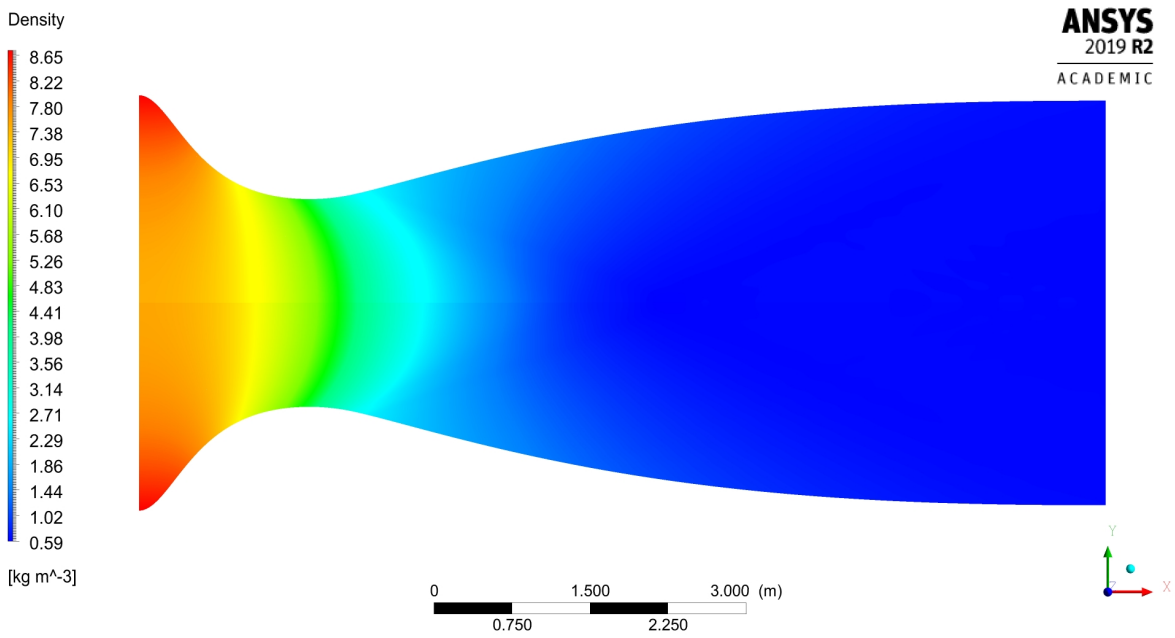

Figure 52.. Contour of the pressure distribution

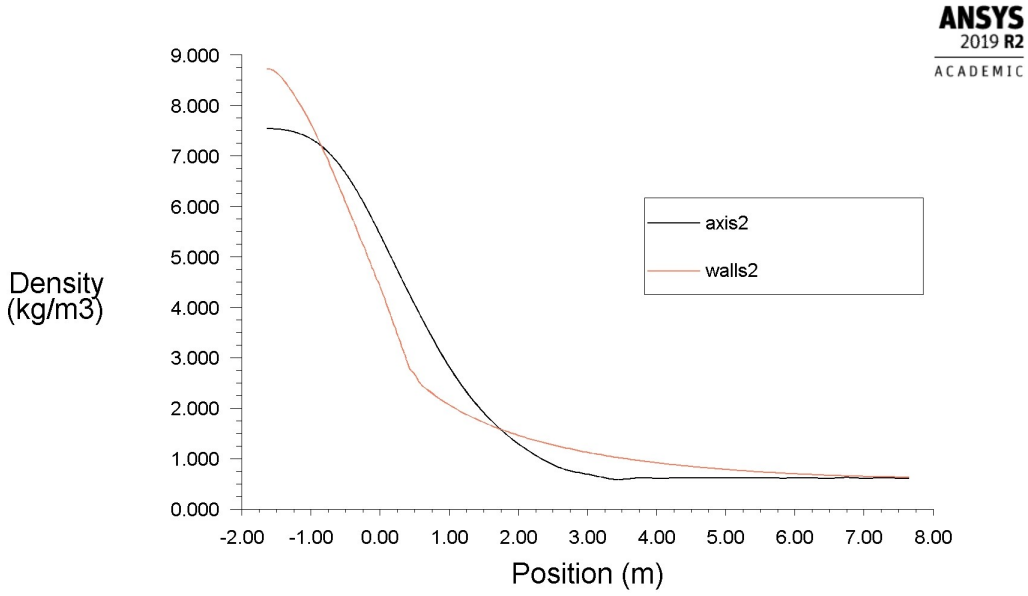

Figure 53.. Pressure distribution on the CD nozzle

Mach number

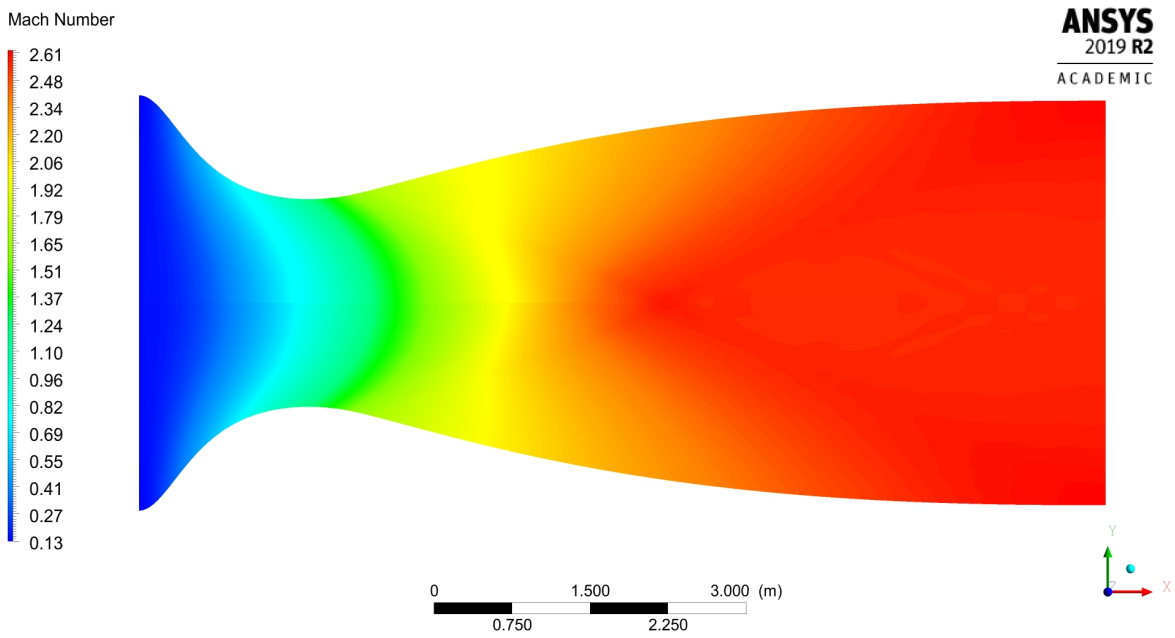

Figure 54.. Contour of the pressure distribution

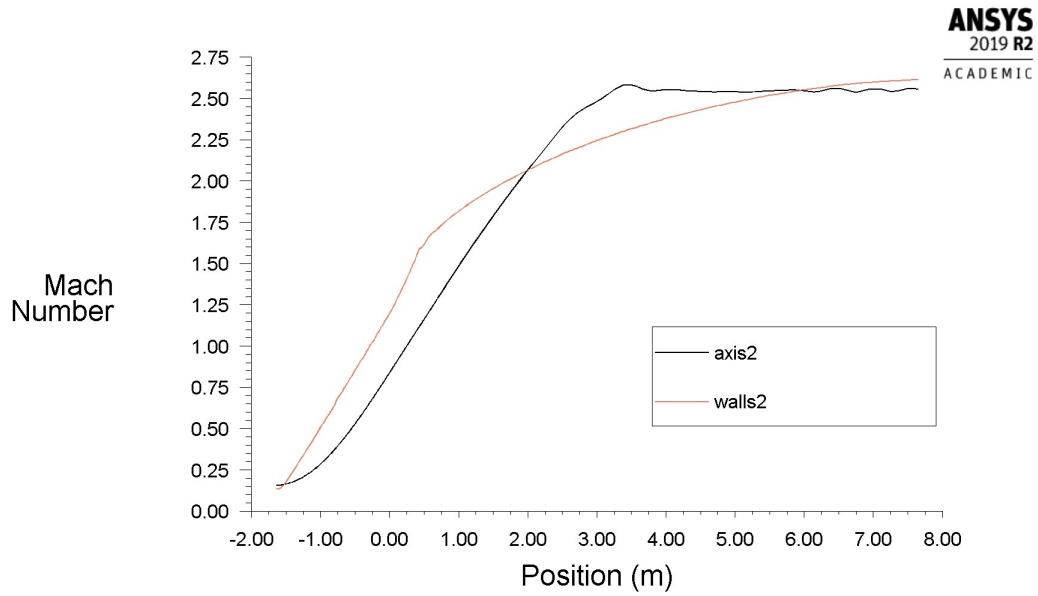

Figure 55.. Pressure distribution on the CD nozzle

The table above shows the maximum and minimum values of the properties that will be used to make a comparison between both methods, the finite volumes of ANSYS-Fluent and the finite differences of the Method fo characteristics.

Table 6. Maximum and minimum values of the numerical simulation results

Maximum and minimum thermodynamics and flow-field properties					
Value	Temperature $[K]$	Pressure $\left[\frac{N}{m^2}\right]$	Total Pressure $\left[\frac{N}{m^2}\right]$	Density $\left[\frac{kg}{m^3}\right]$	Mach number
max	2987.86	$7.49 * 10^6$	$7.59 * 10^6$	8.73	2.62
min	1771.77	$3.05 * 10^5$	$6.56 * 10^6$	0.59	0.14

The charts form figures 49, 51, 53 and 55 shows the two-dimensional analysis of the properties along both the wall and axis. In every chart, at the axis, the value change from the inlet until it arrives at the location of the last point of the kernel design, which is in the coordinate $x = 3; [m]$. On the other hand, the properties have a continue variation along the wall. Both cases mentioned can be corroborated also in the contours from figures 48, 50, 52 and 54 respectively. If we follow the x-axis in the contours, at a distance of three meters, the property measured maintain constant until the axis contrary to what happened in the wall that the property varies along all the distance, from inlet to the outlet.

Although a bit discrepancy in the behavior of the nozzle concerning the wall and the axis is expected, the important thing is that both sides converge to have uniformity in the exit flow, that is the crucial thing of this design.

Last, concerning the values of table 6, the difference between the minimum and maximum of the flow thermodynamics properties except for the total pressure, occurs from the inlet having the maximum values to the exit with the minimum ones.

5.0.5 Validation of the Numerical Simulation Convergence

Since all fluid flow problems are highly nonlinear, computational fluid dynamics (CFD) solutions must be calculated, and hence as it is a numerical

approach, obviously utilize a finite number of grid points making the process iterative. Such numerical solutions are subject to truncation error, due to neglect of the higher-order terms in Taylor's Series. Moreover, because all digital computers round off each number to a specific significant figure, the flow field calculations are also subject to roundoff error.

By refining the grid, the truncation error is reduced. However, the number of steps required to calculate a particular variable is correspondingly increased, therefore increasing the round-off error. Therefore, the total numerical error is a function of how refined is the mesh. It means that there is an optimum value of several elements or cells, at which maximum accuracy is obtained.

Since the point at which the analysis is deemed converged is defined by the judgment of the analyst, a solid understanding of when the analysis has reached its final solution is necessary. Typically, several things are necessary to check before the results of the simulation can reliably be considered. These things to validate the convergence of the solution are:

- Residual RMS error values have acceptable values.
- The variable values of interest have reached a steady solution.
- The domain has imbalances of less than 1%.
- Mesh independence.

Residual RMS error values

Residual RMS error values are one of the most fundamental measures of an iterative solution convergence, as it directly quantifies the error in the solution of the system of equations. In a CFD analysis, the residual measures the local imbalance of a conserved variable in each control volume. Therefore, every cell in your model will have its residual value for each of the equations being solved. In an iterative numerical solution, the residual will never be precisely zero.

For CFD, RMS residual levels of 1E-4 are considered to be loosely converged, levels of 1E-5 are considered to be well converged, and levels of 1E-6 are considered to be tightly converged. For complicated problems, however, it is not always possible to achieve residual levels as low as 1E-6 or even 1E-5.

For the example above, the residual RMS error convergence is:

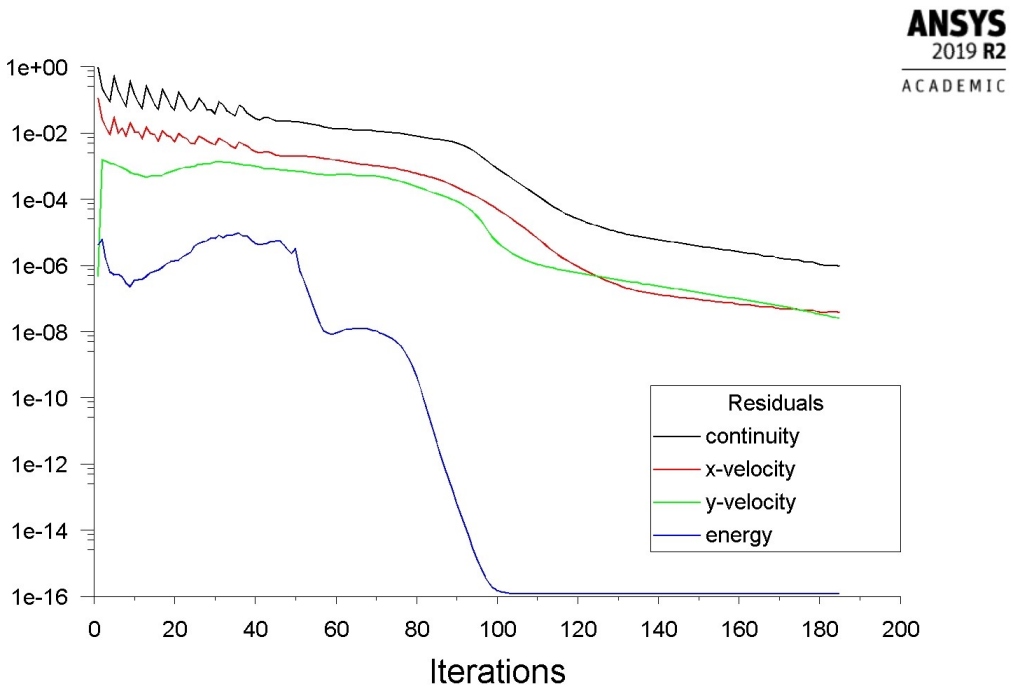

Figure 56.. Error of the flow equations in CFD simulation

Although the input value of iterations in the input setup of ANSYS-Fluent was matched as 500 iterations, the solution stopped at 185 iterations with convergence in the residual RMS error values of:

$$Continuity : 9.5650E-7 \qquad x-velocity : 3.6934E-8$$

$$Energy : 1.2523E-16 \qquad y-velocity : 2.5860E-8$$

Steady solution for variables of interest.

For a steady flow problem, the solution field should not change iteration to iteration for a converged analysis. For ensuring that the solution has reached a

steady-state, the average pressure and temperature, and the maximum Mach number are monitored.

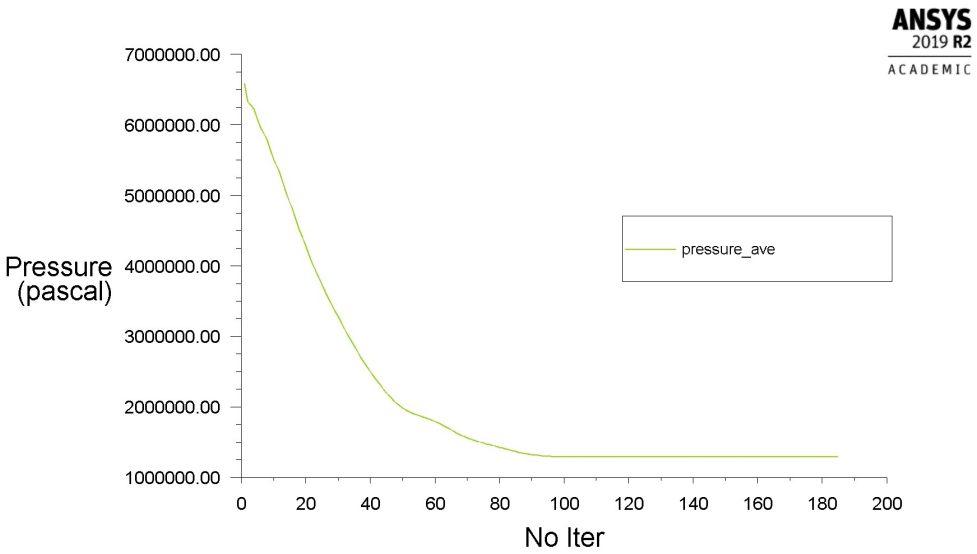

Figure 57.. Steady state reached in the average pressure

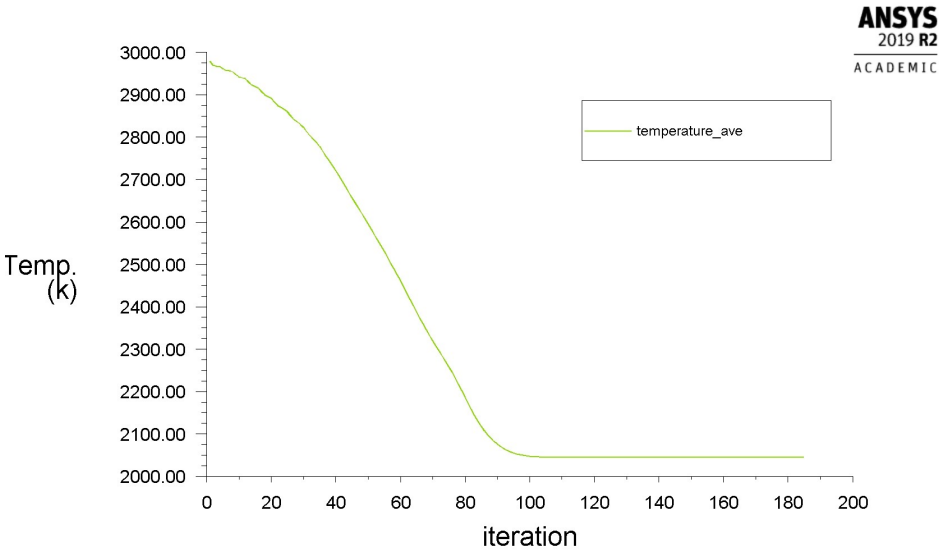

Figure 58.. Steady state reached in the average temperature

The figures above show that the variables of interest reached a steady state in the solution of the simulation. Therefore, the solution converged in reaching steady states in the different variables calculated.

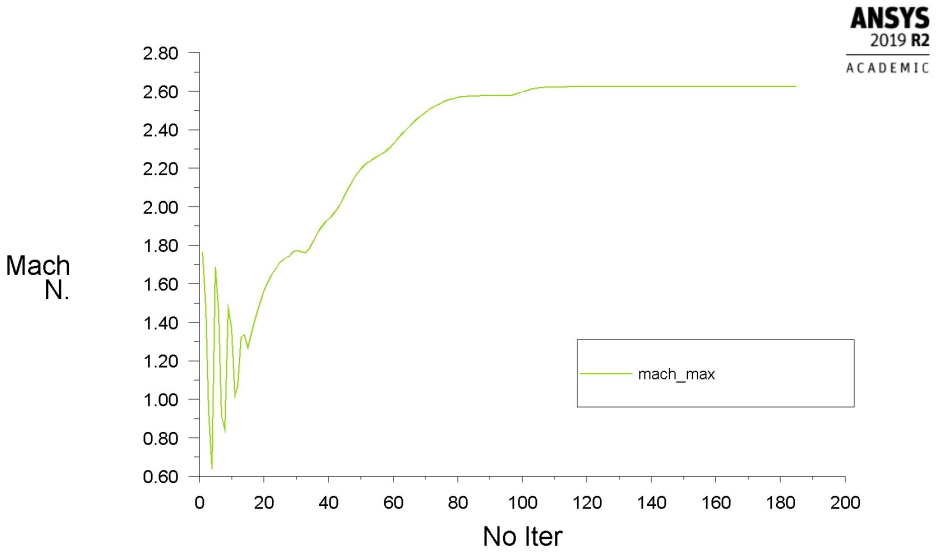

Figure 59.. Steady state reached in the maximum Mach number

Imbalances

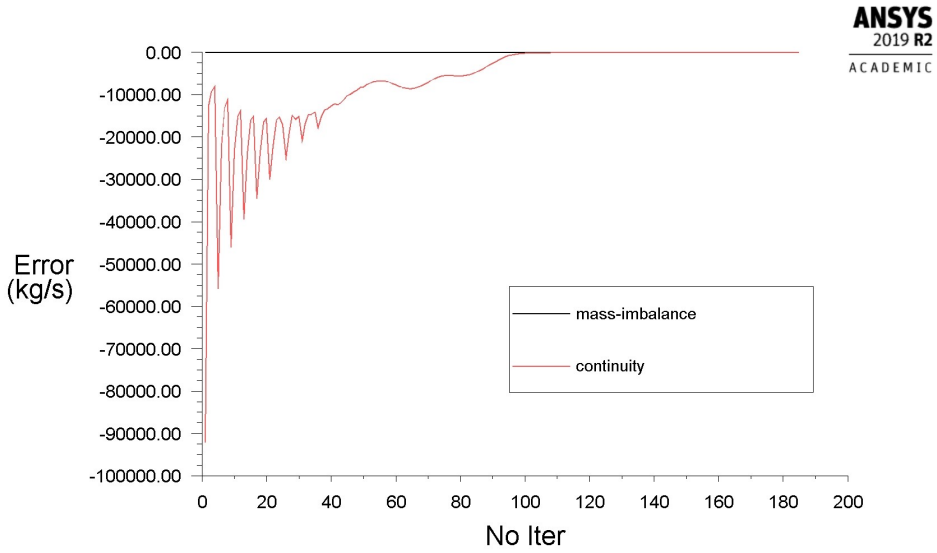

Figure 60.. Imbalance and difference in mass between inlet and outlet

As the numerical simulation of compressible flow works with the conservation equations, it is necessary to ensure that the final solution conserves these quantities. These imbalances will never be precisely zero, as it is a numerical

approach. However, the imbalances should be sufficiently small before considering the solution converged.

The mass imbalance is zero since the beginning of the solution, and indeed, if the difference between the mass entering and the mass leaving the nozzle is measured in every iteration, it gradually decreases as the solution progresses. As it approaches zero, then the imbalance is less than 1%, and it represents the criteria of convergence.

Mesh independence

The convergence outlined above is for a single solution for a mesh defined randomly, and although the solution has converged based on RMS Error values, monitor points, and imbalances, it is crucial to make sure that the solution is also independent of the mesh resolution. Not checking this is a common cause of erroneous results in CFD, and this process should be carried out always, so the results will be reliable.

For carrying out the mesh independence, the first step is to run the initial simulation in the initially chosen mesh and ensure the convergence. Once the converged solution is obtained, it is necessary to parameterize the number of elements as a function of the Edge sizing declared before in the grid generation. Also, another variable needs to be parameterized.

For the mesh independence study in this example, the Edge sizing of the discretized regions in the grid was parameterized as an input variable, and the velocity in the x-direction in conjunction with maximum Mach number, the average temperature, the minimum temperature, and the minimum pressure was parameterized as the output.

After the parameters are declared, the following step is to create different design points where the input parameters are changed to give different responses to the output parameters. In ANSYS, there is a table that is necessary to fill, and it looks like the table below.

In this case, seven more design points were created and executed. The RAM and time consuming can be large, which depends on the computer where the design

Table 7. Input and output parameters in the design points created in the ANSYS Workbench

Table of design points

Design Point	Input parameters			Output parameters		
	Edge sizing 1 (P1, P2, P3)	Edge sizing 2 (P4)	Edge sizing 2 (P5, P6)	$N_{Elements}$ (P22)	Temperature [K] (P24)	x-Velocity $\left[\frac{m}{s}\right]$ (P25)
Dp_3	80	320	160	90000	2045.7	2051.3
Dp_2	70	280	140	68960	2045.7	2051.4
Dp_1	60	240	120	50720	2045.7	2051.6
Dp_0 (Current)	50	200	100	35280	2045.7	2051.7
Dp_4	40	160	80	22640	2045.7	2051.7
Dp_5	30	120	60	12800	2045.8	2051.6
Dp_6	20	80	40	5760	2045.8	2050.8
Dp_7	10	40	20	1506	2046.1	2048.8

is being carried out. After all the design points have achieved its solutions, a parameter parallel chart can be created in ANSYS showing the input and outputs, and how to differ from each other in its values from the maximum value (upper line) to the minimum (lower line).

In the figure 61 can be seen the initial design point that represents the black line and that in the output parameters average temperature (P24), the maximum Mach number (P26), the minimum temperature (P28) and in the x-maximum velocity the values are almost the same except the pink line that diverges of the rest of solutions. In the average pressure (P27), it is not at all deviated from the solution. The number of elements is represented by (P22).

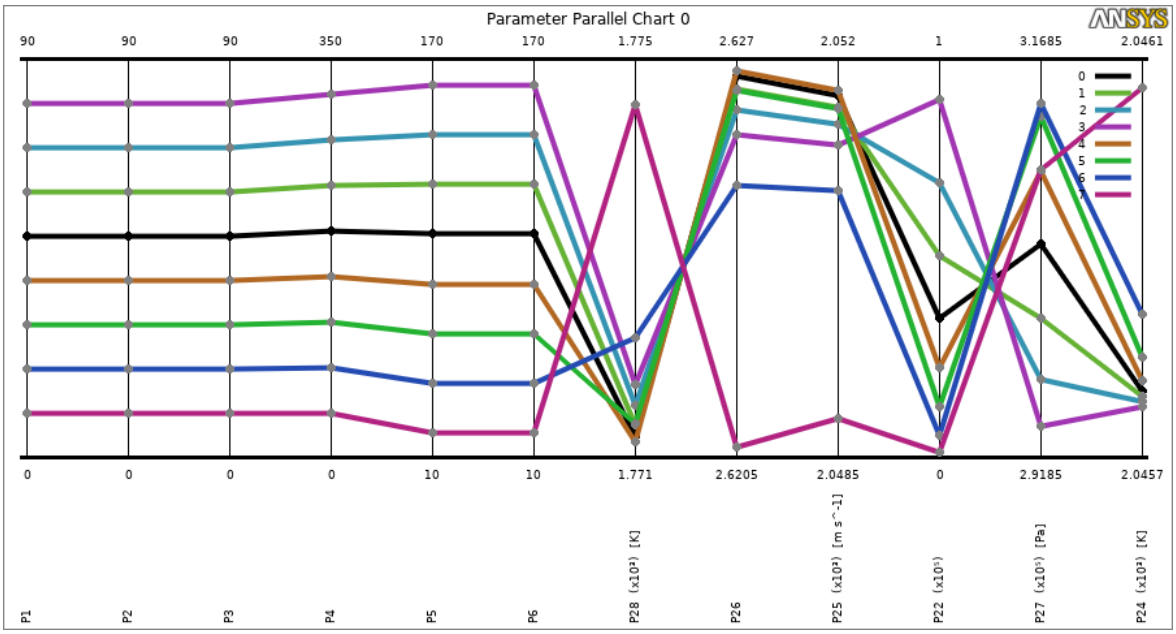

Figure 61.. Parameters parallel chart.

Plotting any of the variables, in this case, the velocity, the optimum number of cells is evident. It will be a point where the solution has almost a constant value in its neighborhood. Out of this neighborhood, the value will vary by either the truncation error because the cell number is less than the adequate or the round-error because the amount of the cell is higher than the optimum.

The figure 62 shows that the initial design point (the yellow point in the graphic) would not have the optimum number of cells as it is at two positions more

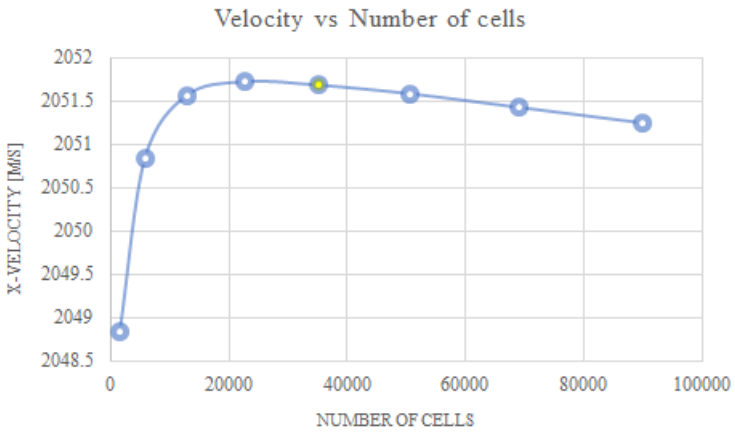

Figure 62.. Maximum axial velocity vs Number of cells

than the ideal value that is the third value when the truncation and round error find an equilibrium. However, this design point works as it is not so far from the ideal point, and the round error will not have a significant consequence in the results. Recalculate all with the ideal value of cells, would be a waste of memory for the computer.

6. Validation of Results

Validating the results require to have a point of comparison. That point will be the result properties at the exit of the nozzle from the Method of characteristics and the results from the ANSYS-fluent numerical simulation.

Results at the exit from the MoC.

$$T_{exit} = 1798.4\ [K]$$
$$p_{exit} = 324886.7\ \left[\frac{N}{m^2}\right]$$
$$\rho_{exit} = 0.629\ \left[\frac{kg}{m^3}\right]$$
$$M_{exit} = 2.58$$

Results at the exit from the Numerical simulation.

Some new results can be obtained from the numerical simulation in ANSYS-Fluent that will help to corroborate the uniformity of the flow at the exit. These data are:

- *Average values*

$$T_{exit} = 1792.5\ [K]$$
$$p_{exit} = 324380.94\ \left[\frac{N}{m^2}\right]$$
$$\rho_{exit} = 0.630\ \left[\frac{kg}{m^3}\right]$$
$$M_{exit} = 2.59$$

- *Standard deviation* The standard deviation is computed in ANSYS-Fluent using the mathematical expression below:

$$\sigma = \sqrt{\frac{\sum_{i=1}^{n}(x - x_0)^2}{n}}$$

The values of the standard deviation in the outlet section of the nozzle are:

$$\sigma_T = 14.83\ [K]$$
$$\sigma_p = 1294.3\ \left[\frac{N}{m^2}\right]$$
$$\sigma_\rho = 0.007\ \left[\frac{kg}{m^3}\right]$$
$$\sigma_M = 0.026$$

- *Uniformity index* The uniformity index represents how a specified field variable varies over a surface, where a value of 1 indicates the highest uniformity. The uniformity index can be weighted by area or mass: the areaweighted uniformity index captures the variation of the quantity, whereas the mass-weighted uniformity index captures the variation of the flux. Here the area-weighted was computed for a specified flow variable ϕ using the expression:

$$\gamma_a = 1 - \frac{\sum_{i=1}^{n}\left[\left(\left|\phi_i - \bar{\phi}_a\right|\right) A_i\right]}{2\left|\bar{\phi}_a\right| \sum_{i=1}^{n} A_i}$$

Where the mean value of the variable is:

$$\bar{\phi}_a = \frac{\sum_{i=1}^{n} \phi_i A_i}{\sum_{i=1}^{n} A_i}$$

The values of the area-weighted uniformity index in the outlet section of the nozzle are:

$$\gamma_T = 0.997$$
$$\gamma_p = 0.999$$
$$\gamma_\rho = 0.996$$
$$\gamma_M = 0.996$$

As can be seen, the uniformity index confirms that the flow is uniform since the maximum value of the index is one. Another measure is the standard deviation, in every value of these, the values deviate one to another from the average value by very little, that digit has not a significant relevance as the values of the properties are considerable, and its deviations are small.

Having in mind that the exit flow in the CFD simulation is uniform, the error between the average values of the properties and the values at the exit from the MoC analysis can be computed. The calculation of the error between both values is made with the equation:

$$Error = \frac{MoC\ resuslt - Simulation\ result}{MoC\ result} * 100\% \tag{6.1}$$

$$Error_T = 0.33\%$$

$$Error_p = 0.16\%$$

$$Error_\rho = 0.16\%$$

$$Error_M = 0.38\%$$

These flow error and thermodynamics properties between both methods corroborate that the design works and is reliable and that one of the specified objectives has been achieved as it was expected an error between 1-5%.

7. Conclusion

Contributions to the Original Work

The derivation of the method of characteristics from the basic concepts of fluid mechanics was taken step by step; It shows how to reach the differential equation of potential flow from these concepts. Once being here, the equations of direction and compatibility of the characteristic lines were obtained. Likewise, it was showed the way that these equations are discretized and its implementation through the Modified Euler predictor-corrector algorithm in the solution of a complete, steady, isentropic, and supersonic flow through a nozzle.

Concerning the methodology, it consists of a general flowchart that is communicated at the time with three more blocks that represent flowcharts of the second level for the design of the subsonic, transonic, and supersonic stages, respectively. The supersonic stage is divided into three other blocks of the third level that perform the initial-value line extends, the kernel design and the turning section design.

In total, there were four predefined processes, each of them with its first level flowchart since they are separated process. These processes are the cases of application of the MoC and the Bisection algorithm of computation.

The sum of the seven flowcharts, along with the other four of the predefined process is equal to the algorithm for programming in Matlab in the design of CD nozzles.

This is the first dissertation where the Vitoshinsky formula is applied along with the Sauer method and the MoC, as usually, the design of supersonic nozzles only shows the transonic and supersonic design. In general, this thesis is the only that shows the union of the three stages, convergent, transonic, and supersonic.

For the example carried out that has a throat radius of one meter, the nozzle reached a length of 9.304 meters. That kind of nozzle was the turning section needs to produce an axial uniform flow that is usually that long. However, this kind of nozzle is used in wind tunnels. For this example, the Matlab code took until 50 min in solving, depending on the requested results.

The numerical simulation showed that the nozzle has a uniform exit flow with uniformity indexes of 0.99, being one uniform.

The axisymmetric two-dimensional flow has the same behavior in either the numerical simulation results or the graphical analysis of the MoC.

The numerical simulation convergence was corroborated through the assessment of the error RMS of the conservation equations as it gave below of 10E-6, the reached stability of the average temperature and pressure, and the maximum Mach number, and the assessment of the imbalances with the error below 1%.

The independence of the mesh was validated through a graphical analysis of several elements vs. the minimum velocity. The data were taken from the simulation of seven design points that took approximately 45min running.

Finally, the error between the results of both methods, the method of characteristics, and the finite volumes of ANSYS-Fluent were inferior to 1%.

Significance of the Contributions

The meaning of the contributions of this thesis lies in the ease that is given to future works. This includes the conceptual part because, due to the number of references accessed, it is considered as a bibliographic reference work and will function as a base and a tool for all works focused on propulsion.

On the other hand, it is always essential to have a reference point, and as the design presented here is ideal, it is an excellent example to compare with similar, more realistic designs. Finally, the methodology of following a step by step simplifies everything, and from that, you can study cases that occur in the nozzles, such as when it works over and underexpanded mode.

Further Work

One of the work purposes is to consolidate a bibliographic reference that serves as the basis for future work. Some of the ideas that were born throughout the development of this thesis and that can be worked on in the future are:

Work on slightly more realistic designs, taking into account the total pressure drop that occurs due to viscosity effects.

Calculate boundary layer formation and apply corrections due to contour

Modify and derive the method of the characteristics for rotational flow, this has already been working, and its research is a matter of study.

Create a user-friendly graphic interface to make the nozzle design faster.

Work with the nozzle non-uniform inlet conditions since, for years, it has been known that this causes a small percentage of turbulence at the exit of the nozzle.

Work with different methods of nozzle designs and shape optimization as there are different proposals by different authors that can be used to investigate.

Use other important variables in the design as boundary conditions, such as the fuel injection ratio, the boattail design, the control that a nozzle must-have, the materials implemented to its manufacturing, and so on.

8. Recommendations

The design always should begin for the convergent part since that is the order of design, and usually, when designing, there is much more data available that will give us a way to compute the discharge coefficient, and with this, the area of the throat can be cleared.

There is no necessity to make a two-dimensional analysis of the divergent part unless it is requested.

Always divide the general design of the contour into three stages, subsonic, transonic, and supersonic. As they are separated design, different methods of design can be mixed. Also, it is useful to save all the computed data as it probably will be needed in another moment.

Try to divide all the programming code by functions as it will make faster the execution of the program. An example is to create a function for calculating the thermodynamic properties with the velocity as the input parameter for applying every time a point is computed.

For the supersonic design recommendations are to divide the design into four parts, as presented in this thesis.

Use the same technique of integration in all the characteristics to avoid any discrepancy between methods; and is recommendable to use the method in its general form as the division between points is not constant.

Save the data in a matrix and have in mind the number of points created in every procedure because these numbers are necessary for al the design.

Bibliographical References

Anderson, J. D. (1995). *Computational fluid dynamics. The basics with applications.* New York: McGraw-Hill Series in Aeronautical and Aerospace Engineering.

ANSYS. (2013). *Ansys Fluent Theory Guide.* USA: ANSYS, Inc.

Baals, D. D., & Corliss, W. R. (2004a). *Ballistic Missiles and Spacecraft Penetrate the Hypersonic Range.* Retrieved 2018-07-26, from https://history.nasa.gov/SP-440/ch5-5.htm

Baals, D. D., & Corliss, W. R. (2004b). *The Era of High-Speed Flight.* Retrieved 2018-07-26, from https://history.nasa.gov/SP-440/ch5-1.htm

Baals, D. D., & Corliss, W. R. (2004c). *How Supersonic and Subsonic Tunnels Differ.* Retrieved 2018-07-26, from https://history.nasa.gov/SP-440/ch5-2.htm

Bernstein, a., Heiser, W., & Hevenor, C. (1967). Compound-compressible nozzle flow. *Journal of Applied Mechanics*, *34*(3), 548–554. Retrieved from https://web.stanford.edu/~cantwell/AA283_Course_Material/Compound_Comp_Nozzle_Flow_Heiser.pdf doi: 10.2514/6.1966-663

Cengel, Y. A., & Boles, M. A. (2015). *Thermodynamics - An Engineering Approach.* (8th ed.; B. Stenquist, Ed.). New York: McGraw-Hill Education. doi: 10.1108/eb031863

DeBonis, J. R. (2010). Gas Turbine Engines: Nozzles. In *Encyclopedia of aerospace engineering* (pp. 15 – 31). American Cancer Society. Retrieved from https://onlinelibrary.wiley.com/doi/abs/10.1002/9780470686652.eae096 (NASA Glenn Research Center) doi: 10.1002/9780470686652.eae096

Decher, R. (1978). Nonuniform flow through nozzles. *Journal of Aircraft*, *15*(7), 416–421. Retrieved from http://dx.doi.org/10.2514/6.1977-957 doi: 10.2514/6.1977-957

De Laval, C. G. P. (1894). *Steam-Turbine* (No. U.S. Patent 522066A).

Deych, M. Y. (1961). *Technical Gas Dynamics (translated from Russian).* Ohio: Foreign Technology Division - Air Force System Command.

DILLAWAY, R. B. (1957). A philosophy for improved rocket nozzle design. *Journal of Jet Propulsion*, *27*(10), 1088-1093. Retrieved from https://arc.aiaa.org/doi/abs/10.2514/8.12463 doi: 10.2514/8.12463

Doty, J. H., Thompson, H. D., & Hoffman, J. D. (1989a). *Maximum Thrust Nozzles With Non-Unlform Inlet Conditions* (Tech. Rep. No. NASP-CR-1069). NASA Lewis Research Center.

Doty, J. H., Thompson, H. D., & Hoffman, J. D. (1989b). Optimum Thrust Airframe Integrated Scramjet Nozzles. In *Seventh national aero-space plane technology symposium.* NASA Lewis Research Center.

El-Sayed, A. F. (2016). *Fundamentals of aircraft and rocket propulsion.* London: Springer-Verlag London Ltd. doi: 10.1007/978-1-4471-6796-9

Farokhi, S. (2014). *Aircraft propulsion* (2nd ed.). Chichester, West Sussex: John Wiley & Sons Ltd. doi: 10.2514/1.J054236

Fay, J. A. (1994). *Introduction to Fluid Mechanics Copyrighted Material Introduction to Fluid Mechanics.* Cambridge: MIT Press.

Guentert, E., & Neumann, H. E. (1959). *Design of Axisymmetric Exhaust Nozzles by Method of Characteristics Incorporating a Variable Isentropic Exponent* (Tech. Rep. No. NASA-TR-R-33). Cleveland, Ohio: NASA LEwis Research Center. Retrieved from https://ntrs.nasa.gov/archive/nasa/casi.ntrs.nasa.gov/19980232191.pdf (Document ID: 19980232191)

Gutkin, M. B., & Chistyakov, Y. A. (2013). A new method of calibration of nozzles for flow metering gas installations. *Measurement Techniques*, *56*(5), 567–569. doi: 10.1007/s11018-013-0245-7

Haddad, A. (1988). *Supersonic Nozzle Design of Arbitrary Cross-Section.* Unpublished doctoral dissertation, Cranfield Institute of Technology.

Hartfield, R., & Ahuja, V. (2011). The Closing Boundary Condition for the Axis-Symmetric Method of Characteristics. In *47th aiaa/asme/sae/asee joint propulsion conference & exhibit* (pp. 1–9). San Diego, California: American Institute of Aeronautics and Astronautics, Inc. doi: 10.2514/6.2011-5943

Hartfield, R. J., & Burkhalter, J. E. (2015). *A Complete and Robust Approach to Axisymmetric Method of Characteristics for Nozzle Design.* Retrieved from http://arc.aiaa.org/doi/10.2514/6.2015-4217 doi: 10.2514/6.2015-4217

Hoffmann, K., & Chiang, S. (2000). *Computational fluid dynamics. Volume I* (4th ed.).

Ishii, R. (2014). A New Method of Nozzle Design. *Contributions to Management Science*, *16*(7), 231–326. doi: 10.1007/978-3-642-53989-3_5

John D. Anderson, J. (2003). *Modern compressible flow with historical perspective* (3rd ed., Vol. 4). New York: McGraw-Hill Series in Aeronautical and Aerospace Engineering. doi: 10.1016/0142-727X(83)90029-2

Kruse, R. (2007). *V-2 Rockets and Rocket Motors | Historic Spacecraft.* Retrieved 2018-07-26, from https://historicspacecraft.com/Rockets_V-2.html

Martinez, I. (2017). *Nozzles.* Retrieved from http://webserver.dmt.upm.es/~isidoro/bk3/c17/Nozzles.pdf

Mattingly, J. D. (2006). *Elements of Propulsion: Gas Turbines and Rockets.* Reston, Virginia: American Institute of Aeronautics and Astronautics, Inc. Retrieved from http://arc.aiaa.org/doi/book/10.2514/4.861789 doi: 10.2514/4.861789

Mattingly, J. D., Heiser, W. H., & Pratt, D. T. (1801). *Aircraft engine design* (2nd ed.; R. Przemieniecki, John S. (Air Force Institute of Technology, Ed.). Reston, Virginia: American Institute of Aeronautics and Astronautics, Inc.

Mulumba, M. J.-B. (2013). *Calculation and Design of Supersonic Nozzles for Cold Gas Dynamic Spraying Using Matlab and Ansys Fluent.* Unpublished doctoral dissertation, University of the Witwatersrand. Retrieved from http://wiredspace.wits.ac.za/bitstream/handle/10539/12865/MScEng{_}DissertationforJean-BaptisteMbuyamba(586572).pdf?sequence=2

NASA Glenn Research Center. (2015). *Nozzles.* Retrieved 2018-07-23, from https://www.grc.nasa.gov/WWW/k-12/airplane/nozzle.html

Oates, G. C. (1989). *Aircraft Propulsion Systems Technology and Design.* Seattle, Washington: American Institute of Aeronautics and Astronautics, Inc. Retrieved from http://books.google.com.tr/books?id=CQLIsf5fi-gC doi: 10.2514/4.861499

O'Byrne, S., Danehy, P. M., & Houwing, A. F. (2006). Investigation of hypersonic nozzle flow uniformity using NO fluorescence. *Shock Waves*, *15*(2), 81–87. Retrieved from https://link.springer.com/article/10.1007/s00193-006-0013-6 doi: 10.1007/s00193-006-0013-6

Ochoa Alvarez, O. M. (2015). *Estudio computacional de la respuesta operacional de un ducto convergente-divergente bajo condiciones de flujo compresible, turbulento*. Unpublished doctoral dissertation, Universidad Nacional de Colombia. Retrieved from http://www.bdigital.unal.edu.co/49782/

Prince, David C., J. (1982). The Method of Characteristics for Supersonic Flow Analysis - A Fresh Perspective. Missouri: American Institute of Aeronautics and Astronautics, Inc. (In AIAA/ASME 3rd Joint Thermophysics, Fluids, Plasma and Heat Transfer Conference) doi: 10.2514/6.1982-996

Quintao, K. K. (2012). *Design Optimization of Nozzle Shapes for Maximum Uniformity of Exit Flow*. Master of science (ms), Florida International University. Retrieved from http://digitalcommons.fiu.edu/etd/779 doi: 10.25148/etd.FI12120505

Rao, G. V. R. (1958). Exhaust Nozzle Contour for Optimum Thrust. *Journal of Jet Propulsion*, *28*(6), 377–382. Retrieved from http://arc.aiaa.org/doi/10.2514/8.7324 doi: 10.2514/8.7324

Rotty, R. M. (2008). *Introduction to Gas Dynamics*. New York: John Willey & Sons, Inc. doi: 10.1007/978-3-540-71343-2_12

Sauer, R. (1947). *General Characteristics of the Flow through Nozzles at Near Critical Speeds* (Tech. Rep. No. 1992). Washington: National Advisory Committee for Aeronautics.

Shapiro, A. H. (1953). *The Dynamics and Thermodynamics of Compressible Fluid Flow* (Vol. I). New York: The Ronald Press Company. Retrieved from http://www.amazon.com/Dynamics-Thermodynamics-Compressible-Fluid-Flow/dp/0471066915/ref=pd{_}sim{_}b{_}59

SIVELLS, J. C. (1970). Aerodynamic design of axisymmetric hypersonic wind-tunnel nozzles. *Journal of Spacecraft and Rockets*, *7*(11), 1292-1299. Retrieved from https://doi.org/10.2514/3.30160 doi: 10.2514/3.30160

Škorpík, J. (2018). Flow of Gases and Steam Through Nozzles. In *Proudění* (chap. 40). Brno, Czech Republic: Jiří Škorpík. Retrieved from http://www.transformacni-technologie.cz

Snelling, S. L. (1991). *Effect of Nonuniform Entrance Flow Profile on Hypersonic Nozzle Pitching Moment*. Master of science (ms), Air Force Institute of Technology. Retrieved from http://www.dtic.mil/dtic/tr/fulltext/u2/a244050.pdf doi: DTICADA244050

Sutton, G. P., & Biblarz, O. (2010). *Rocket Propulsion Elements* (8th ed.). Hoboken, New Jersey: John Willey & Sons, Inc.

Tannehill, J. C., Anderson, D. A., & Pletcher, R. H. (1997). *Computational Fluid Mechanics and Heat Transfer* (Third ed.). Boca Raton. doi: 10.1017/CBO9781107415324.004

Tu, J., Yeoh, G.-H., & Liu, C. (2018). *Computational Fluid Dynamics: A Practical Approach* (Third ed., Vol. 53). Oxford: Butterworth-Heinemann.

Zucrow, M. J., & Hoffman Joe. (1976). *Gas Dynamics - Volume 1.* New York - Santa Barbara - London - Sydney - Toronto: John Willey & Sons, Inc.

Zucrow, M. J., & Hoffman Joe. (1977). *Gas Dynamics - Volume 2: Multidimensional Flow.* New York - Toronto - London - Sydney: John Willey & Sons, Inc. doi: 10.1213/01.ane.0000492743.10184.13